

SEISMIC-WAVE PROPAGATION IN
TWO-PHASE MEDIA AND ITS APPLICATIONS
TO THE EARTH'S INTERIOR

by

GUY THIERRY KUSTER

Licencié ès sciences, Strasbourg (1967)
Ingenieur géophysicien, Strasbourg (1968)

M.S., Massachusetts Institute of Technology (1970)

SUBMITTED IN
PARTIAL FULFILLMENT
OF THE REQUIREMENTS FOR THE
DEGREE OF DOCTOR OF PHILOSOPHY

at the

MASSACHUSETTS INSTITUTE OF TECHNOLOGY

June, 1972

Signature of Author.....

Department of Earth and Planetary Sciences, May 15, 1972

Certified by..... Thesis Supervisor

Accepted by.....
Chairman, Departmental Committee on Graduate Students

WITHDRAWN Lindgren
FROM
MIT LIBRARIES
MASS. INST. TECH.
JUN 28 1972
LIBRARIES

ABSTRACT

Seismic Wave Propagation in Two-Phase Media
and Its Applications to the Earth's Interior

by

Guy Thierry Kuster

Submitted to the Department of Earth and
Planetary Sciences on May 15, 1972
in partial fulfillment of the
requirements for the degree of
Doctor of Philosophy

Theoretical and experimental studies of the macroscopic response of two-phase media to elastic waves are carried out. Theoretical investigations include five separate models: 1. The basic model consists of a solid matrix with spherical inclusions. Wavelengths are much larger than inclusion radii and the inclusions are sufficiently far apart for interactions to be negligible. 2. The inclusions are oblate spheroids. In this case the macroscopic properties depend on the aspect ratio as well as the concentration of the inclusions. 3. Interactions are taken into account in an average sense. Only the macroscopic shear behavior is affected. 4. The matrix is a fluid. It is found that static models cannot be used for wave propagation problems because of inertia effects.

5. The dependence of the macroscopic properties on the wavelength is investigated for a suspension of solid spheres in a fluid. The dispersive effects can be significant.

The velocity of ultrasonic waves is measured in suspensions of solid spheres in a fluid matrix as a function of the concentration of inclusions. In all cases the velocity data are best matched by our theoretical model which takes into account interactions and the dispersive effects resulting from a finite wavelength to inclusion size ratio. The observed attenuation compares satisfactorily to the theoretical values computed by including geometrical scattering, viscous absorption in the fluid matrix and anelasticity of the solid inclusions.

The properties of the earth's core are investigated with the formulations described above. The amplitude spectra of short-period (0.2 to 2.0 Hz) core phases (PKP and PKKP) are measured at LASA. The amplitude ratio technique is used to determine the quality factor Q at the base of the mantle and in the core. On the basis of our data the liquid outer core has a large Q (≈ 2500), whereas the inner core has a low Q (≈ 300). The Q in the transition zone is intermediate (≈ 1200). A highly attenuating layer ($Q \approx 300$) about 150 km thick is required at the base of the mantle. The observed velocities and the low Q values in the inner core and at the base of the mantle can be attributed to small concentrations of melt

(less than 5%). The low velocity gradients and intermediate Q value of the transition zone can be interpreted in terms of partial crystallization of the liquid core.

Thesis Supervisor: M. Nafi Toksöz

Title: Professor of Geophysics

ACKNOWLEDGEMENTS

I am deeply indebted to my advisor, Professor M. Nafi Toksoz, who suggested the topic and guided me throughout this study as well as my stay at MIT.

All along this work I profited from discussions with Professor Keiiti Aki, Professor Sean Solomon and Dr. Joseph Walsh. I owe my thanks to Dr. Bruce Julian for making his ray tracing program available. I would also like to thank Dr. Dai Davies and the Seismic Discrimination Group of Lincoln Laboratory for letting me use their computer facilities.

Finally I would like to express my deepest gratitude to Donald Weidner, my office mate, for countless discussions. His criticisms and suggestions were of invaluable help in shaping my ideas and developing my understanding of the problem.

During my studies at M.I.T. I was fortunate to receive a fellowship from Chevron Oil Company.

This work was supported by the American Petroleum Institute, Project No. 129.

TABLE OF CONTENTS

	Page
ABSTRACT	2
ACKNOWLEDGMENTS	5
LIST OF SYMBOLS	8
1. INTRODUCTION	12
2. THEORETICAL ANALYSIS	17
2.1 Statistical Nature of a Two-Phase Medium	18
2.2 Mal and Knopoff's Model	20
2.3 A Method for Deriving Effective Properties	23
2.4 Spherical Inclusions.	26
2.4.1 Non-interaction model	26
2.4.2 The case of a fluid matrix	29
2.4.3 Average effect of interactions on the effective properties	32
2.5 Spheroidal Inclusions	36
2.6 Effective Attenuation of Elastic Waves	41
2.6.1 Geometrical scattering	42
2.6.2 Viscoelastic attenuation	42
2.6.3 Attenuation in a suspension with a viscous matrix	44
2.6.4 Attenuation in a fluid saturated porous rock	45
2.7 Dispersive Properties of Two-Phase Media	47
2.7.1 Magnitude of the approximation	48
2.7.2 Effective properties as a function of λ/α	49
2.7.3 The size of the representative sphere and its physical meaning	52
Tables	55
Figure Captions	56

3.	EXPERIMENTAL RESULTS	62
3.1	Characteristics of the Suspensions.	63
3.2	Experimental Procedure.	65
3.3	Method of Measurement	66
3.3.1	Velocity	66
3.3.2	Attenuation	67
3.4	Experimental Results.	70
3.4.1	Velocity	70
3.4.2	Attenuation	72
	Tables	75
	Figure Captions	85
4.	APPLICATION TO THE EARTH'S INTERIOR	94
4.1	Method of Analysis.	95
4.2	Data Base	98
4.3	Inversion of the Data	101
4.4	Interpretation.	105
4.4.1	Transition zone.	105
4.4.2	Inner core	110
4.4.3	The base of the mantle and the core- mantle boundary	113
	Tables	118
	Figure Captions	125
5.	CONCLUSIONS.	136
	REFERENCES	139
	APPENDICES	
A.	SCATTERING OF A PLANE P WAVE BY A SPHERICAL OBSTACLE	149
B.	SELF-CONSISTENT MODELS	161
C.	SCATTERING BY SPHEROIDAL INCLUSIONS.	169
D.	EFFECTIVE PROPERTIES FOR INTERMEDIATE WAVELENGTH	183

LIST OF SYMBOLS

A	amplitude of incident plane P wave
A_0	wave incident on the representative sphere (global notation)
A_j	wave incident on an inclusion (global notation)
A_{ijpq}	fourth order tensor
\underline{A}	vector potential
a	radius of a spherical inclusion
B_n	coefficient in the series expansion of scattered P waves
b	radius of matrix shell
C_{12}	constant (Equations 4.3 and 4.4)
ϕ	volume concentration of inclusions
$c(\underline{y})$	volume of an inclusion
c_{ijpq}	elastic tensor, matrix
c'_{ijpq}	elastic tensor, inclusion
d	a/b
d_0	distance
e_{ij}	strain field
e^0_{ij}	incident strain field
f	frequency
G_{ki}	Green's function, matrix
g	acceleration of gravity
$h_n^{(1)}$	spherical Hankel function, first kind
$h_n^{(2)}$	spherical Hankel function, second kind
j_n	spherical Bessel function
K	matrix bulk modulus
K'	inclusion bulk modulus
K^*	effective bulk modulus
K^*_d	dynamic effective bulk modulus

K_L^*	effective bulk modulus, long wavelength limit
K_S^*	static effective bulk modulus
k	wavenumber
l_{ij}	direction cosine
N	number of inclusions in representative sphere
\underline{n}	outward unit normal at \underline{n}
p	wave number, P wave in matrix
p'	wave number, P wave in inclusion
p^*	wave number, P wave in effective material
\mathcal{P}	constant
\mathcal{P}^*	constant
$P_n(\cos\theta)$	Legendre polynomial, order n
Q	elastic quality factor
\mathcal{Q}	constant
\mathcal{Q}^*	constant
R	radius representative sphere
\underline{r}	vector from the center of the representative sphere to the observation point
\underline{r}_j	vector from the center of an inclusion to the observation point
r	$ \underline{r} $
ΔS_{ijpq}	fourth order tensor
s	wave number, S wave in matrix
s'	wave number, S wave in inclusion
T_{ijpq}	4th order tensor depending on matrix & inclusion properties
T_{ijpq}^*	4th order tensor depending on effective and inclusion properties
t^*	anelasticity factor (Equation 4.2)
Δt	time window for spectral estimation
Δt_i	differential travel time
U_{ijpq}	fourth order tensor
\underline{u}	total field
\underline{u}_i	incident field

u	scattered field
u_0	incident displacement vector in matrix
Δu	scattered displacement vector in matrix
$u_1^2, u_2^2, u_3^2, u_4^2, u_5^2, u_6^2$	six row vectors (Equation B1)
u	radial displacement
V	volume of an inclusion
V_0	volume of representative sphere
V_j	volume of jth inclusion in representative sphere
v	displacement vector inside an inclusion
Δv	scattered displacement vector inside an inclusion
v	transverse displacement
v^2	velocity of fluid in the core
x	point in the matrix
x	pa
x'	p'a
x^2	distance between transducers
x_{12}	slope fitted to amplitude ratios
y	center of an inclusion
y, y_a	pa
y'	p'a
y_b	pb
y_R	pR
y_b^*	p*b
y_R^*	p*R
z	point inside an inclusion
z	sa
z'	s'a
α	matrix P wave velocity
α'	inclusion P wave velocity
α^*	effective P wave velocity

α_N	normalized effective P wave velocity
α_L^*	effective P wave velocity, long wavelength limit
$\tilde{\alpha}$	aspect ratio of oblate spheroid
β^*	effective S wave velocity
$\tilde{\gamma}(f)$	attenuation function
γ	attenuation factor
Δ	epicentral distance
δ	constant (Equation 3.3)
Φ	scalar potential
Ψ	scalar potential
λ	wavelength of P wave in matrix material
λ'	wavelength of P wave in inclusion material
λ^*	wavelength of P wave in effective material
$\tilde{\lambda}$	Lamé constant, matrix
$\tilde{\lambda}'$	Lamé constant, inclusion
$\tilde{\lambda}^*$	Lamé constant, effective material
$\Delta\tilde{\lambda}$	$\tilde{\lambda}' - \tilde{\lambda}$
μ	matrix shear modulus
μ'	inclusion shear modulus
μ^*	effective shear modulus
$\Delta\mu$	$\mu' - \mu$
ν	s/p
ρ	matrix density
ρ'	inclusion density
ρ^*	effective density
ρ_g^*	effective gravitational density
ρ_i^*	effective inertial density
$\Delta\rho$	$\rho' - \rho$
σ	matrix properties (global notation)
σ'	inclusion properties (global notation)
σ^*	effective properties (global notation)
$\underline{\eta}$	point on surface of inclusion
η	viscosity of fluid
ω	angular frequency

CHAPTER 1. INTRODUCTION

Heterogeneity is a fundamental characteristic of all real media and it influences the propagation of seismic waves. Heterogeneous media whose properties are known functions of position has been studied extensively (Ewing et al., 1957). When the heterogeneities are of a random nature, one can distinguish two types of media: (i) those where the parameters (velocities, elastic constants, density) are continuous random functions of space and (ii) aggregates resulting of the random juxtaposition of different materials.

Several treatments of the propagation of elastic waves through media of the first type are available (Karal and Keller, 1964; Chernov, 1967; Howe, 1971); in all cases one is to solve the wave equation with random coefficients and it is in general assumed that the fluctuations of the random values about their means are small so that a perturbation method can be used. It is only recently that media of this type have been considered in a seismological context; Aki (1972) and Capon (personal communication) used Chernov's theory to interpret amplitude and phase

fluctuations of seismic signals recorded at the Large Aperture Seismic Array (LASA).

Aggregates of randomly distributed phases have received more attention from geophysicists since they seem to be more representative of actual rocks. An important type of aggregate is a two-phase medium where one phase is an homogeneous and isotropic continuum, the matrix, in which inclusions of the other phase, also homogeneous and isotropic, are randomly embedded. In a two-phase medium the elastic parameters are, therefore, piecewise constant with randomly distributed discontinuities.

Examples of the seismic relevance of two-phase media can be readily found. Seismic velocities and attenuation factors of fluid saturated or partially saturated sedimentary rocks are of utmost importance in seismic prospecting (Born, 1941; Shumway, 1960; Schreiber, 1968). Porosity and the nature of the fluid filling the pores is a major factor affecting the velocities measured on rocks in the laboratory at moderate pressures (Nur and Simmons, 1969). There is increasing evidence for interpreting the zone of low velocity and high attenuation in the upper mantle in terms of partial melting (Anderson et al., 1965; Solomon, 1972). Unexpectedly low velocity gradients may indicate partial crystallization of the fluid's outer core (Toksoz

et al., 1972) and the low inner core shear wave velocity (Julian et al., 1972) suggests partial melting. The puzzling difference between the elastic quality factor Q of moon rocks measured on the earth and in situ may be related to the different behavior of air and vacuum filled pores (Todd et al., 1972).

Theoretical treatment of the propagation of elastic waves in two-phase media (the dynamic problem) is scarce. In two attempts on this subject (Ament, 1959; Mal and Knop-off, 1967), the validity of the results is restricted to the case where the matrix is solid, the inclusions are spheres much smaller than the wavelengths and sufficiently far apart from each other so that interactions are negligible. The theoretical elastic behavior of two-phase media under static loading has been studied in detail (see Hashin, 1964, 1970, for a review). The results of these studies have been applied to seismic problems under the assumption that the conditions prevailing in the propagation of long wavelength waves can be approximated by those under static loading (Walsh, 1969; Solomon, 1972). However, the assumptions (constant strain at infinity) needed for the derivation of static models are incompatible with the nature of the dynamic problem. Furthermore, inertia effects are by definition omitted in static models, whereas they are of

definite importance in wave propagation problems. Finally, static models cannot be extended to cover cases where the relative size of the inclusion and the wavelength is important; they cannot even be used either to define the wavelength at which the long wavelength approximation becomes invalid or to determine the magnitude of the approximation involved. Such questions are quite relevant to laboratory measurements of the elastic properties of rocks where high frequency signals are commonly used. Theoretical studies aimed at a quantitative understanding of both the long wavelength approximation and the interaction effects are therefore necessary.

Measurements of the velocity and attenuation of elastic waves in two-phase media can be found in the literature. The vast majority of these is obtained in the laboratory on porous solids, the pore space being usually filled with air, water, a more viscous fluid or even ice (Wyllie et al. 1956, 1958; Timur, 1968; and Nur and Simmons, 1969); data are also available on media undergoing partial melting (Spetzler and Anderson, 1968). But there are very few data on the velocity and attenuation of elastic waves in two-phase media where the matrix is fluid and the inclusions solid, although such media are of interest in marine geophysics and seismic logging. The only data seem to be those of Knudsen (1946) on the attenuation of acoustic waves in fogs.

In this study we first examine the theoretical response of two-phase media to elastic waves. We review available models (Ament, 1959; Mal and Knopoff, 1967) and extend Ament's approach to obtain additional models. Assuming that the wavelengths are much longer than the inclusion size and that interactions are negligible we derive the effective behavior of (i) a suspension of solid spheres in a non-viscous fluid matrix and (ii) a solid-solid two-phase medium where the inclusions are spheroidal. Assuming that the inclusions are spherical and the wavelengths very long we derive a model where interactions are taken into account by a self-consistent scheme. We also calculate the dependence of the effective properties on the wavelength to inclusion size ratio for a suspension of solid spheres in a non-viscous fluid matrix. In the second part we present our laboratory measurements of the velocity and attenuation of ultrasonic waves in suspensions of solid spheres in a fluid matrix. The experimental results clearly illustrate the validity of our theoretical models. In the final part, we present measurements of the attenuation of short-period P waves having travelled through the earth's core. Our data, combined with available seismic velocity models, are interpreted in terms of partial crystallization in the outer core and partial melting in the inner core and at the base of the mantle.

CHAPTER 2. THEORETICAL ANALYSIS

It has been assumed that the effective elastic moduli derived as solutions of the static problem can be used for computing the effective wave velocities of a two-phase medium when the wavelength is large compared to the inclusion size (Walsh, 1969; Kuster, 1970; Solomon, 1972). Although this approach has led to useful results, it is nevertheless not completely satisfactory. Static results are derived with the assumption that strain or stress is constant over time either at infinity (Eshelby, 1957; Wu, 1966) or on a given surface (Hashin, 1962). This assumption is incompatible with the very nature of the dynamic problem. Inertia effects are omitted in static models by definition, whereas they are an intrinsic feature of wave phenomena. Applying static results to the dynamic problem involves an approximation, but in the same time it does not allow any estimate of the magnitude of the error due to the approximation. As a consequence, the direct treatment of the propagation of elastic waves in two-phase media is important.

2.1 Statistical nature of a two-phase medium.

A two-phase medium is defined as a mixture of two homogeneous isotropic media of different physical properties with well-defined interfaces. A further restriction is that the matrix is a continuum in which inclusions of the other phase are randomly embedded; it is, therefore, a medium whose properties are random but piecewise constant functions of space.

We assume that there exists a volume V_0 , called the representative volume element (RVE), such that wherever we choose to extract the volume V_0 out of the two-phase medium, this volume will have the same average properties as the two-phase medium itself. This assumption, called the quasi-homogeneity assumption, implies that we can define a homogeneous medium, called the effective medium, which will have the same average properties as the two-phase medium. Then the effective wave velocities and effective elastic moduli are related by the usual equations for homogeneous media.

$$\alpha^* = \sqrt{\frac{K^* + 4\mu^*/3}{\rho^*}} \quad \beta^* = \sqrt{\frac{\mu^*}{\rho^*}} \quad (2.1)$$

where α^* and β^* are the effective compressional and shear wave velocities, K^* and μ^* are the effective bulk and shear

moduli and ρ^* is the effective density. The effective elastic moduli and the effective velocities can, therefore, be used interchangeably. The RVE is larger than an inclusion and according to the quasi-homogeneity assumption any volume smaller than the RVE will not exhibit effective properties. Since we want to find the effective behavior of a wave propagating in a two-phase medium, we restrict our study to waves whose wavelength is larger than the RVE size.

Ideally one wishes to find the effective properties from the properties of the constituent phases exactly; but the effective properties obviously depend also on the distribution of inclusions in the medium. An exact solution thus requires a complete statistical description of the distribution. However, what one usually knows about the distribution of inclusions in a real two-phase medium is the relative volume of the two phases. This is clearly not sufficient information for an exact solution. Even if we could obtain an exact solution it would be of no relevance for comparison with data. Because of this practical constraint the question we address ourselves to in the following analysis is: what can we say about the effective properties of a two-phase medium in terms only of the properties and the volume fractions of each phase?

2.2 Mal and Knopoff's model.

Mal and Knopoff (1967) derived an effective wave equation for a two-phase medium with the assumptions that the inclusions are spherical and much smaller than the wavelength of the incident wave. Since part of their derivation is used in appendix C, we shall only outline it here. It basically consists of three steps.

Considering an inclusion isolated in an infinite matrix, and an incident field, they first express the displacement at a point outside the inclusion in terms of the displacement and strain inside. Then they make use of the long wavelength approximation to estimate the displacement and strain inside from the displacement and strain of the incident field. The displacement inside is approximated by the displacement that one would observe if the inclusion was absent (Born's approximation). It is valid for any density contrast between matrix and inclusion materials as long as the wavelengths are large. For the strain, they prove that the lowest-order approximation corresponds to Eshelby's (1957) results under static conditions. Thus, the scattered displacement at \underline{x} due to a sphere located at \underline{y} can be written

$$\Delta u_k(\underline{x}, \underline{y}) = c(\underline{y}) [\omega^2 \Delta \rho u_i^0(\underline{y}) G_{ki}(\underline{x}, \underline{y}) - \Delta S_{ijpq} \frac{\partial u_p^0}{\partial y_q} \frac{\partial G_{kij}}{\partial y_j}] \quad (2.2)$$

where u_i^0 is the incident displacement field, $c(\underline{y})$ is the volume of the sphere, ΔS_{ijpq} is a tensor depending on the matrix and inclusion elastic constants, $G_{ki}(\underline{x}, \underline{y})$ is the i th component observed at \underline{x} of the Green's function due to a point force acting in the k th direction at \underline{y} in an infinite medium with matrix properties, ω is the angular frequency and $\Delta\rho$ is the difference between inclusion and matrix densities. The summation convention is used. The last step which we shall discuss in more detail consists of the application of (2.2) to a cloud of N inclusions randomly distributed in the matrix. The displacement at a point \underline{x} in the middle of the cloud and in matrix material can be written as

$$u_k(\underline{x}) = u_k^0(\underline{x}) + \sum_{s=1}^N \Delta u_k(\underline{x}, \underline{y}^s) \quad (2.3)$$

where $\Delta u_k(\underline{x}, \underline{y}^s)$ is the field scattered by the s th inclusion in presence of all others; it can be estimated by replacing $u_k^0(\underline{x})$ in (2.2) with the field which would exist at \underline{y}^s in the absence of the s th inclusion. Mal and Knopoff make the assumption that this field is the average field which one wants to determine eventually. It is then found that the average field satisfies the wave equation in a homogeneous elastic medium with density and elastic constants

$$\rho^* = \rho(1-c) + \rho'c \quad (2.4)$$

$$K^* = K + \frac{(K'-K)c}{1 + \frac{3(K'-K)}{3K + 4\mu}} \quad (2.5)$$

$$\mu^* = \mu + \frac{(\mu'-\mu)c}{1 + \frac{6(\mu'-\mu)(K + 2\mu)}{5\mu(3K + 4\mu)}} \quad (2.6)$$

where ρ is density, K and μ are the bulk and shear moduli and c is the volume concentration of inclusions. Primed, unprimed and starred variables refer respectively to inclusion, matrix and effective properties.

Note that the effective elastic moduli are the same as those found by Eshelby (1957) in solving the static case. His solution is valid only at low concentrations. Although no such restriction is explicitly stated by Mal and Knopoff, it is actually implicit to their derivation. Equation (2.2) is valid only when the incident field (\underline{u}^0) and the Green's function both satisfy the wave equation in the same medium. In applying (2.2) to the cloud of inclusions Mal and Knopoff replaced u^0 by the average field which satisfies the effective wave equation whereas they conserved Green's function for the matrix. This is valid when the effective and matrix properties are similar.

This is the case when either the concentration of inclusions or the contrast between inclusion and matrix properties is small.

2.3 A method for deriving effective properties.

The method described in this section is due to Ament (1959). It is very simple and powerful, but it has not received much recognition in the literature, except for a brief mention by Hashin (1962). It has not been used to its full extent, not even by Ament himself, possibly because of the rather cumbersome notation he adopted.

Consider a quasi-homogeneous and quasi-isotropic two-phase medium. Let us assume that we can isolate a representative volume element. Because of the quasi-homogeneity assumption, this element will have the same effective properties as the two-phase medium itself. Let us further assume that we can surround this RVE with matrix material extending to infinity, and that we weld the boundaries to obtain the configuration of Figure 2.1(a). A wave incident from infinity will be scattered by the RVE which acts as an isolated obstacle with effective properties embedded in an infinite matrix. The elastic displacement at a point \underline{x} in the matrix can be written as

$$\underline{u}(\underline{x}) = \underline{u}_i(\underline{x}) + \underline{u}_s(\underline{x}, A_0, \sigma, V_0, \sigma^*, \underline{r}) \quad (2.7)$$

where \underline{u}_i is the displacement at \underline{x} due to the incident wave and $\underline{u}_s(\underline{x}, A_0, \sigma, V_0, \sigma^*, \underline{r})$ is the displacement at \underline{x} due to the scattered wave. The scattered wave depends on the incident wave A_0 , the properties of the matrix (σ), the shape and volume of the RVE (V_0), the effective properties of the RVE (σ^*), and the relative location \underline{r} of the RVE and the observation point.

Examine now the geometry of figure 2.1(a) on a finer scale. The RVE actually contains a number of inclusions distributed in matrix material. Thus, the detailed geometry is that indicated on figure 2.1(b); then when a wave is incident from infinity the displacement at \underline{x} can also be written as

$$\underline{u}(\underline{x}) = \underline{u}_i(\underline{x}) + \sum_{j=1}^N \underline{u}_s(\underline{x}, A_j, \sigma, V_j, \sigma', \underline{r}_j) \quad (2.8)$$

This equation simply expresses that the observed displacement at \underline{x} is the superposition of the displacement due to the incident wave and of all displacements due to the waves scattered by each inclusion, the total number of inclusions in the RVE being N . The wave scattered by each inclusion depends on the wave A_j which is incident on that particular inclusion, the matrix properties (σ), the volume and shape of

the inclusion (V_j), the properties of the inclusion material (σ^*) and the relative location \underline{r}_j of the inclusion and the observation point.

All what we have done here is to express the same quantity, the displacement field at \underline{x} in two different ways. In equation (2.7) the RVE is treated as a global entity with effective properties, whereas in equation (2.8) it is treated as the sum of its parts. This is the essence of the method. Equating (2.7) and (2.8), we obtain

$$\underline{u}_s(\underline{x}, A_0, \sigma, V_0, \sigma^*, \underline{r}) = \sum_{j=1}^N \underline{u}_s(\underline{x}, A_j, \sigma, V_j, \sigma^*, \underline{r}_j) \quad (2.9)$$

If all other parameters are known, this equation will yield the effective properties σ^* , provided the scattered displacements can be properly evaluated. The remainder of this chapter is only devoted to the estimation of both sides of equation (2.9) under various conditions. Analytical treatment is possible only when the shape of the inclusions is simple, such as spheres or more generally spheroids. The shape of the RVE will always be spherical in the subsequent analysis and the RVE will thus be called representative sphere. This choice is consistent with the quasi-isotropic assumption made earlier. Finally we must

mention that the essential difficulty of an exact mathematical treatment lies in the estimation of the wave which is actually incident on an inclusion in the presence of neighboring inclusions. Multiple scattering is clearly to be considered but its net effect is difficult to evaluate exactly since the inclusions are randomly distributed.

2.4 Spherical inclusions.

2.4.1. Non-interaction model.

This model has been originally obtained by Ament (1959). Although full credit is to be given to him, we named the model "non-interaction" because it expresses the basic assumption involved in the model.

Consider a quasi-homogeneous and quasi-isotropic two-phase medium. Both phases are assumed to be solid and elastic. Let the incident wave be a plane P wave whose wavelength is much larger than the radius of the representative sphere and a fortiori of the inclusions. The inclusions need not be all of the same size.

We can use the analysis given in appendix A to express the wave scattered by the representative sphere of radius R centered at \underline{x}_0 when illuminated by the plane P wave of amplitude A . If the observation point \underline{x} is at a large

distance the scattered radial and transverse displacements are (equations A27 and A28)

$$u^* = -A[B_0^* - iB_1^* \cos\theta - \frac{B_2^*}{4}(3 \cos 2\theta + 1)] \frac{e^{i(pr-\omega t)}}{p^2 r} \quad (2.10)$$

$$v^* = -A[iB_1^* \sin\theta + \frac{3B_2^*}{4} \frac{s}{p} \sin 2\theta] \frac{s^2 e^{i(sr-\omega t)}}{p^2 r}$$

$$\text{with } B_0^* = i(pR)^3 \frac{K-K^*}{3K^* + 4\mu} \quad (2.11)$$

$$B_1^* = (pR)^3 \frac{\rho - \rho^*}{3\rho}$$

$$B_2^* = i(pR)^3 \frac{20}{3} \frac{\mu(\mu^* - \mu)}{6\mu^*(K+2\mu) + \mu(9K+8\mu)}$$

where p and s are the wavenumbers of P and S waves in the matrix; K, μ and ρ stand for bulk and shear moduli and density, * superscript indicates effective properties; r and θ are defined on Figure 2.1.

We are left with evaluating the right-hand side of equation (2.9). We make the critical assumption that all multiple scattering effects can be neglected so that the wave incident on each inclusion is the undisturbed original plane P wave A . This assumption implies that our model is valid only for small concentrations of inclusions where interactions are weak. Since the observation point is at a large distance from the center of the representative sphere

\underline{x}_0 , we may also assume that every inclusion of the representative sphere is approximately located at \underline{x}_0 . The wave scattered by every inclusion can then also be expressed by equations (2.10) and (2.11), where we simply replace R by a_j , the radius of the j th inclusion, and every quantity with a star superscript by primed quantities which refer to inclusion properties. Then equation (2.9) becomes a set of three equations between the coefficients B_n

$$B_n^* = \sum_{j=1}^N B_n^j \quad n=0, 1 \text{ or } 2 \quad (2.12)$$

Replacing B_n by their expressions we obtain

$$\frac{K-K^*}{3K^* + 4\mu} = c \frac{K-K'}{3K' + 4\mu} \quad (2.13)$$

$$\frac{\rho-\rho^*}{\rho} = c \frac{(\rho-\rho')}{\rho} \quad (2.14)$$

$$\frac{\mu^*-\mu}{6\mu^*(K+2\mu)+\mu(9K+8\mu)} = c \frac{\mu'-\mu}{6\mu'(K+2\mu)+\mu(9K+8\mu)} \quad (2.15)$$

where $c = \sum_{j=1}^N a_j^3/R^3$ is the volume concentration of inclusions.

Equations (2.13), (2.14) and (2.15) give the effective elastic moduli and density in terms of the properties

of the matrix and inclusions and the volume concentration of inclusions. The symmetry of these effective laws clearly show how straightforward it is to extend the results to multiphase media. Written in a somewhat more convenient way, the effective laws are

$$K^* = K + \frac{(K'-K)c}{1 + \frac{3(K'-K)\lambda(1-c)}{3K + 4\mu}} \quad (2.16)$$

$$\rho^* = \rho(1-c) + \rho'c \quad (2.17)$$

$$\mu^* = \mu + \frac{(\mu'-\mu)c}{1 + \frac{6(\mu'-\mu)\lambda K + 2\mu\lambda(1-c)}{5\mu(3K+4\mu)}} \quad (2.18)$$

Comparing our results with those of Mal and Knopoff (equations 2.4 - 2.6) we find that our effective elastic moduli reduce to theirs if c is much smaller than 1. Furthermore, it was implicitly assumed in their model that the matrix and the effective medium are very similar. Because of these two reasons we can conclude that Mal and Knopoff's model is valid for lower concentrations than ours. This result is illustrated in figures 2.3, 3.4, 3.5, and 3.6.

2.4.2. The case of a fluid matrix

In the preceding section the non-interaction

model was derived for a medium consisting of two solid phases, but it can be applied to non-viscous fluid inclusions by letting $\mu'=0$ or to cavities by letting K' , μ' and ρ' vanish. When the two-phase medium is a suspension of solid spheres in a non-viscous fluid matrix, the effective laws for the elastic moduli can also be used, and the effective shear modulus vanishes, except when $c = 1$, as one would have expected. But, as is shown in appendix A, the effective law relating densities is different from (2.17). We have then

$$K^* = K + \frac{(K'-K)c}{1 + \frac{(K'-K)}{K}(1-c)} \quad (2.19)$$

$$\frac{\rho - \rho^*}{\rho + 2\rho^*} = c \frac{\rho - \rho'}{\rho + 2\rho'} \quad (2.20)$$

$$\mu^* = 0$$

Equation (2.20) is not the density law one would expect from the law of conservation of mass in a two-phase medium (equation 2.17). But it must be realized that the effective law involving density is in fact a relation between inertia terms. When the matrix is a fluid, continuity of tangential displacement is not required so that there

can be relative motion between the matrix and inclusion. The net effect of this relative motion can be interpreted as an increase of the inertia of the solid inclusion (Lamb, 1932) which results in a difference between its inertial and gravitational densities. When the matrix is solid this difference does not exist because relative motion is precluded by the capability of the solid to sustain shear. Because of the dynamic nature of a wave, the density to be used in computing the effective velocity is the effective inertial density; thus

$$\alpha^* = \sqrt{\frac{K^*}{\rho_1^*}} \quad (2.21)$$

where K^* and ρ_1^* are given by equations (2.19) and (2.20). As a consequence the effective bulk modulus of a suspension of solid spheres in a fluid matrix is different if it is calculated statically or dynamically; in the static case, K^* is given by the Reuss value (1929)

$$\frac{1}{K_S^*} = \frac{c}{K'} + \frac{1-c}{K} \quad (2.22)$$

which is in fact the same equation as (2.19). But in the dynamic case K^* must be calculated from

$$K_d^* = \alpha^{*2} \rho_g^* \quad (2.23)$$

where ρ_g^* is the effective gravitational density given by (2.17); combining (2.21), (2.22) and (2.23), we find

$$K_d^* = K_s^* \frac{\rho_g^*}{\rho_i^*} \quad (2.24)$$

This result is a clear illustration of the error to which the use of static models can lead when the problem is of a dynamic nature.

2.4.3. Average effect of interactions on the effective properties.

Multiple scattering (or equivalently interactions among inclusions) is a characteristic feature of wave propagation in a two-phase medium. Its effects must be included in a model which is meant to be realistic, especially at large concentrations. However, the exact calculation of the contribution of all multiply scattered waves to the total wave at some point in the medium requires complete knowledge of the inclusion distribution function. This information is generally not available and, consequently, we can only attempt to include the multiple scattering effects in an average sense.

A method which has been used to include the interactions among inclusions in static models is the so-called "self-consistent scheme" (Budiansky, 1965; Wu, 1966), in which it is assumed that, instead of being embedded in matrix material, each inclusion is in fact surrounded by the medium with effective properties. But this assumption seems unsatisfactory because it modifies the boundary conditions on each inclusion. Therefore, we shall slightly modify it by introducing a shell of matrix material between the inclusion and the surrounding effective material. This geometry (figure 2.2) is more general since it contains the particular case of the classical self-consistent scheme, where b the radius of the matrix shell is equal to the radius a of the inclusion. In this analysis, the ratio $d = a/b$ is treated as a free parameter.

In order to obtain the effective laws, we use equation (2.9) with the assumption that the wavelength is much longer than the inclusion radius. On the left-hand side, the wave scattered by the representative sphere is given by the same expression as in the non-interaction model (equations 2.10 and 2.11). On the right-hand side, the wave scattered by an inclusion is to be evaluated. The derivation is given in appendix B; it involves no difficulty, besides algebraic manipulations. The effective density law is the same as in the non-interaction model, for any d .

$$\rho^* = \rho'c + \rho(1-c) \quad (2.25)$$

The effective bulk modulus is given by

$$\frac{K^*-K}{3K^*+4\mu^*} = \frac{c(K'-K)(3K+4\mu)}{(3K'+4\mu)(3K+4\mu^*) - 12(K'-K)(\mu^*-\mu)d^3} \quad (2.26)$$

The analytic expression for the effective shear modulus is extremely complicated; it is given in appendix B, but since the effective moduli are to be determined numerically in general, it seems more reliable to compute the effective shear modulus from the initial determinants (see appendix B).

The essential result here is that the effective moduli depend on the assumed value of the matrix shell radius b . Since this radius is unknown, it seems that the self-consistent scheme is of little help to provide a model where the interactions are taken properly into account. No value of b is a priori better than another. However, by analogy with Mackenzie (1949) and Hashin (1962) we shall favor a model where $d^3 = c$, c being the concentration. With this relationship the effective bulk modulus reduces to the non-interaction model result, but the effective shear modulus is still different. Such a result does not seem too unrealistic from a qualitative point of view. We expect the amplitudes of the multiply scattered waves to

be on the average much smaller than the incident wave. We also know that in the series expansion of the incident wave, the amplitude decreases as one goes from the first-term ($n=0$), which is used in the bulk modulus calculation, to the third term ($n=2$) which is used for the shear modulus calculation. It seems, therefore, that the major influence of the interactions should be upon the effective shear modulus. Although the "evidence" given here is rather thin we shall call this model the interaction model.

If we use the classical self-consistent scheme ($d=1$), we obtain for the effective bulk and shear moduli

$$\frac{K^*-K}{3K^*+4\mu^*} = \frac{c(K'-K)}{3K'+4\mu^*} \quad (2.27)$$

$$\frac{\mu^*-\mu}{5\mu^*(3K^*+4\mu^*)} = \frac{c(\mu'-\mu)}{6\mu'(K^*+2\mu^*)+\mu^*(9K^*+8\mu^*)}$$

The closer d is to 1, the more an inclusion "feels" the influence of the neighboring inclusions. Thus the latter model ($d=1$) is the self-consistent model where the effect of the interactions is maximized. As a consequence we may use the classical self-consistent model ($d=1$) and the non-interaction model as bounds within which any self-consistent model should fall. As an illustration, we plotted the effective P wave velocity computed with our various models for

a typical rock containing spherical inclusions of ice (figure 2.3). Mal and Knopoff's model diverges fairly rapidly as concentration increases. The difference between the two bounds constituted by the non-interaction and classical self-consistent model is quite significant at medium concentrations and it seems that our interaction model can play the role of an average.

2.5 Spheroidal inclusions.

The vector Helmholtz equation is not separable in spheroidal coordinates (Morse and Feshbach, p. 1765); therefore, when the inclusion is spheroidal we cannot expand the expressions for the amplitude of the scattered waves in series whose coefficients can be found by solving the boundary conditions as we did for spheres in appendix A. If we are to use equation 2.9 for obtaining the effective properties, we must find an alternative way of expressing the scattered waves.

The derivation outlined below is given in detail in appendix C. The displacement field due to the waves scattered by an inclusion of arbitrary shape can be written in terms of the displacement and strain inside the in-

clusion (Mal and Knopoff, 1967). When the wavelength is much larger than the inclusion size, the displacement inside can be approximated by the displacement that we would observe at the point where the inclusion is centered if the inclusion was absent. Mal and Knopoff (1967) showed that the approximation to the strain inside a spherical inclusion in terms of the incident strain is given by the same expression as that found by Eshelby (1957) in solving the static problem. By analogy we assume that we can use Eshelby's expression for spheroidal inclusions. It is then possible to express the scattered field in terms of the incident field (equation C23 in the appendix); the result depends on the orientation and shape of the spheroid.

We can now use equation (2.9) and obtain the effective properties. For the left-hand side we use Mal and Knopoff's expression for the field scattered by a sphere (equation C15) in the appendix). For evaluating the right-hand side we neglect all interactions and, therefore, assume that the field incident on each spheroid is the original incident field; we also assume that the spheroids are oblate and that their orientations are uniformly distributed over all directions to ensure quasi-isotropy. We finally obtain the effective laws

$$\frac{K^*-K}{3K^*+4\mu} = c \frac{T_{iijj}(\tilde{\alpha})}{3} \frac{(K'-K)}{3K+4\mu} \quad (2.28)$$

$$\rho^* = \rho(1-c) + \rho'c \quad (2.29)$$

$$\frac{\mu^* - \mu}{6\mu^*(K+2\mu) + \mu(9K+8\mu)} = \frac{c(\mu' - \mu)}{25\mu(3K+4\mu)} \left[T_{ijij}(\tilde{\alpha}) - \frac{T_{ijjj}(\tilde{\alpha})}{3} \right] \quad (2.30)$$

The scalars $T_{ijij}(\tilde{\alpha})$ and $T_{ijjj}(\tilde{\alpha})$ are functions of the aspect ratio $\tilde{\alpha}$ of the inclusions; they are given in appendix C.

The essential result here is that the effective elastic moduli depend not only on the concentration but also on the shape of the inclusions (i.e. aspect ratio $\tilde{\alpha}$). This conclusion is in agreement with experimental data on porous rocks (Nur and Simmons, 1969). It is important to note that our assumption of non-interaction among the spheroids is violated when the ratio $c/\tilde{\alpha}$ is larger than 1 (Solomon, 1971) since the inclusions are then overlapping, at least partially; it is even probable that the assumption is reasonable only when $c/\tilde{\alpha}$ is smaller than about 1/4. We have given the results found for spheroids having all the same aspect ratio; however, the results can be easily extended to cover the case of a discrete spectrum of aspect ratio. The concentration is then a function of $\tilde{\alpha}$ and the effective bulk modulus is given for instance by

$$\frac{K^* - K}{3K^* + 4\mu} = \frac{K' - K}{3K + 4\mu} \sum_{m=1}^M c(\tilde{\alpha}_m) \frac{1}{3} T_{ijij}(\tilde{\alpha}_m) \quad (2.31)$$

Of course, the non-interaction assumption must still be valid and it can be expressed as

$$\sum_{m=1}^M \frac{c(\tilde{\alpha}_m)}{\tilde{\alpha}_m} < 1 \quad (2.32)$$

We can compare our results (2.28) and (2.30) with those obtained by Walsh (1969) for a two-phase medium with non-interacting spheroidal inclusions. Walsh used the formulas derived by Wu (1966) for the static problem with the self-consistent scheme; for the effective bulk modulus, Wu obtained

$$K^* - K = \frac{c}{3} T_{ii jj}^*(\tilde{\alpha}) (K' - K) \quad (2.33)$$

where T^* now depends on inclusion and effective properties whereas T in (2.28) depends on inclusion and matrix properties. Walsh removed the self-consistent scheme in (2.33) by replacing T^* with T so that he obtained

$$K^* - K = \frac{c}{3} T_{ii jj}(\tilde{\alpha}) (K' - K) \quad (2.34)$$

which is different from our result (equation 2.28) although in both cases the result is supposed to represent the effective properties of the same two-phase medium. The comparison becomes more fruitful if one takes the case

of spheres. Then

$$\frac{1}{3} T_{ii jj}^* (1) = \frac{3K^* + 4\mu^*}{3K' + 4\mu^*} \quad (2.35)$$

$$\frac{1}{3} T_{ii jj} (1) = \frac{3K + 4\mu}{3K' + 4\mu} \quad (2.36)$$

If we use Walsh's procedure, and substitute (2.36) in (2.34) we obtain Mal and Knopoff's result. If we use (2.36) in our equation (2.28) we obtain the bulk modulus of the non-interaction model for spheres. Similar results hold for the effective shear modulus. The conclusion is that Walsh's results compare to ours (equations 2.28 and 2.30) in the same way Mal and Knopoff's model compares to the non-interaction model for spheres. Walsh's results are, therefore, valid only for lower concentrations of inclusions than ours, which are themselves limited to fairly low concentrations.

If we attempt now to take into account the interactions by using the classical self-consistent scheme, we obtain the following effective laws (the derivation is given in appendix C)

$$K^* - K = \frac{c}{3} T_{ii jj}^* (\tilde{\alpha}) (K' - K) \quad (2.37)$$

$$\rho^* = \rho(1-c) + \rho'c \quad (2.38)$$

$$(\mu^* - \mu) = \frac{c}{5}(\mu' - \mu) [T_{ijij}^*(\tilde{\alpha}) - \frac{1}{3}T_{iijj}^*(\tilde{\alpha})] \quad (2.39)$$

(2.37) and (2.39) are the same as those obtained by Wu (1966) in solving the corresponding static problem. They are the counterpart of (2.27) valid for spheres. They may also be considered as bounds for the effective moduli when interactions are included with a self-consistent scheme. We did not derive the analog of our interaction model for spherical inclusions in the case of oblate spheroids.

2.6 Effective attenuation of elastic waves.

So far we have only discussed the effective response of a two-phase medium to elastic waves when both phases are perfectly elastic. However, any realistic medium has some anelastic behavior, resulting in damping of the waves. When a wave propagates through a two-phase medium, the attenuation it experiences is essentially due to three processes: (i) Internal friction phenomena which constitute usually the dominant mechanism. (ii) Geometrical scattering which represents the fraction of the incident energy which is carried away by the scattered waves; this mechanism is usually important only at high frequencies. (iii) Losses due to compressibility and thermal conduction

which are usually very small and will be neglected here.

2.6.1. Geometrical scattering

The contribution of geometrical scattering to the attenuation of a plane P wave propagating through a two-phase medium with spherical inclusions has been computed by Yamakawa (1962) for the long wavelength approximation. The decay law for the amplitude is

$$A = A_0 e^{-\gamma d_0}$$

$$\text{where } \gamma = \frac{3}{4} cp(pa)^3 [2B_0^2 + \frac{2}{3}(1+2v^3)B_1^2 + \frac{(2+3v^5)}{5}B_2^2]$$

$$\text{with } B_0 = \frac{K-K'}{3K'+4\mu} \quad (2.40)$$

$$B_1 = \frac{\rho-\rho'}{3\rho}$$

$$B_2 = \frac{20}{3} \frac{\mu(\mu'-\mu)}{6\mu'(K+2\mu) + \mu(9K+8\mu)}$$

c is the volume concentration of inclusions, p is the wave number of P waves in the matrix, a is the radius of the inclusions and v is the ratio of P to S wave velocity in the matrix, d_0 is the distance.

2.6.2. Viscoelastic attenuation

For a two-phase medium consisting only of solid phases

the attenuation due to anelastic behavior can be evaluated in a straightforward manner from the effective laws for elastic media by using the correspondence principle. If the viscoelastic behavior of each phase is represented by complex moduli, the effective moduli will also be complex and the effective velocities and attenuation coefficients are given by (Bland, 1960)

$$\begin{aligned} 1/\alpha^* &= \text{Real} [\rho^*/(K^* + 4\mu^*/3)]^{1/2} \\ 1/\beta^* &= \text{Real} [\rho^*/\mu^*]^{1/2} \end{aligned} \quad (2.41)$$

$$\begin{aligned} \gamma_\alpha^* &= -\omega \text{Imag} [\rho^*/(K^* + 4\mu^*/3)]^{1/2} \\ \gamma_\beta^* &= -\omega \text{Imag} [\rho^*/\mu^*]^{1/2} \end{aligned} \quad (2.42)$$

However, the effective laws for the elastic moduli were derived with the long wavelength approximation; they can be used for the corresponding viscoelastic problem if and only if both the wavelength and the characteristic attenuation length, i.e. $1/\gamma^*$ (length over which the amplitude is reduced by e) are much larger than the inclusion size a . In particular when one of the phases is a viscous liquid, the effective viscoelastic behavior can only be obtained from the effective elastic behavior by letting the shear modulus become purely imaginary ($\mu \rightarrow i\omega\eta$) if the

shear waves in the fluid satisfy the conditions given above. This may very often not be the case, especially for low viscosity liquids.

2.6.3. Attenuation in a suspension with a viscous matrix.

Consider a suspension of elastic spheres in a fluid matrix which is elastic in compression but Newtonian viscous in shear. In such a suspension the attenuation due to matrix viscosity cannot in general be calculated by using long wavelength models and the correspondence principle, since the attenuation mechanism is the absorption of the scattered S waves in the very neighborhood of each inclusion. Epstein (1941) has calculated the attenuation due to this mechanism, in connection with his study of sound absorption in fogs. The decay law is

$$A = A_0 e^{-\gamma d_0}$$

$$\text{where } \gamma = cp(\delta-1)\text{Real} \left[\frac{i + b_0 - ib_0^2/3}{\delta - i\delta b_0 - (2+\delta)b_0^2/9} \right]$$

$$\text{with } \delta = \rho/\rho' \quad (2.43)$$

$$b_0 = (1+i)a \sqrt{\frac{\omega f \rho}{\eta}}$$

where c is concentration of inclusion, p is the wavenumber

of a P wave in the matrix, a is the inclusion radius, f is frequency, η is the matrix Newtonian viscosity, ρ and ρ' are the densities of matrix and inclusion.

2.6.4. Attenuation in fluid saturated porous rocks.

Recently geophysicists have shown interest in the anelastic behavior of solids containing a small volume of inclusions filled with a viscous liquid (Spetzler and Anderson, 1968; Walsh, 1969; Solomon, 1972); the inclusions are commonly modeled as oblate spheroids with small aspect ratios ($\tilde{\alpha} \leq 10^{-3}$). Experimental results on low porosity rocks (Nur and Simmons, 1969) indicate that the attenuation of elastic waves is very sensitive to the presence of a small volume of fluid-filled cracks. The thickness of such cracks may be less than a micron which is smaller than the wavelength and damping length of all waves. Even S waves in water at 1 MHz have characteristic lengths of about 2μ . Hence, the attenuation in such materials can be calculated with our non-interaction model (equations 2.28-2.30) for oblate spheroids modified via the correspondence principle ($\mu' \rightarrow i\omega\eta$).

On figure 2.4 we show the shear wave attenuation factor Q_{β}^{-1} calculated with our non-interaction model as a function of the product $f\eta$ (frequency \times viscosity) for different values of concentration and the aspect ratio. Aspect ratios smaller than 10^{-6} are not considered because

their thickness would be of the order of a few angstroms. Such narrow cracks can probably not be fluid-saturated in a realistic rock. The matrix is assumed perfectly elastic and its elastic moduli correspond to those of a typical rock:

$$K = \mu = 4 \times 10^{11} \text{ dynes/cm}^2$$

and the bulk modulus of the inclusion is 2.15×10^{10} dynes/cm². It is clear that the attenuation due to fluid-filled cracks can be sizeable when the product $f\eta$ is larger than 10^{+4} , which corresponds to high frequency waves (in the MHz range) when water ($\eta=1\text{cp}$) is the saturating fluid. In these cases relaxation phenomena are then the dominant sources of damping according to our model. With an adequate distribution of inclusion shapes, the Q may even be frequency independent, different frequencies being then affected by different relaxation peaks. The attenuation is proportional to $c/\tilde{\alpha}$, but it must be recalled that the validity of the model is restricted to values of $c/\tilde{\alpha}$ smaller than 1. When $f\eta$ is small, i.e. low frequencies for water-filled cracks, the relaxation phenomena due to the presence of fluid inclusions produce very little attenuation. It is known from seismic field experiments ($f \approx 100$ Hz, $Q \approx 50$) that the attenuation is not negligible (McDonal et al., 1958). It may be due to anelastic behavior of the matrix, which can roughly be modeled by letting the elastic moduli of the matrix become complex (Anderson et al,

1965). It also seems that the presence of a liquid modifies the surface properties at grain boundaries and cracks in a way to enhance attenuation, even at low frequencies (Tittman, 1972). These phenomena are at present little understood and cannot be explained with our model.

2.7 Dispersive properties of two-phase media.

All models presented in the preceding sections were derived with the assumption that the wavelength λ of the waves is much larger than the radius of the representative sphere and inclusion size. This assumption involves an approximation which corresponds mathematically to the truncation of the series expansions of the waves after the leading terms. Neither the magnitude nor the implications of this approximation has been discussed in the previous section. This question is important, not only for the sake of completeness, but also for the application of laboratory data to porous rocks in field measurements. In the laboratory frequencies are typically of the order of 1 MHz and wavelengths are probably not always much larger than the pore size. Here we examine this approximation more closely and evaluate its effects on the determination of the effective properties.

2.7.1. Magnitude of the approximation.

Consider for simplicity a solid elastic sphere isolated in a non-viscous fluid matrix. When a plane P wave of any wavelength is incident on it, we know from appendix A that we can obtain an exact solution in the form of an infinite series by satisfying the boundary conditions for $n = 0$ to ∞ where n is the summation index in the series. The far field dilation due to the scattered waves can be written as

$$\Delta = \frac{e^{i(pr-\omega t)}}{pr} \sum_{n=0}^{\infty} (-i)^{n+1} B'_n P_n(\cos \theta) \quad (2.44)$$

where p is the wave number of a P wave in the matrix, $P_n(\cos \theta)$ is the Legendre polynomial of order n and

$$B'_n = x^3 [B_{n0} + \sum_{j=2}^{\infty} B'_{nj} x^j] \quad n=0 \text{ or } 1 \quad (2.45)$$

$$B'_n = x^{2n-1} \sum_{j=2}^{\infty} B'_{nj} x^j \quad n \geq 2 \quad (2.46)$$

with $x = 2\pi a/\lambda$ (2.47)

The B'_{nj} are coefficients depending only on the inclusion and matrix properties and are obtained by solving the boundary conditions; the first few (n and j small) are given in appendix D.

In the long wavelength approximation, only the dominant terms are kept, that is the terms of order x^3 . Terms of order x^5 are neglected so that the magnitude of the approximation is of order x^2 with respect to 1. From equation (2.47) we find that this approximation implies an error of the order of 1% when $\lambda/a = 60$ and 10% when $\lambda/a = 20$.

2.7.2. Effective properties as a function of λ/a .

Consider now a suspension of equal size solid spheres in a non-viscous fluid matrix. Our method of deriving effective properties involves the estimation of the waves scattered on one hand by an individual inclusion and on the other hand by the representative sphere (equation 2.9). The radius R of the representative sphere is larger than that of an individual inclusion; thus for a fixed wavelength, the approximation involved in evaluating the effective properties by keeping only the leading terms depends essentially on the ratio λ/R and not λ/a . Hence as a first simplification let us assume that λ/a is sufficiently large so that we can use the long wavelength approximation in expressing the waves scattered by each individual inclusion. Assuming also that multiple scattering effects can be neglected, the far field dilatation due to the waves

scattered by each inclusion is

$$\Delta' = -\frac{e^{i(pr-\omega t)}}{pr} [iB_0' + B_1' \cos \theta] \quad (2.48)$$

where $B_0' = iAx^3 \frac{K-K'}{3K}$ (2.49)

$$B_1' = Ax^3 \frac{\rho-\rho'}{\rho+2\rho'} \quad (2.50)$$

The terms which are neglected are of order x^5 . The far field dilatation due to the waves scattered by the representative sphere is calculated by keeping the next higher order terms of order y_R^5 where $y_R = 2\pi R/\lambda$. We have according to appendix D.

$$\Delta^* = -\frac{e^{i(pr-\omega t)}}{pr} [iB_0^* + B_1^* \cos \theta] \quad (2.51)$$

where $B_0^* = iAy^3 \frac{K-K^*}{3K^*} \left[1 + \frac{Ky_R^2}{3K^*} - \frac{3y_R^2}{5} + \frac{(y_R^{*2} - y_R^2)K}{15(K-K^*)} \right]$ (2.52)

$$B_1^* = Ay^3 \frac{\rho-\rho^*}{\rho+2\rho^*} \left[1 + \frac{30 \rho\rho^*(y_R^2 - y_R^{*2}) + 3y_R^2(\rho^* - \rho^2)}{5(\rho-\rho^*)(\rho+2\rho^*)} \right] \quad (2.53)$$

with $y_R^* = 2\pi R/\lambda^*$, λ^* being the wavelength of a P wave in the effective material. The terms neglected are of order y_R^7 . Using again equation 2.9 for deriving the effective laws we obtain, if N is the number of inclusions in the represen-

tative sphere.

$$B_0^* = N B_0^j \quad (2.54)$$

$$B_0^* = N B_0^j$$

since all inclusions have the same radius. We can solve this system of two equations for the two unknowns ρ^* and K^* as a function of the free parameter y_R . The analytical solution is given in appendix E, but a numerical example is a more fruitful basis of discussion. Since we have data on a suspension of polystyrene spheres in water (next chapter), we apply our analysis to this two-phase medium. The two quantities to compare are the effective P wave velocity α_L^* calculated with the long wavelength approximation (equation 2.29) and the effective velocity obtained from the solution of system (2.54) by

$$\alpha^* = \sqrt{\frac{K^*}{\rho^*}} \quad (2.55)$$

The values of α^* computed for different concentrations and for different values of λ/R are given in table 2.1; α_L^* is also given for comparison. It is seen that α^* approaches α_L^* when λ/R is large, as it should be. For smaller λ/R

α^* is smaller than the long wavelength limit and the difference can become significant. When λ/R becomes small, say about 5 or 10, the various simplifications introduced for obtaining the result are not valid any more and the values of α^* are questionable. For such low values of λ/R the concept of effective properties becomes marginal because of the quasi-homogeneity assumption (cf. section 2.2). The decrease of the velocity as the wavelength becomes smaller can be interpreted as destructive interference of the scattered waves; each inclusion acts as a source and as the wavelength decreases the sources within the representative sphere become more and more out of phase. Karal and Keller (1964) and Howe (1971) obtained very similar results for media whose properties are continuous random functions of position, the fluctuations about the average properties being small. They found that the actual velocity was smaller than the average velocity. The decrease of the velocity depended on both the magnitude of the fluctuations and the length within which they were correlated.

2.7.3. The size of the representative sphere and its physical meaning.

All along the analysis we treated λ/R as a free parameter because the radius of the representative sphere is essentially unknown; we only know that it is at least larger than an inclusion radius. But if we have velocity measure-

ments in a suspension where the inclusion radius, the wavelength and the concentration are known, we can determine the relative size of the representative sphere and an inclusion; this can be done by combining our velocity data of the water-polystyrene suspension (figure 3.4) and Table 2.1. At 50% and 68% concentration the measured velocity is about 1% and 2% lower than the long wavelength limit; thus we find that λ/R is of the order of 20. Since λ/a is about 50, we conclude that R is about 3 inclusion radii. By analogy with the results of Karal and Keller (1964) and Howe (1971), R may be interpreted as a correlation length or in other words as the length over which interactions among inclusions are significant. It is therefore not too surprising that R is fairly small, since one expects only very near neighboring inclusions to interact significantly. This interpretation of the radius R of the representative sphere implies that it is a constant for a given two-phase medium which is consistent with our estimate of R from two different concentrations (table 2.1). It follows then from analysis that the velocity is a function of the frequency of the incident wave, or in other words that a two-phase medium is dispersive. This was already known qualitatively because the long-wavelength limit is different from the short-wavelength limit in which the average velocity

is given by the average sum of the travel times in each phase:

$$\frac{1}{\alpha_*} = \frac{1-c}{\alpha} + \frac{c}{\alpha'} \quad (2.56)$$

However, instead of knowing only two limiting estimates, we can now draw a tentative dispersion curve for our suspension (figure 2.5). Since the velocity is larger for $\lambda \ll a$ than for $\lambda \gg a$ and since it starts decreasing as λ/a decreases from infinity to about 50, the velocity must pass through a minimum. This minimum cannot be found precisely since our approach breaks down when the wavelength becomes too small, but it may be about $\lambda \approx a$.

For the sake of clarity in illustrating the method, we treated only the case of a suspension and we did not calculate higher order approximations. There is no additional difficulty in treating a solid-solid two-phase medium or in including more terms, except for algebraic manipulations.

Table 2.1

DEPENDENCE OF THE EFFECTIVE VELOCITY ON THE WAVELENGTH

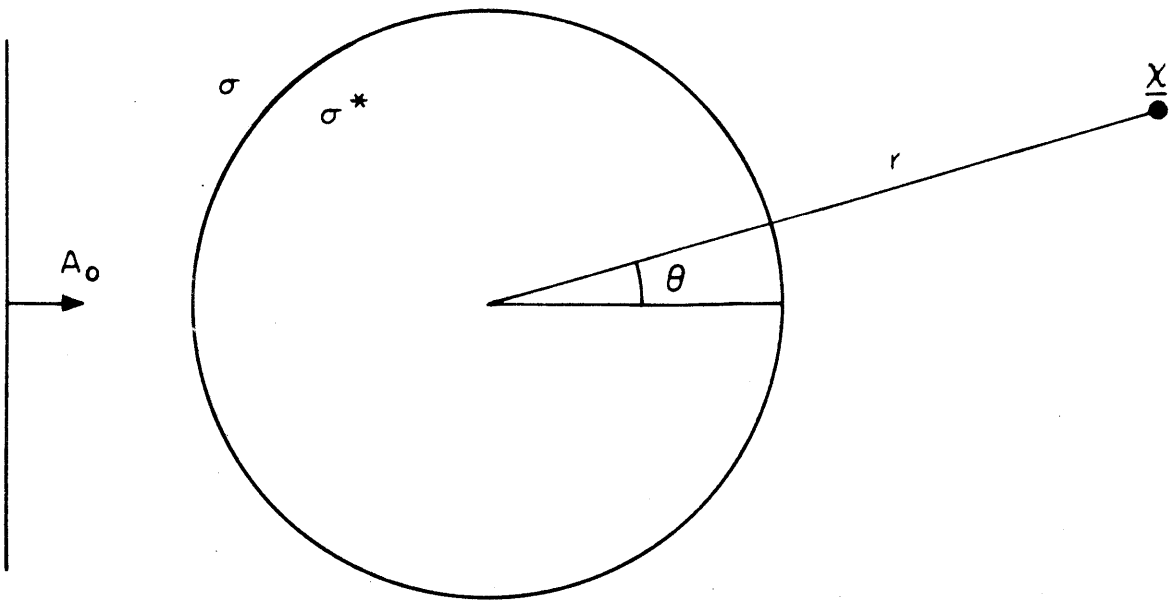
c = 50%			c = 68%		
$\alpha_L^* = 1.6373$			$\alpha_L^* = 1.7199$		
λ/R	α^* (km/s)	$\Delta\alpha^*/\alpha^*$ (%)	λ/R	α^* (km/s)	$\Delta\alpha^*/\alpha^*$ (%)
6.79	1.5373	6.3	7.52	1.5989	7.2
7.47	1.5446	5.5	9.47	1.6218	5.9
9.41	1.5643	4.6	10.43	1.6324	5.2
13.57	1.5929	2.7	15.04	1.6682	3.0
17.10	1.6066	1.9	18.95	1.6847	2.0
21.54	1.6168	1.25	23.87	1.6966	1.35
36.84	1.6297	0.46	40.82	1.7114	0.5
67.86	1.6350	0.14	75.18	1.7173	0.15
94.10	1.6361	0.08	104.26	1.7185	0.08
188.2	1.6370	0.02	208.5	1.7195	0.02
>1500	1.6373	0	>1500	1.7199	0

c is concentration of inclusions; α_L^* is the effective velocity calculated with the long wavelength approximation (Equation 2.21). α^* is the effective velocity calculated for a given ratio of the wavelength λ to the representative sphere radius R.

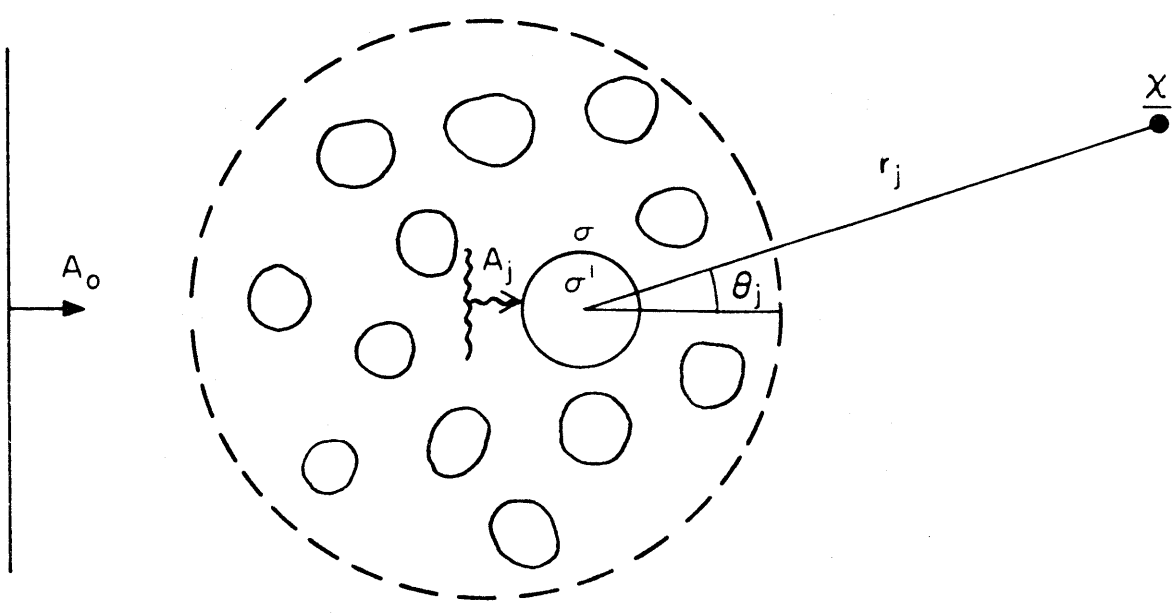
$$\Delta\alpha^* = \alpha_L^* - \alpha^*$$

FIGURE CAPTIONS

- Figure 2.1. Scattering of a plane wave by (a) the representative sphere (b) the individual inclusions. Symbols are defined in the text.
- Figure 2.2. Geometry used for the generalized self-consistent models.
- Figure 2.3. P wave velocity versus concentration in a rock containing spherical inclusions of ice. NON refers to the non-interaction model, INT refers to the interaction model ($d^3=c$), SCS refers to the classical self-consistent model ($d=1$) and MK to the model of Mal and Knopoff.
- Figure 2.4. Shear wave attenuation factor versus frequency (or viscosity) in a rock with fluid-filled penny-shaped cracks. Each relaxation peak corresponds to a different aspect ratio given at the maximum of the peak.
- Figure 2.5 Velocity versus wavelength to inclusion size ratio, water-polystyrene suspension.



(a)



(b)

FIGURE 2.1

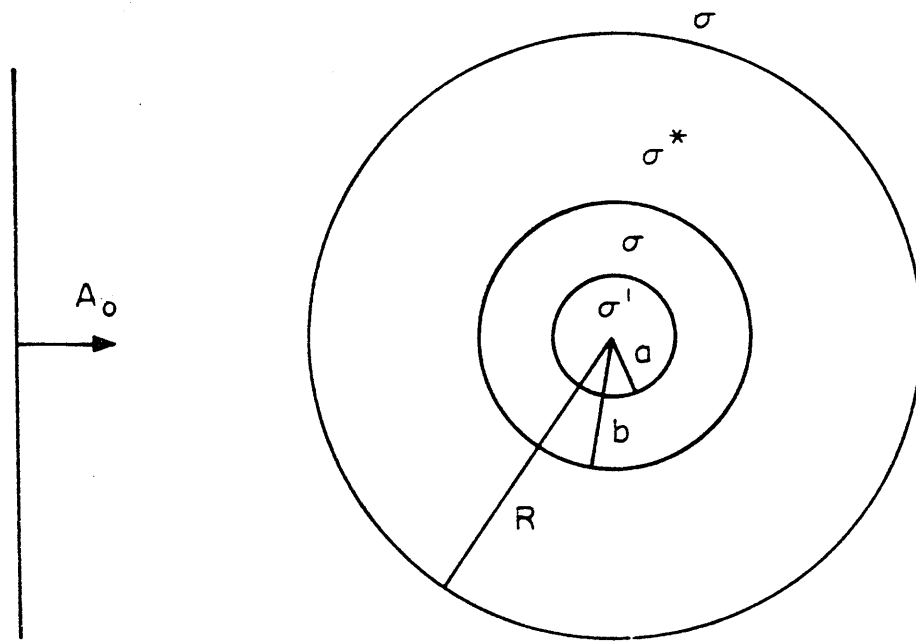


FIGURE 2.2

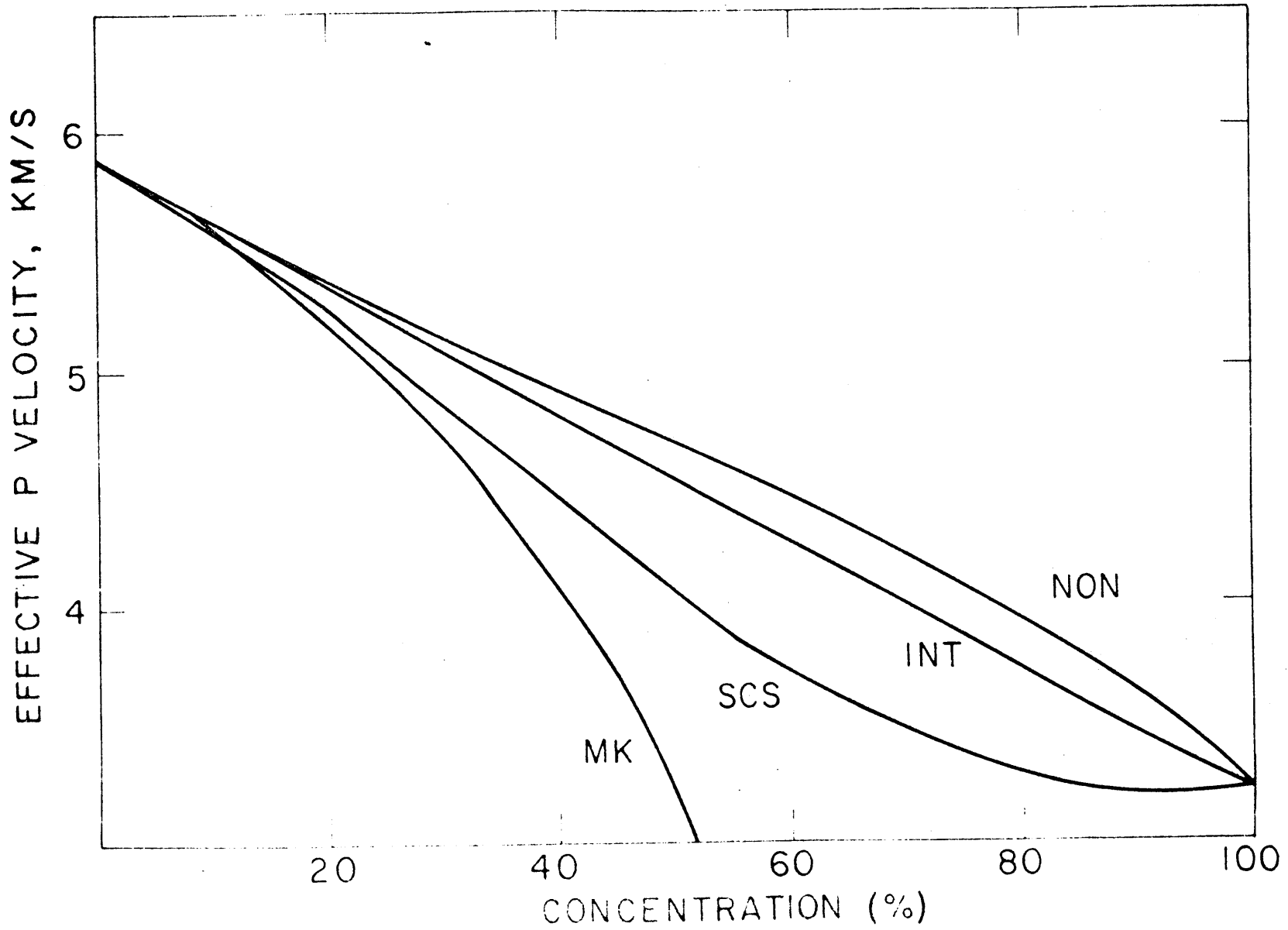


FIGURE 2.3

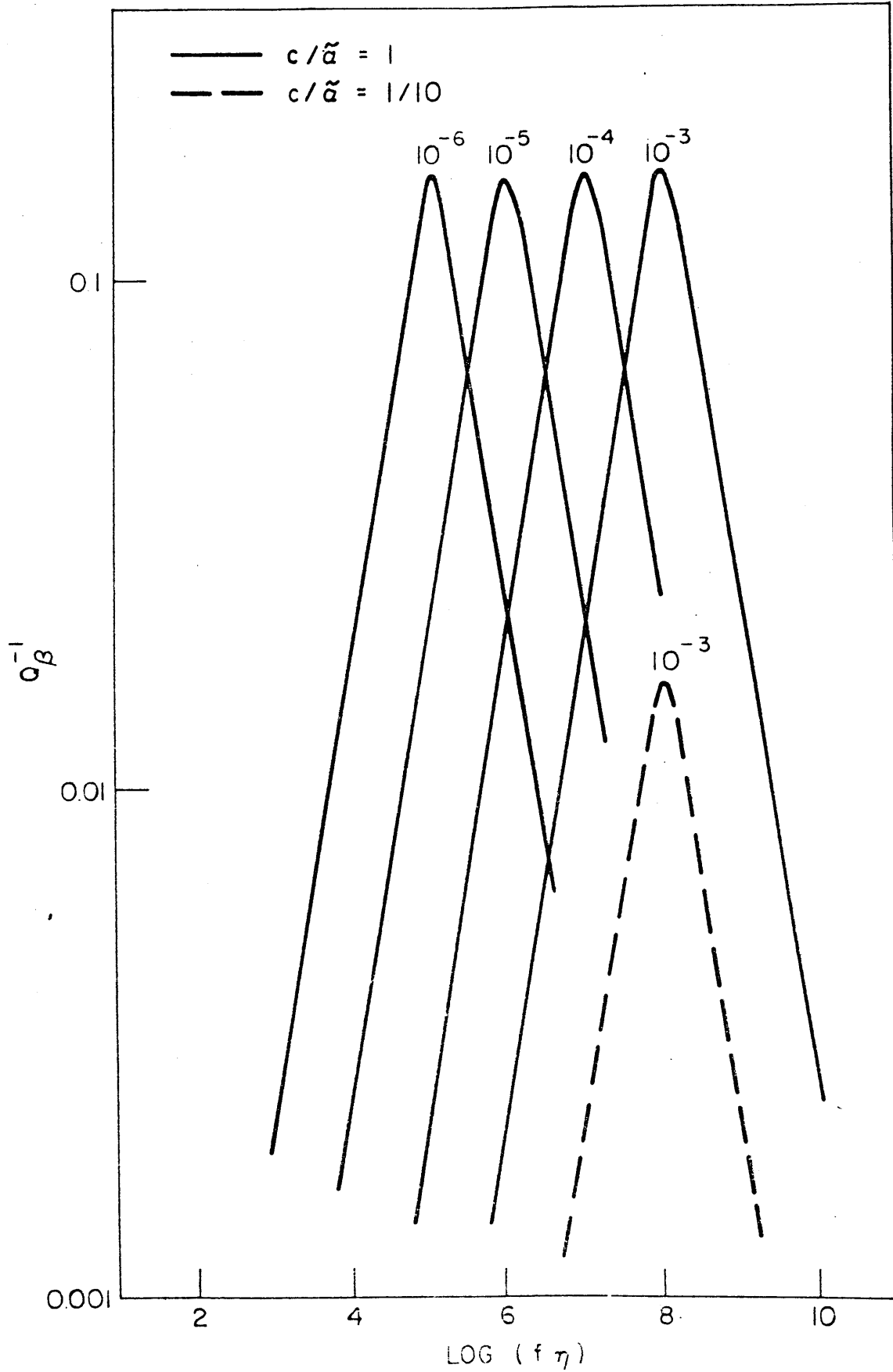


FIGURE 2.4

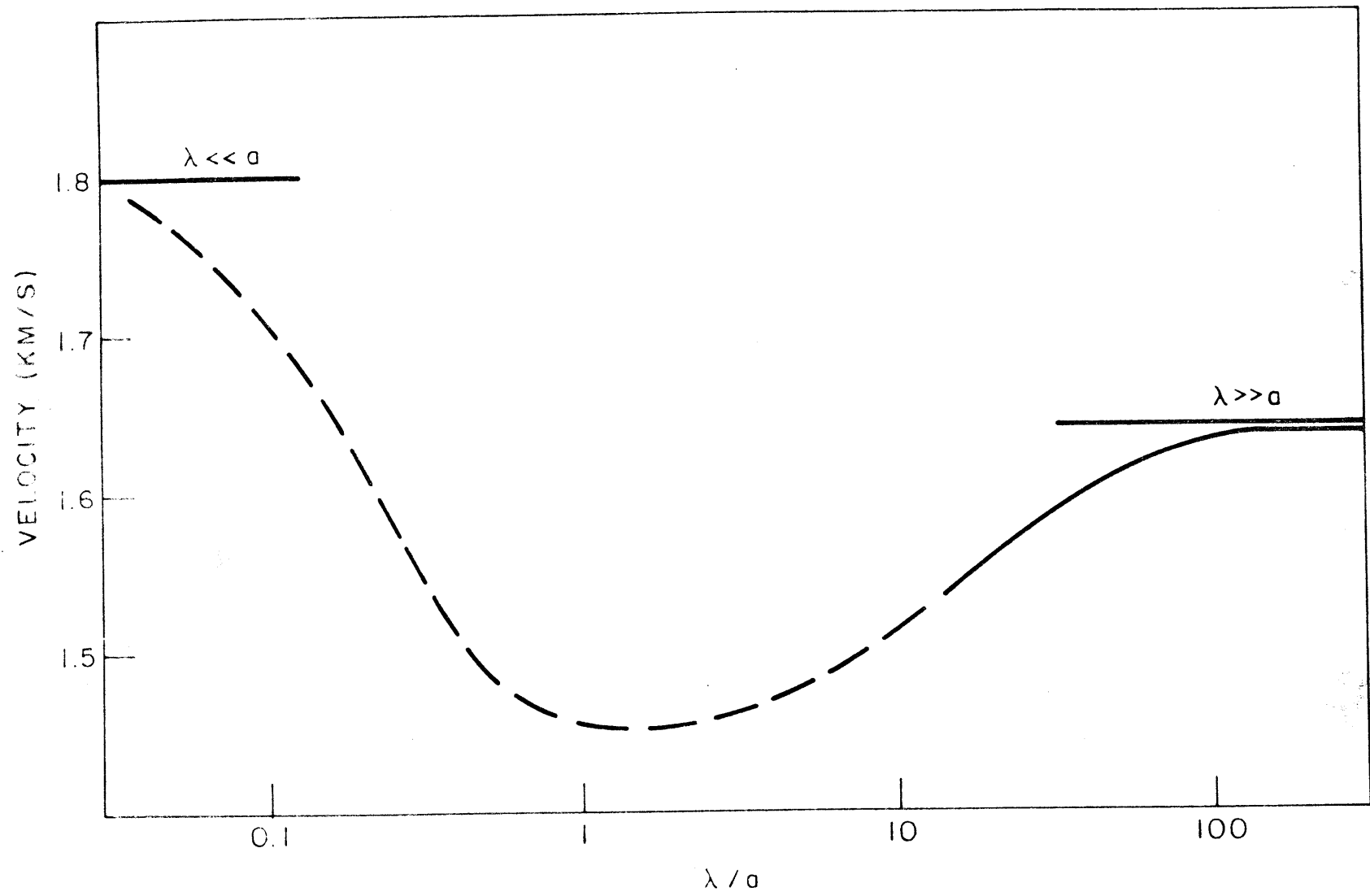


FIGURE 2.5

CHAPTER 3. EXPERIMENTAL RESULTS

Experimental data on the velocity and attenuation of elastic waves in two-phase media are widely available in the literature. Most of the experimental results have been obtained on partially or fully saturated porous rocks (Born, 1941; Wyllie et al., 1956, 1958; Shumway, 1960; Nur and Simmons, 1969) or on media where partial melting takes place (Spetzler and Anderson, 1968). These data are relevant to a variety of seismic problems. An important problem in seismic prospecting is to identify fluid saturated sedimentary layers. Also, there is increasing evidence for partial melting in the upper mantle (Anderson et al., 1965; Solomon, 1972). On the contrary experimental data on suspensions of solid inclusions in a fluid matrix are scarce, except for sound attenuation in fogs (Knudsen, 1946). In this chapter we present measurements of the compressional wave velocity and elastic quality factor in three suspensions of solid spheres in viscous matrices; the data are also compared with the values

calculated by using the theoretical models derived in the preceding chapter.

3.1. Characteristics of the suspensions.

The choice of suitable solid particles to be suspended in a fluid matrix is limited by a number of constraints if one wants to make accurate and precise measurements and compare them with theoretical results: (i) the inclusions should preferably be of spherical shape and of small size because the working frequencies are typically of the order of 200 KHz; (ii) the properties of the inclusion material should be either known or measurable. The latter condition implies that it be also available as a bulk material and not only as a powder; (iii) the densities of the matrix and inclusions must be close so that the inclusions remain in suspension for a sufficiently long period; and (iv) both materials must be chemically compatible. We used the three combinations for laboratory measurement: polystyrene beads in water (WPS), polystyrene beads in oil (OPS) and glass beads in a mixture of benzene and acetylene tetrabromide (ATBG). The physical constants of the constituents are given in Table 3.1.

The polystyrene spheres were provided by Sinclair-

Koppers Co. and soda-lime glass beads are commercially available from Potters Brothers Inc. The densities of both materials were measured in the laboratory. For soda-lime glass we adopted the elastic velocities tabulated by Press (1966). For polystyrene we measured the velocities on a disc of polystyrene provided by the manufacturer. Given the uncertainty in attenuation measurements, we simply adopted the Q values observed on Lucite (Toksoz, personal communication) as representative of polystyrene. The trade mark of the oil we used is Nujol. Its density and viscosity were measured in the laboratory at 20°C. We mixed benzene and acetylene tetrabromide in order to obtain a mixture density slightly lower than that of glass; they are perfectly miscible, but the rate of evaporation of benzene is larger than that of acetylene tetrabromide so that the density of the matrix was slowly increasing along the experiment. For this reason, the experiment was carried out in a few hours and no attenuation measurements were performed since these require a long time. The size distribution of the polystyrene spheres (figure 3.1) was obtained by passing 680g of them through a tower of 16 sieves ranging from 707 to 53 microns in opening; it can be approximated by a normal probability density function with mean 140 μ and standard deviation 30 μ . Since all glass beads were smaller than 50 μ in

radius, the knowledge of their size distribution is not crucial.

3.2. Experimental procedure.

The experimental set-up is illustrated in Figure 3.2. The suspension is contained in a ten gallon tank. The transducers are PZT-5 compressed discs. The transmitter and receiver are moveable along a rail fixed on the top of the tank and are submerged in the suspension. They are located so that all waves reflected and refracted by the tank boundaries arrive at the receiver well after the direct wave. The input signals shown on Figure 3.3 are provided by a pulse generator for velocity determinations and a tone-burst generator for amplitude measurements. The output signals also shown on figure 3.3 are displayed on an oscilloscope. A delay line incorporated in the oscilloscope is used for travel time measurements and the peak to peak amplitudes are read on the scale of the oscilloscope screen. Two electric stirrers are used to maintain the solid spheres in suspension and assure uniform concentration.

3.3. Methods of measurement.

3.3.1. Velocity.

The distance separating both transducers is determined on the rail fixed on the top of the tank and the corresponding travel time of the first peak of the received signal is read on the delay line triggered by the input signal. These measurements are repeated 20 times with different separations of the transducers, all other parameters of the suspension being held constant. A straight line is fitted to the measured values by linear regression (figure 3.4); its slope gives the velocity of the wave. The fit is usually quite good; a typical value for the standard error of estimate of the slope is 2 out of 1500. For the sake of clarity and consistency, we adopt the 90% confidence limits on the fitted slope as the error bounds on the measured velocity. They are given in tables 3.3, 3.4 and 3.5. It is necessary to correct measured values for temperature variations, since a change of a few degrees Celsius modifies the velocity by a larger amount than the error bounds. Therefore, all velocity measurements are reduced to a common temperature of 20° C. We use the tabulated values of the temperature dependence of the velocity and density of both components of the suspension and compute the dependence of the effective velocity

on temperature via our non-interaction model. The temperature corrections we thus obtained are given in table 3.2. for the WPS and OPS suspensions. No correction is needed for the ATBG suspension because all measurements were made in a few hours under a hood.

The volume concentration of inclusions is determined by the ratio of the volume of solid put into suspension to the total volume. It is known with less than 1% relative error, but it reflects the actual concentration of inclusions between the transducers only if the concentration is maintained uniform throughout the tank. There was never any evidence during the experiments that this condition was not fulfilled by our continuous stirring: we never observed beads accumulating anywhere in the tank.

3.3.2. Attenuation.

The damping characteristics of our suspensions are determined from the amplitude of sinusoidal wave packets as a function of frequency. Absolute amplitudes are difficult to use because they are strongly affected by geometric effects and response of the recording system besides anelasticity of the medium; these unwanted effects can be eliminated by use of the amplitude ratio technique. The amplitudes of an elastic wave propagating on one hand

in pure matrix material (subscript m) and on the other hand in a suspension of concentration c (subscript s) can be written as functions of frequency f

$$A_m(f) = G_m(\tilde{x}) T_m(f) e^{-\tilde{\gamma}_m(f)\tilde{x}} e^{i(2\pi ft - k_m\tilde{x})}$$

$$A_s(f) = G_s(\tilde{x}) T_s(f) e^{-\tilde{\gamma}_s(f)\tilde{x}} e^{i(2\pi ft - k_s\tilde{x})}$$
(3.1)

where \tilde{x} is the distance between the transducers and k the wave number, G is a factor depending only upon geometry, T is the frequency response of the recording system and $\gamma(f)$ is the attenuation factor. If the geometry and recording system are kept the same for both measurements, we obtain

$$\ln \left| \frac{A_s}{A_m} \right| = \tilde{x} [\tilde{\gamma}_m(f) - \tilde{\gamma}_s(f)]$$
(3.2)

For a wide variety of materials $\tilde{\gamma}$ is approximately a linear function of frequency (Knopoff, 1964). This is certainly not the case for suspensions over a broad frequency range. For geometrical scattering alone, $\tilde{\gamma}$ is proportional to the fourth power of frequency (equation 2.40). However, our data indicate that we can use the linear approximation at least over some frequency range (200 to 450 KHz). Then we have

$$\tilde{\gamma}(f) = \gamma f + \delta \quad (3.3)$$

where γ and δ do not depend on frequency; γ is called the attenuation coefficient and is related to the quality factor Q by

$$\gamma = \frac{\pi}{Qv} \quad (3.4)$$

where v is the wave velocity. Combining (3.2) and (3.3) we obtain

$$\ln \left| \frac{A_s}{A_m} \right| = (\gamma_m - \gamma_s) f \tilde{x} + (\delta_m - \delta_s) \tilde{x} \quad (3.5)$$

If the geometry is known, the relative Q of a suspension with respect to the Q of pure matrix can be determined from the slope of a line fitted to the logarithm of the amplitude ratio versus frequency. This is the procedure we follow. The amplitudes that we use are those of the second cycle in the sinusoidal wave packets (see arrows on figure 3.3) for frequencies increasing from 100 to 480 KHz in steps of 20 KHz. They are also corrected for the variation of the amplitude of the same cycle in the input signal. No amplitude measurements were made on the ATBG suspension because of the short amount of time we had

because of the fast evaporation of benzene.

3.4. Experimental results.

3.4.1. Velocity

The velocities measured in our three suspensions at various concentrations are given in Table 3.3, 3.4 and 3.5. The normalized effective velocity α_N , that is the ratio of the effective velocity at concentration c to the velocity of the matrix, is plotted versus concentration on figures 3.5, 3.6 and 3.7. On these plots we also indicate the effective velocities calculated with Mal and Knopoff's model where $\mu = 0$ (equations 2.1, 2.4 and 2.5) and our model (equations 2.19, 2.20 and 2.21).

In all cases both models are in good agreement with our data at low concentrations. It is clear, especially with the ATBG suspension, that our interaction model comes closest to the measured velocities at large concentrations. Nevertheless the velocities computed with our model fall consistently above the data; in the WPS suspension at 50% and 68% concentration the discrepancy is of the order of 1% and 2% which is significantly larger than the errors of measurement. Because of its consistency it is unlikely that the difference could be attributed to a miscalculation of

the actual concentration between the transducers. For the ATBG suspension it may be due to a slight discrepancy between the actual properties of the glass we used and the tabulated values, but such a reason cannot be invoked for the other two suspensions since we measured the polystyrene velocities with great care in order to assure sufficient accuracy and precision.

The difference between the observed and calculated velocities can be explained in terms of the dispersive effects due to a finite wavelength to inclusion size ratio. The wavelength of the wave is of the order of 7mm, or about fifty inclusion radii, in both the WPS and OPS suspensions. It was shown in the previous chapter that under such conditions significant bias can result from the use of models based on the long wavelength approximation; the model we used for comparison with the data contains this approximation. Recalling the results of chapter two, we know that for our suspensions the long wavelength velocity is larger than the velocity of a wave which does not satisfy the long wavelength approximation. The sign of the predicted dispersive effect is the same as the observed one. However, the magnitude of the dispersive effect cannot be predicted because it depends on the unknown radius of the representative sphere which is in fact the length over which interactions are significant. Alternatively we can use

our data for estimating this effective interaction distance. It was found in chapter two that it is of the order of three inclusion radii, indicating, as could be expected, that interaction is significant only between very near neighbors. It is also consistent with the better agreement between the long wavelength model and the data at low concentrations where the separation of the inclusions is larger than the effective interaction distance. In summary our velocity data clearly illustrate the practical interest of our theoretical formulation of the problem and the improvement it constitutes over previous models, all limited to the long wavelength approximation.

3.4.2. Attenuation.

On figure 3.8 we show the amplitude ratios measured on the OPS suspension at 5%, 20%, 40%, 50% and 62% concentration, and on the WPS suspension at 68% concentration. They illustrate that the assumption of a linear decay is not valid over the full frequency range; in particular there seems to be a systematic increase at low frequencies, most obvious on the OPS suspension at 40%. No explanation could be found for this behavior. But for the largest concentrations where the attenuation is most significant, and thus the data most reliable, the plots exhibit the expected variation fairly well. The second conclusion one can draw from figure 3.8 is that the attenuation becomes significantly different from that in pure matrix only for large

concentrations ($c > 40\%$). The values of Q obtained from the fit of a linear law to the data over a limited frequency band are given in Table 3.6 for $c > 40\%$. At smaller concentrations the stability and precision of the fitted Q is very poor, because the slope which is proportional to Q^{-1} is small. Comparison of the data on both suspension at concentrations around 65% shows that the viscosity of the matrix is not a negligible parameter, even when the filling solid is a highly attenuating medium.

The theoretical Q values of our suspensions are computed by taking into account the three major sources of attenuation: the geometrical scattering, the viscosity of the matrix and the anelasticity of polystyrene. The contribution of the geometrical scattering is evaluated with equation (2.40) where the inclusions are assumed perfectly elastic and the matrix non-viscous. The contribution of the matrix viscosity is obtained from equation (2.43) and the attenuation due to polystyrene anelasticity is calculated with equations (2.42) and (2.19) by letting the inclusion bulk modulus be complex (Table 3.1). The part of the total attenuation stemming from each mechanism is given in Table 3.7 for various frequencies; it is clear that the theoretical Q is slightly frequency dependent, but for the sake of comparison with the observations we adopt an

average Q over the band of interest. It also illustrates well the strong frequency dependence of the geometrical scattering effects and the importance of the viscosity of the matrix. The Q computed with Mal and Knopoff's model is also given in table 3.7, but it only reflects the attenuation due to polystyrene anelasticity.

The comparison of the computed with the observed Q values is satisfactory (table 3.6), given the large uncertainty of attenuation measurements. The reasonable agreement indicates that we took into account the major sources of attenuation in our calculation. If we had neglected the contributions of geometrical scattering and matrix viscosity, the calculated Q in the OPS suspension at 62% would have been 153 instead of 87, and thus about twice as large as the observed Q . It is to be noted that the attenuation due to either matrix viscosity or geometrical scattering cannot be evaluated with a long wavelength model modified via the correspondance principle, since the wavelengths of S waves in the fluid are smaller than the inclusion radius. Our attenuation data constitute thus another example of the errors which the use of static models can lead to.

Table 3.1
 PHYSICAL CONSTANTS OF THE MATERIALS USED
 IN THE EXPERIMENTS

	<u>Water</u>	<u>Oil</u>	<u>ATB</u>	<u>Polystyrene</u>	<u>Glass</u>
ρ (g/cm ³)	0.9982	0.8794	2.365	1.045	2.405
α (km/s)	1.4632	1.4554	1.025	2.334	6.790
β (km/s)				1.163	3.265
Q_α				55	
Q_β				40	
K (10 ¹⁰ dynes/cm ²)	2.137	1.863	2.485	3.808	76.71
K' (10 ¹⁰ dynes/cm ²)				0.056	
μ (10 ¹⁰ dynes/cm ²)				1.413	25.64
μ' (10 ¹⁰ dynes/cm ²)				0.035	
η (poise)	0.01	1.8			

All values are valid at a temperature of 20°C. ρ is density, α and β are P and S wave velocity, Q_α and Q_β are P and S wave attenuation factors; K and μ are the real parts of the bulk and shear moduli, whereas K' and μ' are the imaginary parts; η is Newtonian viscosity. ATB refers to the mixture of acetylene tetrabromide and benzene.

Table 3.2

TEMPERATURE CORRECTION

	Water	Oil	Polystyrene
$\frac{\partial \rho}{\partial T} (\text{g/cm}^3 \text{ } ^\circ\text{C})$	$-2 \cdot 10^{-4}$ (i)	$-4.9 \cdot 10^{-4}$ (ii)	$-2.65 \cdot 10^{-4}$ (iii)
$\frac{\partial \alpha}{\partial T} (\text{m/s } ^\circ\text{C})$	2.4 (i)	-3.0 (ii)	
$\frac{1}{K} \frac{\partial K}{\partial T} (^\circ\text{C}^{-1})$	$30 \cdot 10^{-4}$ (iv)	$-47 \cdot 10^{-4}$ (iv)	0 (assumed)

- (i) Weast (1971)
(ii) measured in the laboratory
(iii) Rudd (1965)
(iv) calculated from $\partial \rho / \partial T$ and $\partial \alpha / \partial T$

c (%)	WPS	OPS
	$\frac{\partial \alpha^*}{\partial T} (\text{m/s } ^\circ\text{C})$	$\frac{\partial \alpha^*}{\partial T} (\text{m/s } ^\circ\text{C})$
10	2.27	-2.90
20	2.18	-2.78
30	2.06	-2.64
40	1.94	-2.44
50	1.77	-2.23
60	1.59	-1.95
70	1.34	-1.59

$\partial \alpha^* / \partial T$ is the variation of the effective compressional velocity with temperature at a concentration c . It is calculated with equation (2.21) and the values of $\partial \rho / \partial T$ and $\partial \alpha / \partial T$.

Table 3.3

MEASURED VELOCITIES IN THE WATER-POLYSTYRENE SUSPENSION

c (%)	α^* (km/s)	$\Delta\alpha^*$ (m/s)	α_N	$\Delta\alpha_N$ (10^{-3})
0	1.4632	0.5	1.0	0.4
0.66	1.4644	2.5	1.0008	2.0
	1.4670	2.2	1.0026	1.8
1.75	1.4648	2.5	1.0011	2.0
	1.4689	1.9	1.0039	1.6
	1.4676	2.6	1.0030	2.1
	1.4676	1.4	1.0030	1.3
2.78	1.4726	1.7	1.0064	1.5
	1.4726	2.2	1.0064	1.8
3.65	1.4723	1.4	1.0062	1.3
	1.4731	1.7	1.0068	1.5
	1.4759	2.4	1.0087	1.9
	1.4745	2.0	1.0077	1.7
5.07	1.4810	1.5	1.0122	1.3
	1.4817	1.1	1.0126	1.1
5.13	1.4797	1.1	1.0113	1.1
	1.4784	0.9	1.0104	0.9
6.16	1.4850	1.2	1.0149	1.1
	1.4838	1.2	1.0141	1.1
6.76	1.4869	3.7	1.0162	2.8

c (%)	α^* (km/s)	$\Delta\alpha^*$ (m/s)	α_N	$\Delta\alpha_N$ (10^{-3})
6.76	1.4887	0.7	1.0174	0.8
7.91	1.4888	0.9	1.0175	0.9
	1.4886	0.7	1.0174	0.8
8.76	1.4912	1.9	1.0191	1.6
	1.4894	0.8	1.0179	0.9
9.64	1.4923	2.9	1.0199	2.3
	1.4939	1.2	1.0210	1.1
	1.4903	1.3	1.0185	1.2
10.1	1.4929	2.8	1.0203	2.2
	1.4943	0.8	1.0213	0.9
	1.4986	0.9	1.0242	0.9
11.7	1.4959	0.8	1.0223	0.9
13.1	1.5044	0.9	1.0282	0.9
14.6	1.5090	2.4	1.0313	1.9
	1.5103	2.3	1.0322	1.9
15.7	1.5109	3.3	1.0326	2.5
	1.5116	3.2	1.0331	2.5
17.6	1.5146	3.3	1.0351	2.5
	1.5198	2.7	1.0387	2.1
	1.5151	1.3	1.0355	1.2
	1.5128	1.3	1.0339	1.2
19.5	1.5247	1.7	1.0420	1.5
	1.5210	1.3	1.0395	1.2

c (%)	α^* (km/s)	$\Delta\alpha^*$ (m/s)	α_N	$\Delta\alpha_N$ (10^{-3})
21.7	1.5254	1.3	1.0425	1.2
	1.5261	3.3	1.0430	2.5
	1.5283	2.1	1.0445	1.7
23.5	1.5362	4.7	1.0499	3.5
	1.5377	3.3	1.0509	2.5
25.1	1.5410	1.7	1.0532	1.5
	1.5429	2.4	1.0545	1.9
26.6	1.5510	4.7	1.0600	3.5
	1.5457	1.3	1.0564	1.2
28.0	1.5529	3.9	1.0613	2.9
	1.5519	2.7	1.0606	2.1
29.9	1.5606	2.4	1.0666	1.9
	1.5573	1.9	1.0643	1.6
32.2	1.5618	2.5	1.0674	2.0
	1.5653	2.4	1.0698	1.9
33.9	1.5671	5.2	1.0710	3.7
	1.5699	2.8	1.0729	2.2
38.1	1.5791	1.6	1.0792	1.4
	1.5786	1.7	1.0789	1.5
	1.5790	1.7	1.0792	1.5
	1.5816	1.1	1.0809	1.1
41.0	1.5953	3.9	1.0903	2.9
	1.5934	1.3	1.0890	1.2

c (%)	α^* (km/s)	$\Delta\alpha^*$ (m/s)	α_N	$\Delta\alpha_N$ (10^{-3})
45.0	1.6095	2.2	1.1000	1.8
	1.6072	2.2	1.0984	1.8
48.4	1.6157	1.3	1.1042	1.2
	1.6164	1.5	1.1047	1.3
51.6	1.6303	1.6	1.1142	1.4
	1.6293	1.3	1.1135	1.2
56.2	1.6540	3.5	1.1304	2.7
	1.6452	3.2	1.1244	2.5
68.0	1.6912	1.2	1.1558	1.1
	1.7038	1.7	1.1644	1.5

c is the volume concentration of inclusions

α^* is the effective compressional wave velocity in the suspension

$\Delta\alpha^*$ is the 90% confidence limit on α^*

α_N is the normalized effective compressional wave velocity

$\Delta\alpha_N$ is the 90% confidence limit on α

Note: the same notation is used in tables 3.4 and 3.5

Table 3.4

MEASURED VELOCITIES IN THE OIL-POLYSTYRENE SUSPENSION

c (%)	α^* (km/s)	$\Delta\alpha^*$ (m/s)	α_N	$\frac{\Delta\alpha_N}{\alpha_N}$ (10^{-3})
0	1.4554	0.5	1.0	0.4
5.2	1.4646	2.7	1.0063	2.3
	1.4653	1.5	1.0068	1.4
	1.4683	0.8	1.0089	1.0
	1.4650	2.9	1.0066	2.4
	1.4708	1.7	1.0106	1.6
	1.4780	1.3	1.0155	1.3
10.0	1.4774	1.3	1.0151	1.3
	1.4902	1.2	1.0239	1.2
14.6	1.4898	1.7	1.0236	1.6
	1.4989	1.2	1.0299	1.2
19.8	1.5012	1.5	1.0315	1.4
	1.5246	1.7	1.0475	1.6
30.0	1.5259	1.6	1.0484	1.5
	1.5666	1.1	1.0764	1.2
39.6	1.5664	1.5	1.0763	1.4
	1.5988	1.3	1.0985	1.3
51.6	1.5995	1.6	1.0990	1.5
	1.6590	1.7	1.1399	1.6
62.7	1.6579	1.3	1.1391	1.3

Note: symbols are defined in table 3.3

Table 3.5

MEASURED VELOCITIES IN THE ATBG SUSPENSION

<u>c (%)</u>	<u>α^* (km/s)</u>	<u>$\Delta\alpha^*$ (m/s)</u>	<u>α_N</u>	<u>$\Delta\alpha_N (10^{-3})$</u>
0	1.025	1	1.0	1
10.2	1.073	1	1.047	2
	1.974	2	1.048	3
14.9	1.092	2	1.075	3
21.6	1.141	2	1.113	3
	1.141	2	1.113	3
28.6	1.189	1	1.160	2
	1.191	2	1.162	3
35.0	1.234	3	1.204	4
	1.238	2	1.208	3
43.0	1.315	2	1.283	3
	1.318	1	1.286	2

Note: symbols are defined in Table 3.3.

Table 3.6

OBSERVED AND CALCULATED Q IN WPS AND OPS SUSPENSIONS

	Concentration(%)	Q _{calculated}	Q _{observed}	Frequency Band (kHz)
OPS	40	155	230	240-440
OPS	50	115	150	200-440
OPS	62	87	80	160-440
WPS	68	112	160	200-440

Table 3.7

CONTRIBUTION OF DIFFERENT MECHANISMS TO THE TOTAL ATTENUATION FACTOR γ

	Frequency (KHz)	Geometrical Scattering (10^{-9} s/cm)	Matrix Viscosity (10^{-9} s/cm)	Polystyrene Anelasticity (10^{-9} s/cm)	Total (10^{-9} s/cm)	Q	Q_{MK}
OPS c=62%	100	1	100	124	225	84	280
	200	4	78	124	206	92	280
	300	14	66	124	204	93	280
	400	34	59	124	217	87	280
	480	59	54	124	237	80	280
WPS c=68%	100	0	1	147	149	124	224
	200	3	1	147	152	121	224
	300	11	0	147	159	116	224
	400	26	0	147	174	106	224
	480	45	0	147	193	96	224

c is concentration of inclusions

Q is related to the total attenuation factor γ by $Q = \pi/v\gamma$, where v is the wave velocity

Q_{MK} is the quality factor computed with the model of Mal and Knopoff.

FIGURE CAPTIONS

- Figure 3.1 Distribution of the radius (in microns) of the polystyrene beads.
- Figure 3.2 Experimental set-up.
- Figure 3.3 A. Input signal, pulse generator. B. Input signal, tone-burst generator. C. Output signal, pulse generator. D. Output signal, tone-burst generator. Vertical scale is arbitrary.
- Figure 3.4 Distance between the transducers versus travel time of the wave. Data and fitted line.
- Figure 3.5 Normalized effective velocity versus concentration, WPS suspension. INT refers to our model for a fluid matrix (equation 2.21) and MK refers to the model of Mal and Knopoff.
- Figure 3.6 Normalized effective velocity versus concentration, OPS suspension. INT and MK are defined in figure 3.5.
- Figure 3.7 Normalized effective velocity versus concentration, ATBG suspension. INT and MK are defined in figure 3.5
- Figure 3.8 Amplitude ratios versus frequency, WPS and OPS suspensions. Data and fitted lines.

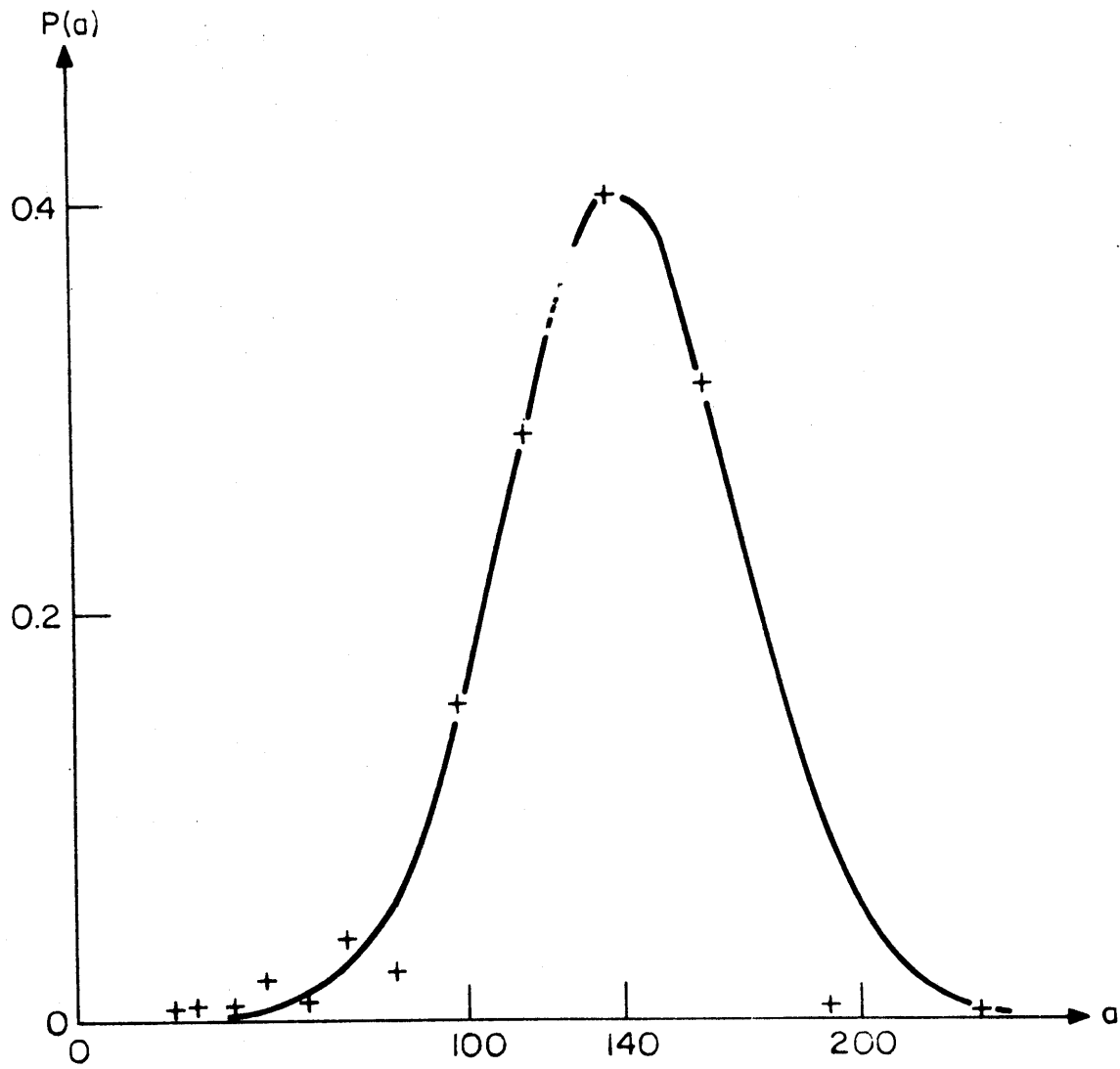


FIGURE 3.1

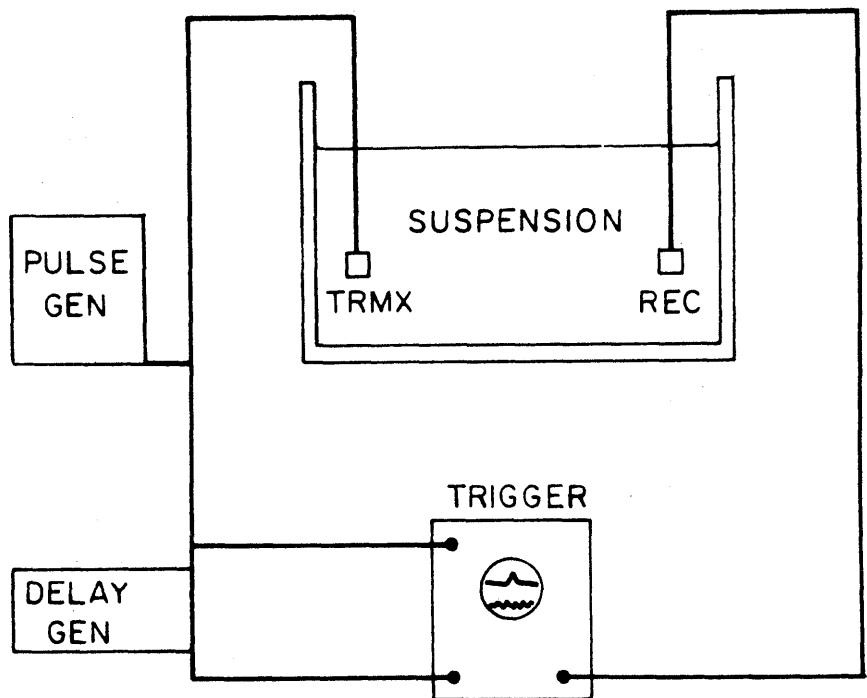


FIGURE 3.2

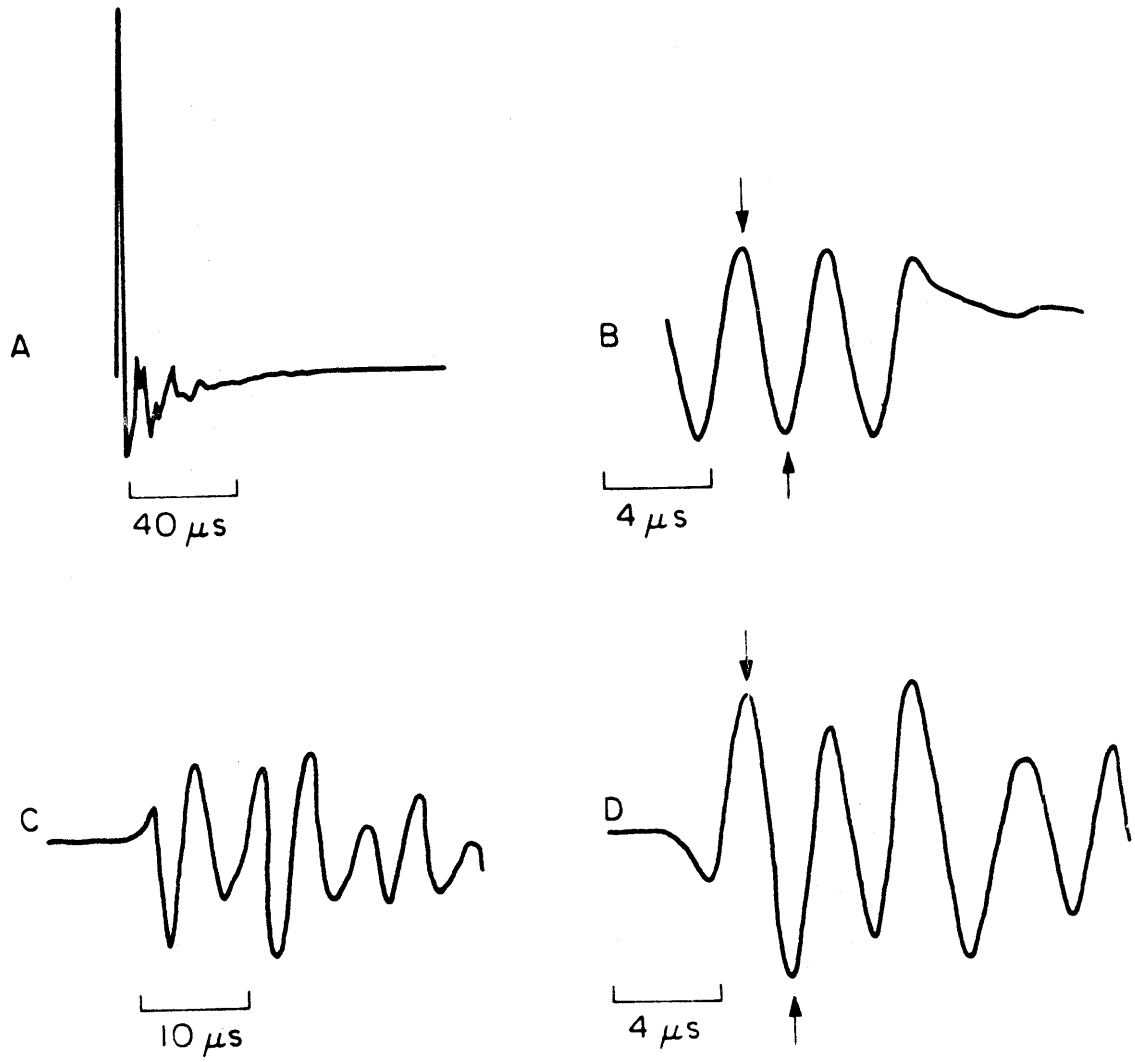


FIGURE 3.3

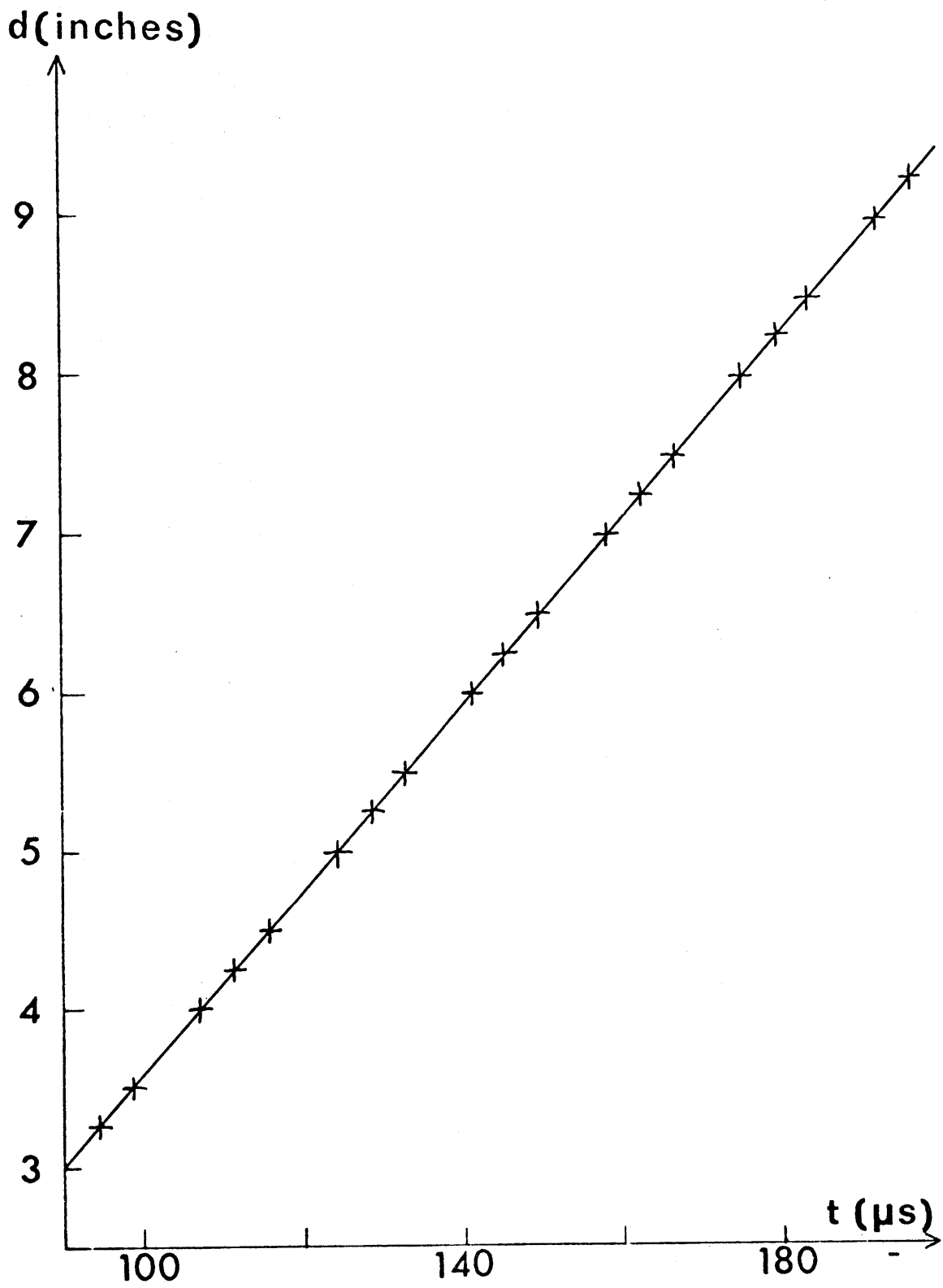


FIGURE 3.4

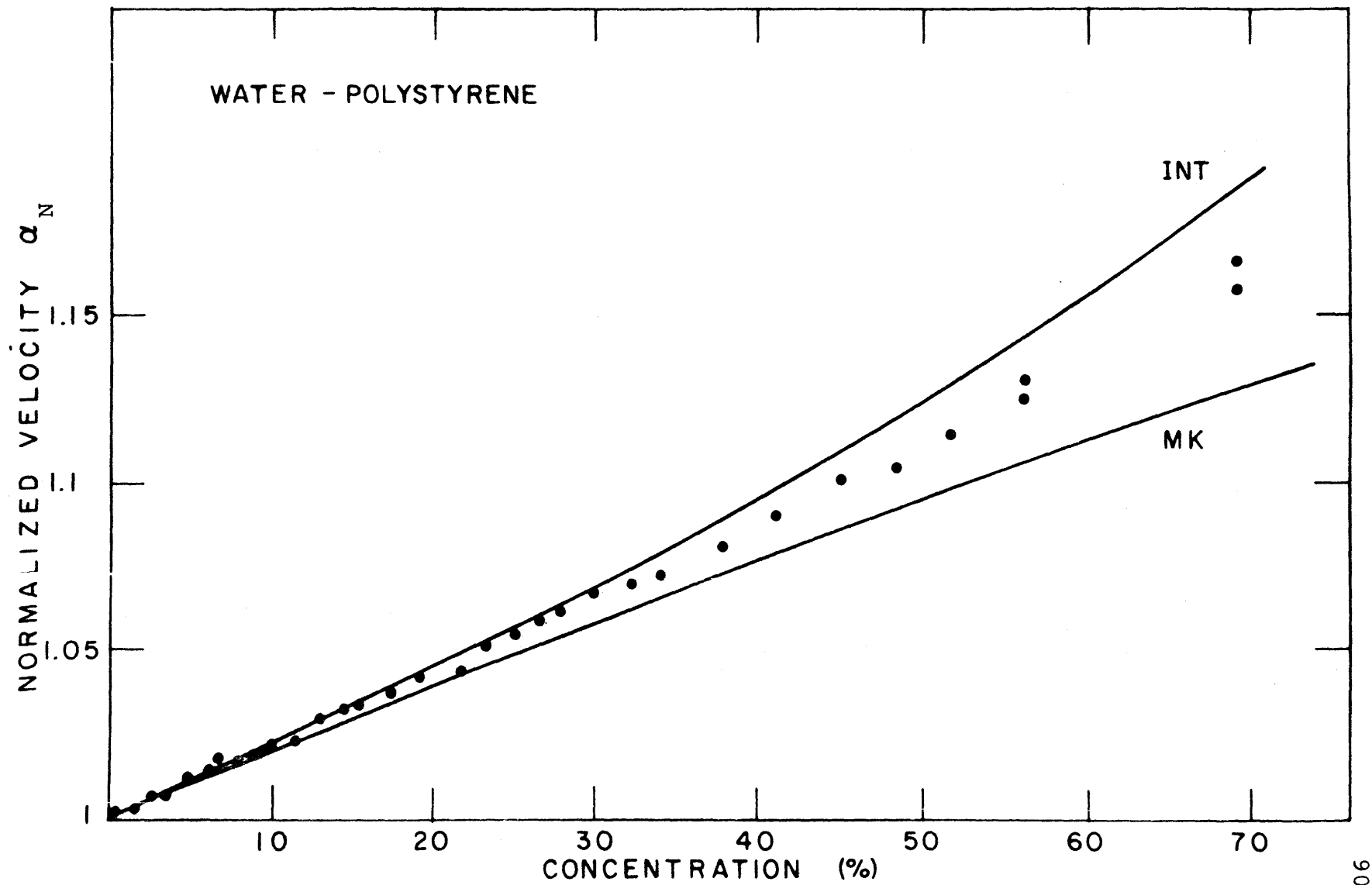


FIGURE 3.5

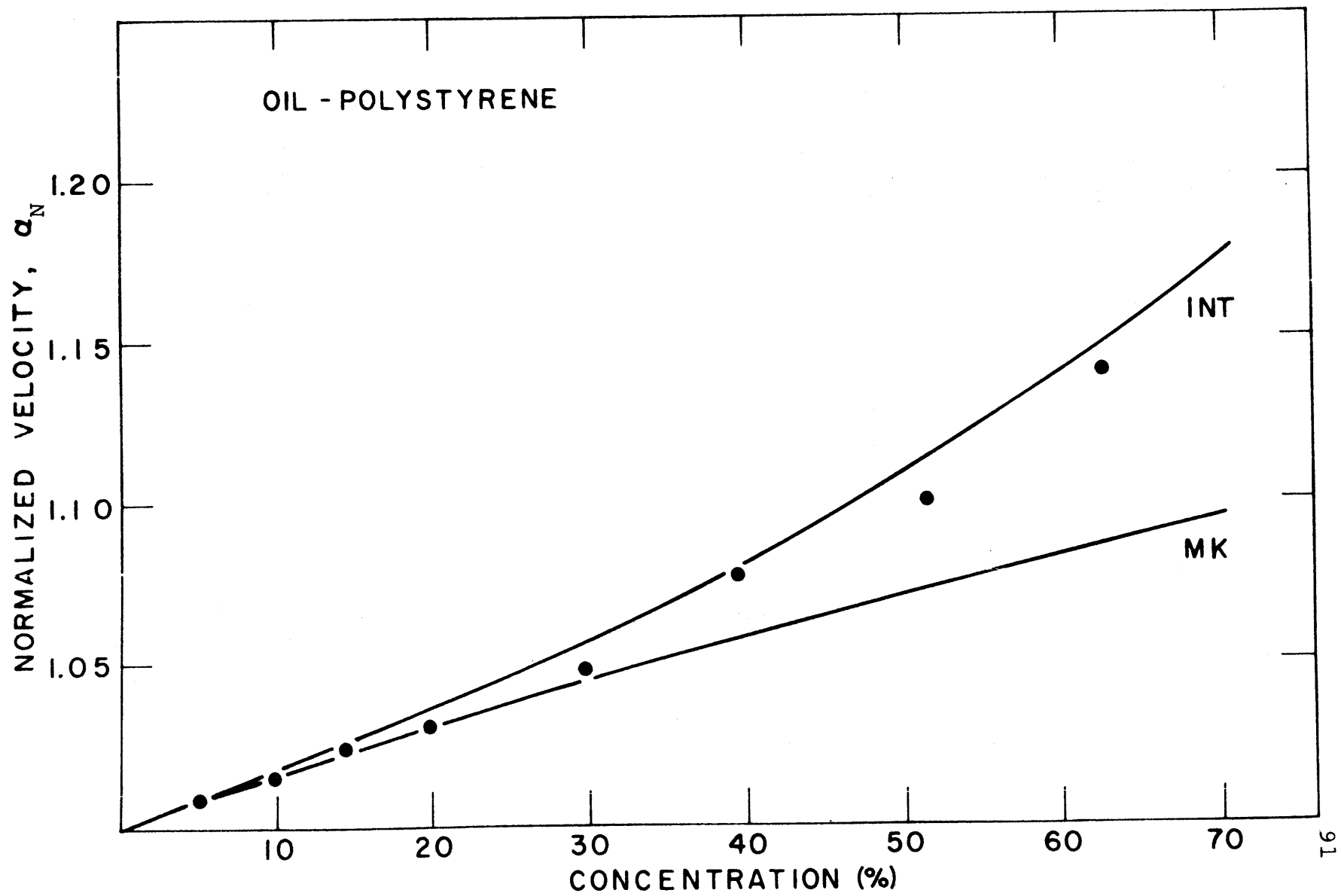


FIGURE 3.6

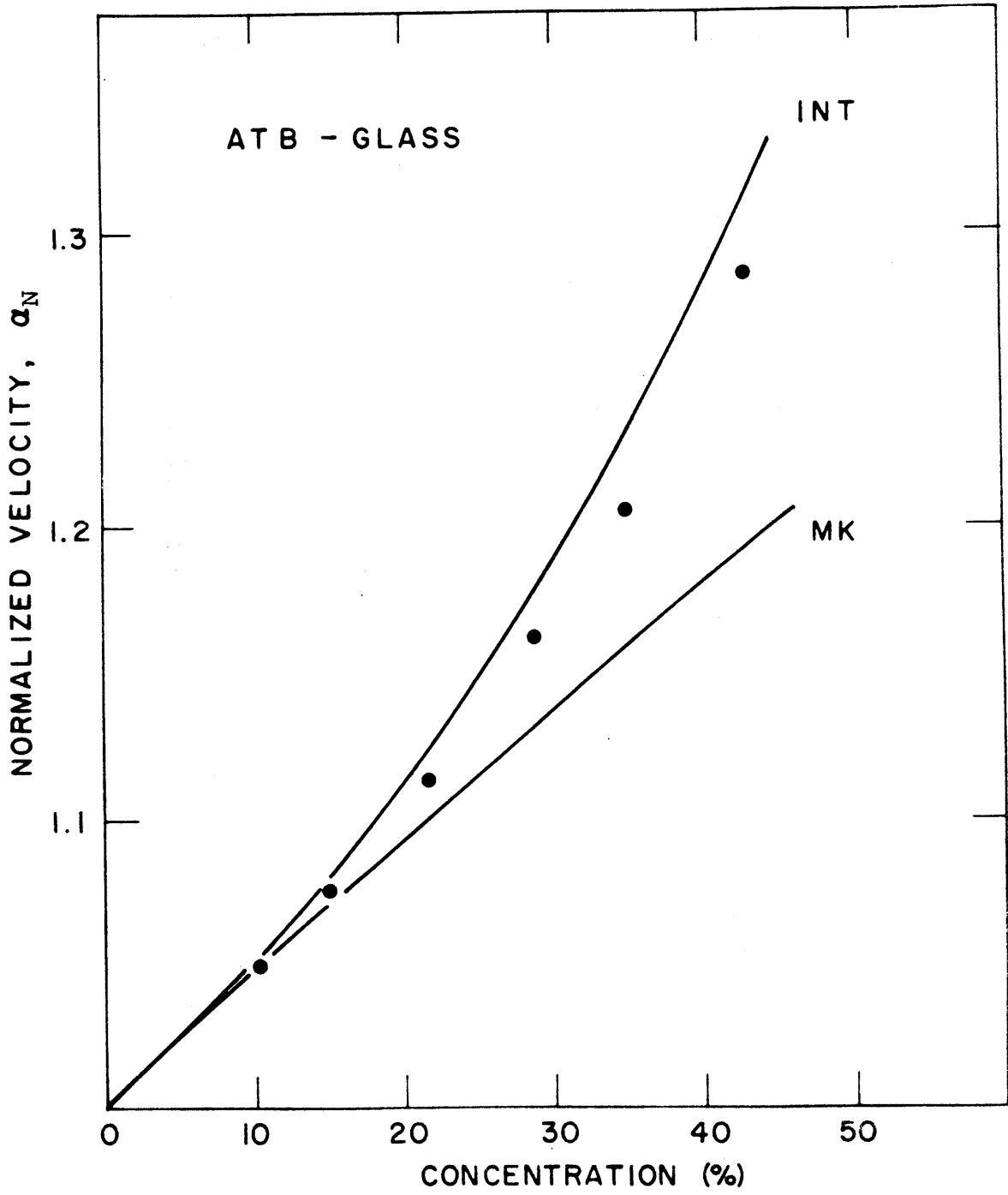


FIGURE 3.7

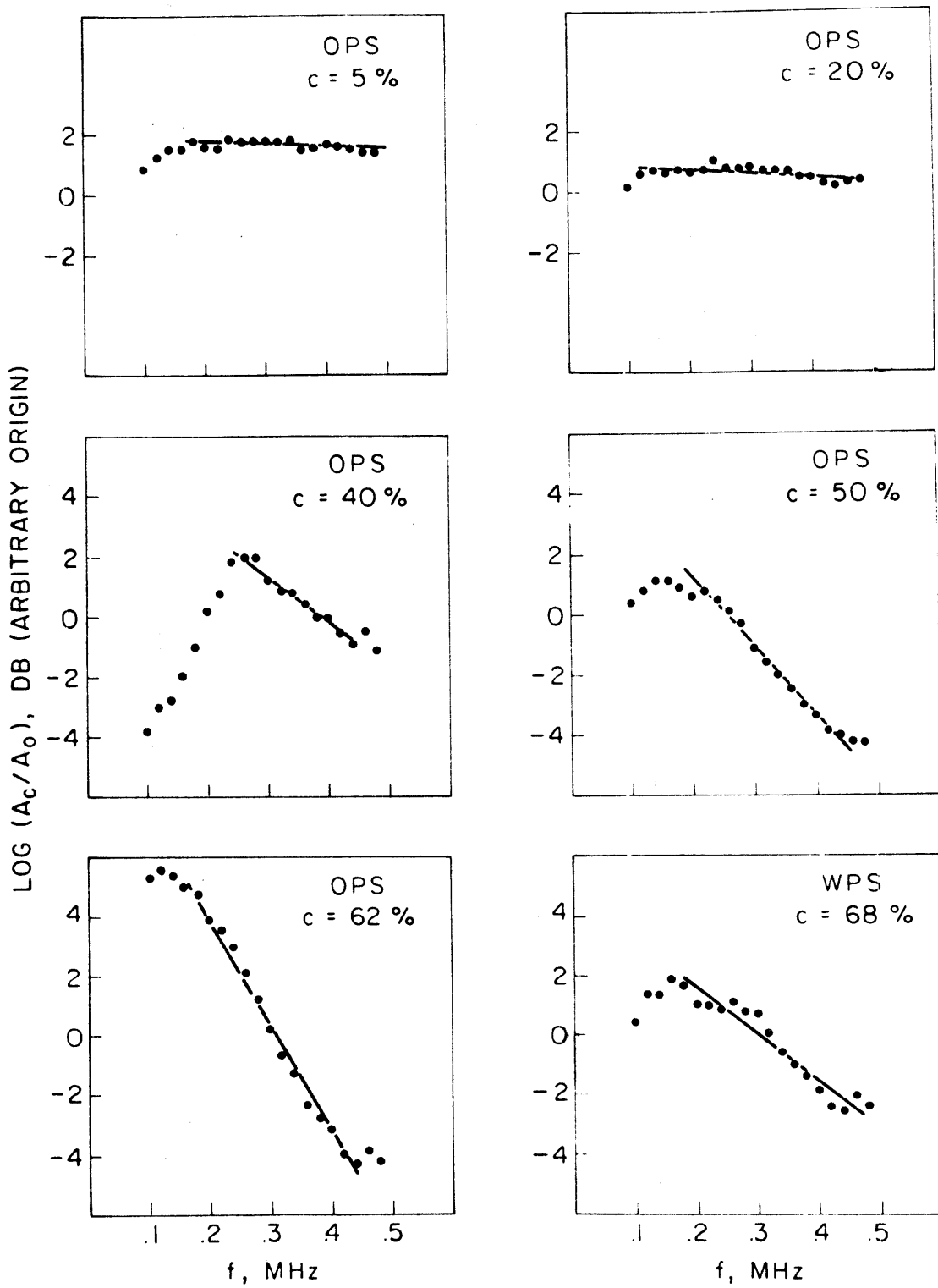


FIGURE 3.8

CHAPTER 4. APPLICATION TO THE EARTH'S INTERIOR

A major feature of the earth's deep interior is the existence of a central core. From the center of the earth up, the core can be divided into three regions (Bullen, 1965): (i) the presumably solid inner core extends from the center to a radius of about 1200 km; (ii) the approximately 500 km thick transition zone surrounding the inner core owes its name to the uncertainty of its seismic velocities and (iii) the fluid outer core extending up to the core-mantle boundary at a depth of about 2900 km. The combination of shock wave data, seismic observations and geochemical arguments seem to indicate that the outer core is an iron melt containing a lighter alloying element, probably sulfur or silicon (Anderson et al., 1971); the solid inner core may simply be the high pressure solid phase of this system with probably little S or Si and even some nickel (Press 1968). The occurrence of this phase change led Verhoogen (1961) to postulate progressive crystallization of the core. He showed that partial crystallization of the outer core with corres-

ponding growth of the inner core can provide enough heat to maintain convection and thus the magnetic field. Recent observations of PKJKP (Julian et al., 1972) and the inversion of free oscillating data (Dziewonski and Gilbert, 1972) are a confirmation of the solidity of the inner core, but at the same time the low shear velocity may indicate partial melting.

The theory of two-phase media combined to seismic observations can provide a useful test of these hypotheses about the state of the earth's core. Seismic velocity profiles of the core are readily available but only crude estimates, if not guesses, of the elastic quality factor Q have been made. Since the latter is of vital importance for interpreting seismic data in terms of two-phase media, we present in this chapter a model for Q in the core and show the compatibility of the attenuation and velocity data with the hypothesis of partial melt and partial crystallization in the deep interior.

4.1. Method of analysis.

The spectrum of a seismic signal is affected by a number of factors besides anelasticity of the earth. Such factors are the near-source and near-receiver crustal structures,

the geometrical spreading of the wave front, reflections and refractions that the wave undergoes on its path to the receiver, the instrument response and processing method. In order to eliminate these unwanted contributions we use the amplitude ratio technique (Teng, 1966, 1968) for attenuation measurements. The observed amplitude spectrum of a P wave may be written as

$$A(f) = S(f,i,i') G(\Delta) T(\Delta) R(f,e) I(f) e^{-t^*f} \quad (4.1)$$

where $S(f,i,i')$ is the source spectrum in general a function of the frequency f , azimuth i' and take-off angle i of the body wave. $G(\Delta)$ is the geometrical spreading factor independent of frequency. $T(\Delta)$ represents the effects of reflections and refractions along the path and may be taken as independent of frequency for short-period body waves. $R(f,e,e')$ is the near-receiver transfer function dependent on frequency, azimuth e' , and angle of emergence e of the wave; $I(f)$ is the instrument response. The exponential term represents the attenuation of P waves due to anelasticity with factor

$$t^* = \pi \int \frac{ds}{\alpha(s)Q(f,s)} \quad (4.2)$$

where α is the P wave velocity and Q the quality factor, the integration being taken along the ray path. The ratio of the spectra of two P waves from the same event recorded at the same station can now be written as

$$\frac{A_1(f)}{A_2(f)} = C_{12} \frac{S(f, i_1)R(f, e_1)}{S(f, i_2)R(f, e_2)} e^{-(t_1^* - t_2^*)f} \quad (4.3)$$

where C_{12} is independent of frequency. For P waves originating from surface focus events and sampling the core the rays are nearly vertical. Thus we may assume that the effects of crustal structure and source radiation pattern are the same for any pair of core phases. As a consequence equation (4.3) may be written as

$$\ln \frac{A_1(f)}{A_2(f)} = (t_2^* - t_1^*)f + \ln C_{12} \quad (4.4)$$

where C_{12} is independent of frequency. If we make the common assumption that Q is independent of frequency (the validity of this assumption will be discussed later), then by combining equations (4.2) and (4.4) we can obtain the distribution of Q within the core from the slope of a line fitted to a plot of the logarithm of the amplitude ratio of two core phases vs. frequency, provided we know the velocity distribution.

4.2. Data base.

The PKP and PKKP phases used in this study are from the events listed in Table 4.1 as recorded at LASA. Origin time, hypocenter location and magnitude are from the United States Coast and Geodetic Survey Bulletin. The events are chosen so that at least two core phases are observed at LASA, thus allowing the use of equation (4.4). All amplitude spectra are computed from the beam of the subarray sums with the Seismic Data Analysis Console program (Fleck, 1968). When the onset of the signal is clear enough, our own time picks are used to form the beam; otherwise the beam is obtained by steering the array to the expected azimuth and $dt/d\Delta$ of the wanted phase. Typical processed signals are shown on Figure 4.1. The length of the time window used for the spectral estimations is typically four seconds, but it is variable from one event to another depending on the noise level and signal duration. However, the same window is used for all phases from a same event so that the window length has no effect on the spectral ratio, besides resolution. Because of the nearly vertical incidence of all core phases the spectral estimates are not corrected for the damping of the high frequencies due to the use of subarray sums. This effect

would amount to an artificial damping of about 2 db of the AB branch relative to the DF branch of PKP at 2 Hz; at this frequency the noise level is already significant and this correction is not felt to be crucial.

Typical spectra of two phases from the same event and their spectral ratio are shown on Figure 4.2. The scatter is due to a large extent to the occurrence of pronounced but narrow peaks or troughs in one of the two spectra. Such detailed features are not significant because of the resolution of our estimates and since we are interested in the overall trend of the spectral ratios, we smooth them by taking the average over three adjacent frequencies; the resulting smoothed spectral ratio is also shown on Figure 4.2.

We have computed 28 spectral ratios which are to be divided into four groups according to the pair of core phases used (i) PKP_{AB}/PKP_{DF} (ii) PKP_{AB}/PKP_{BC} (iii) $PKP_{DF}/PKKP_{AB}$ and (iv) $PKKP_{BC}/PKKP_{AB}$. The subscripts refer to the various branches of the travel time curve (Figure 4.3) and they correspond to various depths of penetration as indicated on the velocity model (Toksoz et al, 1972) that we used (Figure 4.4). Typical paths of the core phases we used are shown on Figure 4.5. Several amplitude ratios are given as examples on Figure 4.6.

The least one can say is that the linear dependence on frequency postulated in connection with equation (4.4) is not obvious in all cases. However, on a global basis, the general trend is indeed linear as is shown by the averages of all spectral ratios within a group (Figure 4.7). It seems then that there is no strong evidence to reject our earlier assumption that Q is independent of frequency. But it is clearly shown in Table 4.2 that the great scatter between the estimate of the slope of the spectral ratio from individual events allows use of the data only for the determination of gross average features. As a consequence we take the average of all spectral ratios within a same group and fit straight lines to these four average spectral ratios. The fitting is performed over two frequency bands: 0.5 to 1.5 Hz and 0.2 to 2.0 Hz. The corresponding fitted slopes are given in table 4.2; they are called "average 1" and "average 2" respectively. On one hand, "average 1" is more reliable than "average 2" because it is less contaminated by noise (signal to noise ratio approaches 1 when $f \approx 2.0$ Hz). On the other hand "average 1" is less reliable because it is obtained from a narrower frequency band than "average 2". Thus in the following section we shall use the "average 1" and "average 2" estimates separately in the interpretation. Comparing both will give an indication of the stability of our results.

4.3. Inversion of the data.

We assume that the Earth is a spherically symmetric body and that it can be divided in concentric layers, each layer having a constant Q . If a velocity model is assumed, we can find the travel time of the P wave in each layer and by using equations (4.2) and (4.4) we can write

$$x_{12} = 27.3 \sum_{i=1}^N \frac{\Delta t_i}{Q_i} \quad (4.5)$$

where x_{12} is the slope (in db/Hz) of the amplitude ratio of wave 1 to wave 2, Δt_i is the travel time difference (wave 2 minus wave 1) in the i^{th} layer in seconds, and Q_i is the quality factor in the i^{th} layer. This is our working equation to invert the amplitude ratio data for the Q structure of the deep interior.

The travel times of P waves in each layer are computed with the ray tracing program written by Julian; the velocity model which is used is given in Table 4.3. A particular choice of mantle P wave velocities is not crucial since all published models are very similar at least down to a depth of 2750 km. Thus for the mantle we choose the values given by Buchbinder (1971) except for the 150 km thick low velocity layer just above the core-mantle boundary (CMB) where the velocities are those reported by Bolt

(1972). The velocity model of the core is from Toksoz et al. (1972).

We have four estimates of the differential attenuation of core phases (the four average slopes). From the velocity model of Toksoz et al. (1972) it seems reasonable to divide the core in four layers: the inner core, the transition zone, the lower outer core (depths between 3570 and 4670 km) and the upper outer core (depths between 2900 and 3570 km). In order to determine the Q within these layers, we adopt a Q of about 200 for short-period P waves in the upper mantle (from the surface to a depth of 700 km) and a Q of about 2000 for the rest of the mantle (Archambeau et al., 1969). The choice of an upper mantle Q is not critical because all core phases spend about the same time in the upper mantle. Then using a set of four equations of the type (4.5) we can calculate the Q values in the four layers of the core. Whether we use the average slopes estimated over the 0.5 to 1.5 Hz or the 0.2 to 2.0 Hz frequency band, the general features of the solution are the same. We find a negative Q in the lower outer core (about -2000) and a Q of the order of 700 in the upper outer core. The fact that we find a negative but large Q does not indicate that the solution is meaningless. We determine in fact Q^{-1} so that a small uncertainty on Q^{-1} when Q^{-1} is

close to zero may lead to very large Q values either positive or negative. The result essentially means that Q in the lower outer core is very large. More important is the relatively low Q (700) found for the upper outer core. This result seems inconsistent with the observations of short period multiply reflected core phases such as P_4^{KP} and P_7^{KP} (Qamar and Eisenberg, 1972). With a Q of 700 in the upper outer core the amplitude ratio of P_7^{KP} to PKP would be of the order of 10^{-4} at 1 Hz since these phases spend about 2100 seconds and 300 seconds respectively in the upper outer core. This ratio is clearly too small for allowing observations of P_7^{KP} even from high magnitude events. Therefore we may conclude that the observed attenuation cannot be solely attributed to regions within the core.

An alternative is that part of the attenuation originates in the mantle. Since there is good evidence that Q is high in most of the mantle and since most of the travel time difference between two different core phases in the mantle comes from very near the core-mantle boundary, we introduce an additional layer at the base of the mantle. The evidence given by Bolt (1972) for the existence of a low velocity zone above the core-mantle boundary (CMB) leads us to adopt 150 km as the thickness of this layer. The six layers into which we divide the Earth are (i) the

upper mantle (0 to 700 km) with a Q of 200, (ii) the mantle (700 to 2750 km) with a Q of 2000, (iii) the layer at the base of the mantle (2750 to 2900 km), (iv) the outer core (2900 to 4670), (v) the transition zone (4670 to 5170 km) and (vi) the inner core (5170 to 6370 km). In table 4.4 we give the average travel time difference in each of the six layers for each pair of core phases we observed. Solving the resulting system of the type of equation (4.5) we obtain the following Q values.

For the 0.5 to 1.5 Hz frequency band

$Q = 200$ in the layer above the CMB

$Q = 2200$ in the outer core

$Q = 800$ in the transition zone

$Q = 270$ in the inner core

For the 0.2 to 2.0 Hz frequency band

$Q = 380$ in the layer above the CMB

$Q = 2900$ in the outer core

$Q = 1700$ in the transition zone

$Q = 400$ in the inner core

The general features of both estimates are very similar. The Q in both the inner core and the layer above the CMB is low and comparable to the Q value of the upper mantle. The Q is large in the outer core and somewhat lower in the transition zone. On the basis of our data it does not seem

that Q can be as large as 6000 or 10000 as was suggested by Bolt (.972) and Qamar and Eisenberg (1972). But it must be emphasized that differences between large values of Q are not very significant since one actually determines Q^{-1} . The essential point is that the Q value which we find for the outer core is not in contradiction with observations of multiply reflected core waves. Our most significant results are the low Q values found in the inner core and in the layer above the CMB. Since it is difficult to estimate exactly which of our two sets of estimates is the most reliable (is the bias due to noise contamination more serious than the bias due to the use of a fairly narrow frequency band?) and since they are similar, we shall adopt the following average Q values for the remaining discussion:

$Q \approx 300$ in the layer above the CMB

$Q \approx 2500$ in the outer core

$Q \approx 1200$ in the transition zone

$Q \approx 300$ in the inner core

4.4. Interpretation.

4.4.1. Transition zone.

A large variety of velocity distributions have been proposed for the "anomalous" zone between the outer core and

the solid inner core (Adams and Randall, 1964; Buchbinder, 1971; Qamar, 1971; Toksoz et al., 1972). Nevertheless there seems to be general agreement on two features, (i) the transition zone is delimited at the bottom by the inner core boundary (ICB) which constitutes a sharp P wave velocity discontinuity as is evident from the observations of PKiKP (Engdahl et al., 1970), (ii) the velocity gradients are lower than in the outer core.

As a consequence of these uncertainties there has been little speculation about the state of the transition zone. Bolt (1971) and Buchbinder (1971) seem to favor the hypothesis of a solid transition zone possibly partially molten. It conveniently explains the velocity discontinuities apparently required by the observations of precursors to PKP at short epicentral distances. But then, are the low velocity gradients to be explained by an increase of partial melt with depth or unduly large temperature gradients? Would the ICB discontinuity represent a solid-solid phase change and why would it be much larger than the shallower discontinuity? Since the velocity discontinuity between the outer core and the transition zone may be as small as 0.1% (Buchbinder, 1971) it seems more appropriate to base any interpretation on the definitely low velocity gradients.

If the outer core velocities are linearly extrapolated

to the ICB, the P wave velocity just outside the inner core would be about 10.40 km/s whereas it is 10.15 km/s in the model of Toksoz et al., (1972). This decrease in velocity seems too large to be attributed to a temperature effect. But it could be due to partial crystallization. The effective P wave velocity in a suspension of solid spheres in a fluid matrix can be smaller than the velocity of the fluid, provided the density and bulk modulus ratios of the solid to the liquid phase meet certain conditions. Using formula (2.19), (2.20) and (2.21) we find that the 2.4% decrease in velocity is compatible with a suspension where the concentrations of solid is 60% with a density ratio of 1.10 and a bulk modulus ratio of 1.01. Smaller concentrations of solid larger density ratios and vice-versa; in all cases, however, the bulk modulus ratio must be nearly 1. These values are not incompatible with the probable increase in density upon freezing of liquid core material and the K - P hypothesis of Bullen (1965) who suggested that at pressures in the megabar range the bulk modulus of most materials in the earth is a smoothly varying function of pressure. In shallower parts of the transition zone the difference between the observed velocity and the extrapolated velocity is smaller. Following our hypothesis of partial crystallization, we conclude that the concentration of solids in suspension in the fluid increases with depth, indicating progressive

settling and growth of the inner core.

Our interpretation requires a rather large density ratio between the solid phase and the melt so that it may be questionable whether the solidified particles will remain in suspension or sink. The motion of a sphere of solid material with respect to the surrounding fluid can be found from Stokes' drag law. If

$$6 \pi a \eta \tilde{v} = \frac{4}{3} \pi a^3 \Delta \rho \quad (4.6)$$

the solid sphere of radius a with excess density $\Delta \rho$ will sink with a velocity \tilde{v} in the fluid of viscosity η ; g is the acceleration of gravity. Taking $g = 600 \text{ cm/s}^2$, $\Delta \rho = 1 \text{ g/cm}^3$ we obtain in CGS units

$$\frac{\eta \tilde{v}}{a^2} \approx 100 \quad (4.7)$$

From here on, any argument becomes rather speculative since neither η , \tilde{v} or a is known; but let us proceed, essentially to show that the assumed density ratio does not necessarily preclude the possibility of a stable suspension in the transition zone.

If we assume that the inner core has been formed over the past three billion years by solidification of the outer core at a constant rate, we find that its radius increases

at present times by about 0.1 mm/year. If there is no independent motion of the fluid, our hypothesis would then require that the sinking velocity of a solid particle is of the same order, that is about 10^{-10} cm/s. The viscosity of the fluid can be estimated from the Q values given in the preceding section. If we attribute all attenuation of short period P waves to shear viscosity we can use the approximate relation

$$\frac{1}{Q} \approx \frac{\omega\eta}{K} \quad (4.8)$$

where K is bulk modulus and $\omega = 2\pi \times$ frequency. Taking $K \approx 10$ megabars in the outer core on the average and $Q \approx 2500$ for P waves of frequency 1 Hz we obtain $\eta \approx 5 \times 10^8$ poises. In the transition zone, with $Q \approx 1200$ and $K \approx 12$ megabars we have $\eta \approx 10^9$ poises. Since there are probably other mechanisms contributing to the total attenuation it seems that we can take 10^8 poises as a rough estimate for the fluid viscosity. Such a value seems more appropriate than the estimate of Sato and Espinosa (1967), who found 10^{11} poises which by use of equation (4.8) gives a Q of 10. Combining our viscosity estimate with the required sinking velocity, we find that the radius of the solid particles must not be larger than 0.1mm on the average. Whether such a size is reasonable or not is an open

question, but it probably cannot be proved impossible. A larger size can be allowed for if there is fluid motion which is probable if partial crystallization takes place because the associated heat release can sustain convection. If the velocity of the fluid in the convection cells is 10 km/year (Stacey, 1969), a particle with a radius of 1m would remain in suspension, provided the fluid motion is vertical and upwards. This is of course not the case in all parts of the convection cell. Thus if the solid particles are large and if convection is existing in the transition zone, it is likely that this region of the Earth is laterally inhomogeneous. There are as yet no data indicating such features.

In summary, the hypothesis of partial crystallization in the transition zone is compatible with observed velocity gradients. The resulting suspension of solid matter in the fluid is denser as depth increases and is not necessarily unstable.

4.4.2. Inner core.

The inner core boundary (ICB) is a sharp, well-defined interface (Engdahl et al., 1970). It probably corresponds to a liquid-solid phase change since there is little evidence that the transition zone is solid as we saw in the previous section whereas evidence for a solid

inner core is accumulating (Dziewonski and Gilbert, 1972; Julian et al., 1972). The rigidity of the inner core is apparently very low, about 1/12 of its bulk modulus if one adopts a 3.0 km/s for the shear wave velocity (Julian et al., 1972). This result combined with the low Q of P waves determined in this study may indicate partial melting.

The concentration of melt may be estimated from seismic data by using the non-interaction model for a solid matrix containing spheroidal inclusions derived in Chapter 2 (equations 2.28-2.30). The effective elastic constants of the inner core can be determined from the seismic velocities. Taking 12.8 g/cm^3 for the density and 11.0 and 3.0 km/s as the P and S velocities, we obtain 14.0 and 1.16 megabars for the effective bulk and shear moduli. The Q of P waves is about 300. The major difficulty in estimating the melt concentration arises from the fact that we do not know the properties of the solid matrix. As a first approximation we shall assume that the bulk moduli of the liquid and solid phases are equal as was suggested in the previous section. But for the shear modulus of the matrix the best we can do is guessing. Let us first take a value close to the effective value, say $\mu = 1.25$ megabars. Then we can compute the effective moduli and Q_α for various values of the concentration of

melt c and of the aspect ratio $\tilde{\alpha}$ of the melt pockets. It is to be recalled that there is no unique distribution of c and $\tilde{\alpha}$ for which the observed and calculated effective properties are matched. Taking our estimate of 10^8 poises as the viscosity of the melt and a frequency of 1 Hz, the observed values can be obtained for instance with roughly $c = 10^{-4}$ and $\tilde{\alpha} = 3 \times 10^{-4}$ or $c = 5 \times 10^{-5}$ and $\tilde{\alpha} = 10^{-4}$ (Figure 4.8). The significant result is that the velocity and attenuation data can be explained with a very low volume of melt (about 0.1% or less) concentrated in flat penny-shaped pockets. If on the other hand the matrix is a Poisson solid (Poisson's ratio equal 1/4), then a larger amount of melt is required for matching the low effective shear modulus; about 5% of melt occurring in pockets with $\tilde{\alpha} = 10^{-2}$ would be needed. The actual matrix shear modulus is probably between the two values we considered, but as a result it seems that a small amount of melt in the inner core would be sufficient to explain the low shear velocity and Q value of P waves which one observes.

There is, however, one piece of data which seems to be in conflict with this interpretation. In our calculation we attributed all attenuation to shear dissipation. Then a Q of 300 for P waves corresponds to a Q of 30 for shear waves. In this case PKJKP would not be observable since the wave remains a long time in the

inner core as a shear wave. However Julian et al. (1972) reported observations of PKJKP and they also gave 500 to 1000 as a rough estimate for the Q of shear waves in the inner core. This value is probably excessive since they did not account for the sizable attenuation of PKKP which they used as a reference. A value for Q_{β} of 100 to 200 seems more adequate but it would imply that a large part of the P wave attenuation is due to volume dissipation. Modifying our model by introducing a bulk viscosity comparable to the shear viscosity and by allowing for a slight difference between the bulk moduli of the solid and melt does not produce sufficient damping. If the mechanism for P wave attenuation is intrinsic anelasticity of the solid phase, the only remaining argument supporting the partial melting hypothesis is the anomalously low shear velocity.

4.4.3. The base of the mantle and the core-mantle boundary.

An interesting result of this study is that a highly attenuating layer is required at the base of the mantle, just above the core-mantle boundary (CMB). According to Bolt (1971, 1972) this region is also a zone of low P and S wave velocity and he proposed 150 km as its thickness. We take 2750 km as the depth of the top of this "anomalous" zone because it is the depth at which the

velocities start departing from their normal behavior (Johnson, 1969). The interpretation of the data is based here on a procedure similar to that used in the section on the transition zone.

At a depth of 2750 km we adopt the values given by Johnson (1969) for the P velocity and by Press (1970) for the shear velocity and density. We also used the gradients of these parameters between 2500 and 2750 km depths to extrapolate the velocities and density to the CMB, which we located at a depth of 2900 km; these extrapolated values will be called "matrix values at the CMB". The actual or effective values of the seismic velocities at the CMB in the mantle are those reported by Bolt (1972). Finally we took the P wave velocity and density in the core at the CMB from Toksoz et al. (1972) and Press (1970). All parameters mentioned above are given in Table 4.5.

We now postulate that the anomalous zone is a two-phase medium consisting of inclusions of liquid core material embedded in a solid matrix of mantle material. By analogy with work on the upper mantle (Solomon, 1972) this hypothesis is qualitatively supported by the low seismic velocities and the high attenuation. In the following we show the compatibility of the hypothesis with the data on a quantitative basis and we estimate the required concentration of liquid material. The analysis

can be simplified a bit by realizing that the bulk moduli of the matrix and inclusion materials are very similar, about 6.4 and 6.5 megabars respectively. The effective bulk modulus will, therefore, be very close to the matrix bulk modulus, in particular when the concentration of **inclusions** is small. Thus, to a first approximation we can write

$$2 \frac{\Delta\alpha}{\alpha} = \frac{4\Delta\mu}{3K + 4\mu} - \frac{\Delta\rho}{\rho} \quad (4.9)$$

$$2 \frac{\Delta\beta}{\beta} = \frac{\Delta\mu}{\mu} - \frac{\Delta\rho}{\rho}$$

where α , β , K , μ , ρ are P and S velocity, bulk and shear modulus and density and where Δ refers to the difference between the effective value and the matrix value at the CMB. Using Table 4.5, we find $\Delta\mu/\mu \approx 5.9\%$ and $\Delta\rho/\rho \approx 4.5\%$. From the density change we find that the volume concentration of liquid core material is about 5%. This figure is to be taken only as a rough estimate of the volume of liquid core material which can account for the available seismic velocities at the CMB; at shallower depths the concentration of liquid would be smaller and would vanish at a depth of 2750 km according to this model.

We can use the models derived in Chapter 2 to have an estimate of the shape distribution of the liquid pockets.

Taking 10^8 poises for the viscosity of the liquid, we can calculate the effective elastic constants and the attenuation of 1 Hz P waves for various aspect ratios of the inclusions. If we attribute all attenuation to shear viscosity, a Q of 130 for shear waves corresponds to our observed Q of 300 for P waves. From Figure 4.9 it is found that all attenuation can be accounted for by a concentration of about 7.5×10^{-6} when the aspect ratio is 10^{-4} ; if all attenuation is attributed to pockets with aspect ratio 10^{-2} , the needed concentration is about 2.5% , but this would also imply an effective shear modulus of about 1.6 megabars, whereas the observed shear modulus is between 2.60 and 2.85 megabars.

If the shear velocity near the CMB is somewhat lower than that reported by Bolt (1972) , say 6.9 km/s, system (4.9) yields $\frac{\Delta\mu}{\mu} \approx 10\%$ and $\frac{\Delta\rho}{\rho} \approx 2.7\%$, which corresponds to $c \approx 3.2\%$. This set of values allows a fit with a more satisfactory distribution of shapes and concentrations; an example of a distribution which matches both the attenuation and the velocities is given on Table 4.6.

In summary it seems that by using our models for two-phase media we can satisfactorily explain the observed velocities and P wave attenuation at the base of the mantle. A small amount of liquid core material dispersed in the solid mantle material as penny-shaped pock-

ets is sufficient to lower the Q of short period P waves by an order of magnitude throughout the lowermost 150 km of the mantle. As one approaches the core-mantle boundary, the liquid phase may be concentrated in thicker pockets and amount to as much as 3 or 5% in relative volume.

Table 4.1

EVENTS USED FOR DETERMINING Q IN THE CORE

Event	Origin Time (h min s)	Latitude (Degrees)	Longitude (Degrees)	Depth (km)	Body-Wave Magnitude	Distance To LASA (Degrees)	Observed Phases
4 13 67	19 53 42	27.3N	128.7E	38	6.0	91.2	PKKP(AB , β C)
6 17 67	5 0 12	58.3S	26.6W	140	6.1	123.4	PKP(DF) ,PKKP(AB)
8 30 67	4 22 2	31.7N	100.3E	3	6.1	98.4	PKKP(AB , β C)
9 20 67	9 39 15	49.8S	163.4E	30	6.1	123.7	PKP(DF) ,PKKP(AB)
9 29 67	17 29 40	31.8S	57.3E	22	5.0	160.5	PKP(AB ,DF)
10 9 67	17 21 34	25.0S	179.0W	619	6.7	97.0	PKKP(AB , β C)
10 18 67	16 23 26	25.1S	71.5E	33	5.7	158.4	PKP(AB , β C ,DF)
10 25 67	0 59 22	24.5N	122.2E	65	6.0	96.7	PKKP(AB , β C)
11 14 67	5 28 37	5.4S	147.1E	201	5.8	105.3	PKKP(AB , β C)
5 20 68	7 13 3	30.9S	178.3W	22	6.0	100.9	PKKP(AB , β C)
8 3 68	4 54 33	25.6N	128.5E	19	6.4	92.7	PKKP(AB , β C)
9 12 68	22 44 7	21.6S	179.4W	635	5.9	94.6	PKKP(AB , β C)
9 14 68	1 25 19	24.5S	80.4E	33	5.5	157.2	PKP(AB , β C ,DF)
9 14 68	13 48 31	28.4N	53.1E	33	5.8	103.0	PKKP(AB , β C)
9 16 68	13 55 36	6.1S	148.7E	59	5.8	104.8	PKKP(AB , β C)
9 26 68	14 37 46	20.9S	177.0W	250	5.8	92.6	PKKP(AB , β C)
10 8 68	7 43 23	39.9S	87.7E	33	6.0	167.8	PKP(AB ,DF)
10 23 68	21 4 41	3.3S	143.3E	12	6.1	106.4	PKKP(AB , β C)
11 4 68	9 7 39	14.2S	172.0E	585	5.8	94.7	PKKP(AB , β C)
1 24 69	2 33 3	21.9S	179.6W	595	5.9	94.9	PKKP(AB , β C)
2 11 69	22 16 14	6.7S	126.8E	450	6.0	119.7	PKP(DF) ,PKKP(AB)
3 10 69	6 54 18	5.6S	147.2E	206	5.8	105.4	PKKP(AB , β C)
3 20 69	20 46 56	27.5S	66.0E	33	5.5	159.9	PKP(AB ,DF)
7 31 69	5 5 4	27.6S	66.2E	33	5.3	160.0	PKP(AB ,DF)
11 7 69	18 34 00	27.9N	60.1E	35	6.1	104.7	PKKP(AB , β C)
12 14 69	18 37 10	8.2N	58.5E	33	6.0	123.7	PKP(DF) ,PKKP(AB)

Table 4.2

SLOPES FITTED TO AMPLITUDE RATIOS

Event	Δ (°)	PKKP _{BC} /PKKP _{AB}		Δx_{12} (db/Hz)	Δt (s)
		x_{12} (db/Hz)			
4 13 67	91.2	11.9		1.2	2.0
9 26 68	92.6	18.2		4.0	6.0
8 3 68	92.7	7.1		2.4	7.5
9 12 68	94.6	15.7		1.1	3.0
11 4 68	94.7	19.8		1.0	3.7
1 24 69	94.9	8.1		2.2	4.0
10 25 67	96.7	7.6		3.6	4.1
10 9 67	97.0	13.9		2.1	5.0
8 30 67	98.4	25.9		4.3	3.8
5 20 68	100.9	14.0		3.0	5.0
9 14 68	103.0	19.4		1.3	2.5
9 16 68	104.8	4.3		3.2	3.0
11 7 69	104.7	0.1		0.9	6.5
11 14 67	105.3	7.9		1.6	2.0
3 10 69	105.4	3.3		1.1	4.0
10 23 68	106.4	15.2		2.2	7.3
"Average 1"		12.2		0.9	
"Average 2"		7.4		0.6	

Event	Δ (°)	PKP _{AB} /PKP _{DF}		Δx_{12} (db/Hz)	Δt (s)
		x_{12} (db/Hz)			
10 8 68	167.8	2.8		1.5	5.5
9 29 67	160.5	-0.3		2.1	4.5
7 31 69	160.0	12.4		0.6	3.5
3 20 69	159.9	12.8		1.4	4.3
10 18 67	158.4	-2.8		1.2	5.0
9 14 68	157.2	13.9		4.9	4.0
"Average 1"		7.1		1.0	
"Average 2"		3.8		0.5	

Event	Δ (°)	PKP _{DF} /PKKP _{AB}		Δx_{12} (db/Hz)	Δt (s)
		x_{12} (db/Hz)			
6 17 67	123.4	0.3		3.6	5.1
9 20 67	123.7	5.8		2.0	20.1
2 11 69	119.8	22.9		3.2	10.0
12 14 69	123.7	-6.9		5.1	4.5
"Average 1"		5.5		1.5	
"Average 2"		6.0		0.8	

Table 4.2 (Continued)

SLOPES FITTED TO AMPLITUDE RATIOS

Event	$\Delta(^{\circ})$	$x_{12}(\text{db/Hz})$	$\Delta x_{12}(\text{db/Hz})$	$\Delta t(\text{s})$
		$\text{PKP}_{AB}/\text{PKP}_{BC}$		
10 18 67	158.4	-4.4	2.6	5.0
9 14 68	157.2	-0.8	1.5	4.0
Average 1		-2.6	1.2	
Average 2		-3.2	1.1	

Δt is the time window used for spectral estimation, x_{12} is the slope fitted to the amplitude ratio and Δx_{12} is its standard deviation. "Average 1" and "Average 2" are obtained by fitting a line to the average spectral ratios over the frequency band 0.5 to 1.5 Hz and 0.2 to 2.0 Hz, respectively. They are not the average of all slopes within a group. For individual events the frequency band used in the fit is 0.5 to 1.5 Hz.

Table 4.3

VELOCITY MODEL FOR P WAVES

Radius (km)	Velocity (km/s)	Radius (km)	Velocity (km/s)	Radius (km)	Velocity (km/s)
0	11.26	2100	9.73	4270	12.90
100	11.25	2200	9.64	4370	12.78
200	11.25	2300	9.55	4470	12.66
300	11.24	2400	9.45	4570	12.55
400	11.22	2500	9.39	4670	12.43
500	11.20	2600	9.27	4770	12.32
600	11.20	2700	9.18	4870	12.19
700	11.20	2800	9.09	4970	12.05
800	11.19	2900	8.94	5070	11.91
900	11.13	3000	8.81	5170	11.76
1000	11.05	3100	8.65	5270	11.60
1100	10.97	3200	8.50	5370	11.44
1200	10.97	3300	8.35	5470	11.27
1200	10.14	3400	8.18	5570	11.08
1300	10.16	3470	8.05	5670	10.74
1400	10.18	3470	13.33	5770	10.20
1500	10.17	3620	13.63	5870	9.64
1600	10.16	3670	13.60	5970	9.13
1700	10.16	3770	13.49	6070	8.68
1700	10.03	3870	13.37	6170	8.33
1800	9.96	3970	13.25	6270	8.12
1900	9.90	4070	13.13	6330	8.05
2000	9.80	4170	13.01	6370	6.75

Table 4.4

TRAVEL TIME DIFFERENCES FOR PAIRS OF CORE PHASES
IN A SIX-LAYER EARTH

Depth (km)	$PKP_{AB} - PKP_{BC}$ (s)	$PKP_{AB} - PKP_{DF}$ (s)	$PKP_{DF} - PKKP_{AB}$ (s)	$PKKP_{BC} - PKKP_{AB}$ (s)
0- 700	+ 7	+ 10	-6.5	- 6
700-2750	+141	+160	- 92	-156
2750-2900	+ 46	+ 74	- 20	-106
2900-4670	+ 60	+108	-654	+ 80
4670-5170	-220	-110	+161	+154
5170-6370		-182	+ 20	

Table 4.5

SEISMIC PROPERTIES AT THE BASE OF THE MANTLE

	A	B	C
Depth (km)	2750	2900	2900
α (km/s)	13.63	13.78	13.33
β (km/s)	7.28	7.37	6.9-7.0
ρ (gkm ³)	5.28	5.36	5.5
$\frac{\partial \alpha}{\partial z}$ (s ⁻¹)	10^{-3}		
$\frac{\partial \beta}{\partial z}$ (s ⁻¹)	$4 \cdot 10^{-4}$		

Column A refers to the properties in the mantle, assumed to be pure matrix material. Column B refers to the properties of the matrix at the CMB (extrapolated from Column A). Column C refers to the actual effective properties at the CMB.

TABLE 4.6

A possible distribution of the concentration and shape of the melt pockets at the base of the mantle.

concentration	aspect ratio
2.5×10^{-2}	1
6.0×10^{-3}	10^{-1}
1.0×10^{-3}	10^{-2}
7.5×10^{-6}	10^{-4}

- Figure 4.1 Typical waveforms of core phases recorded at LASA. All are full-array beams. Time scale is in seconds.
- Figure 4.2 Power spectra of two core phases and the calculated amplitude ratios versus frequency. The smoothed amplitude ratio is obtained from the unsmoothed amplitude ratio by averaging three adjacent frequencies.
- Figure 4.3 Travel time and ray parameter versus epicentral distance for PKP and PKKP. (From Toksoz et al., 1972)
- Figure 4.4 P wave velocity in the core versus radius. (From Toksoz et al., 1972)
- Figure 4.5 Ray paths of PKP and PKKP in the earth, corresponding to the travel time curves in figure 4.3.
- Figure 4.6 Examples of smoothed amplitude ratios of two core phases from four events.
- Figure 4.7 Average amplitude ratios for each group of core phases and fitted lines.
- Figure 4.8 Q of P waves versus frequency (or viscosity) in a partially molten inner core with a matrix shear modulus equal to 1.25 megabars. The arrows indicate the observed value ($Q=300$). The relaxation peaks A,B,D,E,F and G are

calculated for inclusions with aspect ratios 10^{-5} , 10^{-4} , 3×10^{-4} , 10^{-3} , 10^{-2} and 10^{-5} respectively.

Figure 4.9 Q of P waves versus frequency (or viscosity) at the core mantle boundary. The arrows indicate the observed value ($Q=300$). The relaxation peaks A, B, D, E, and F are calculated for inclusions with aspect ratios 10^{-5} , 10^{-4} , 10^{-3} , 10^{-2} and 10^{-5} respectively.

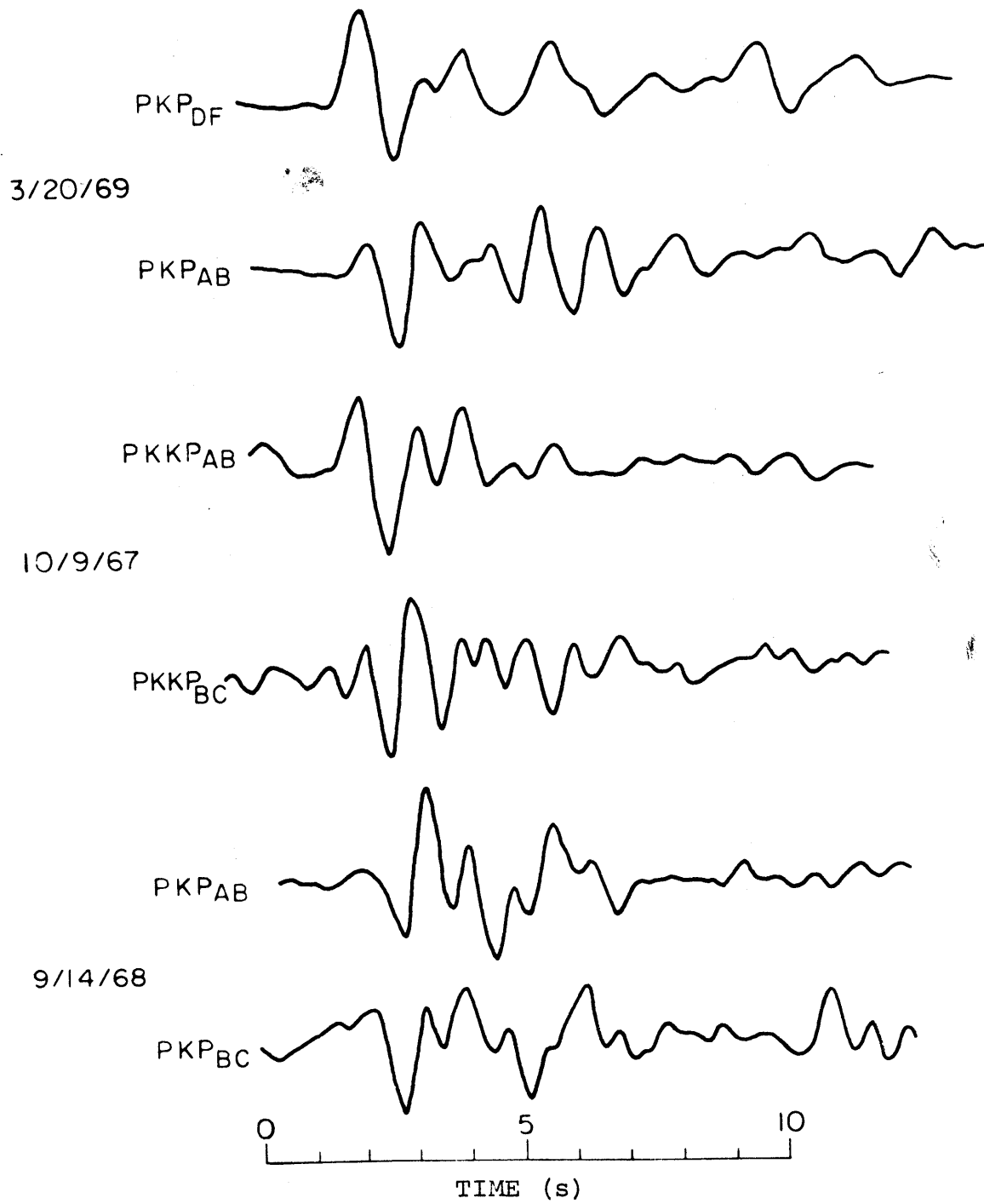


FIGURE 4.1

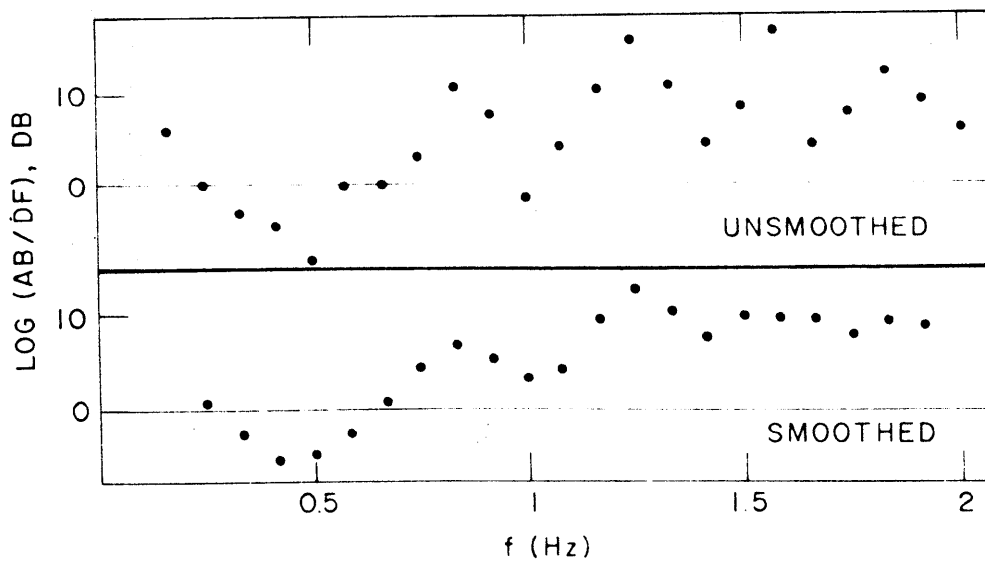
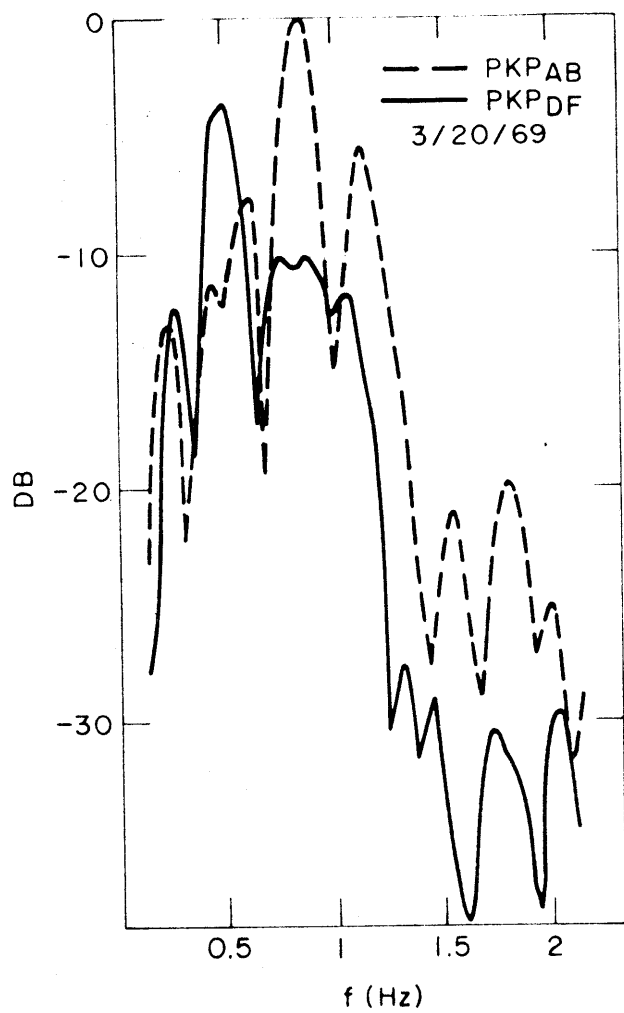


FIGURE 4.2

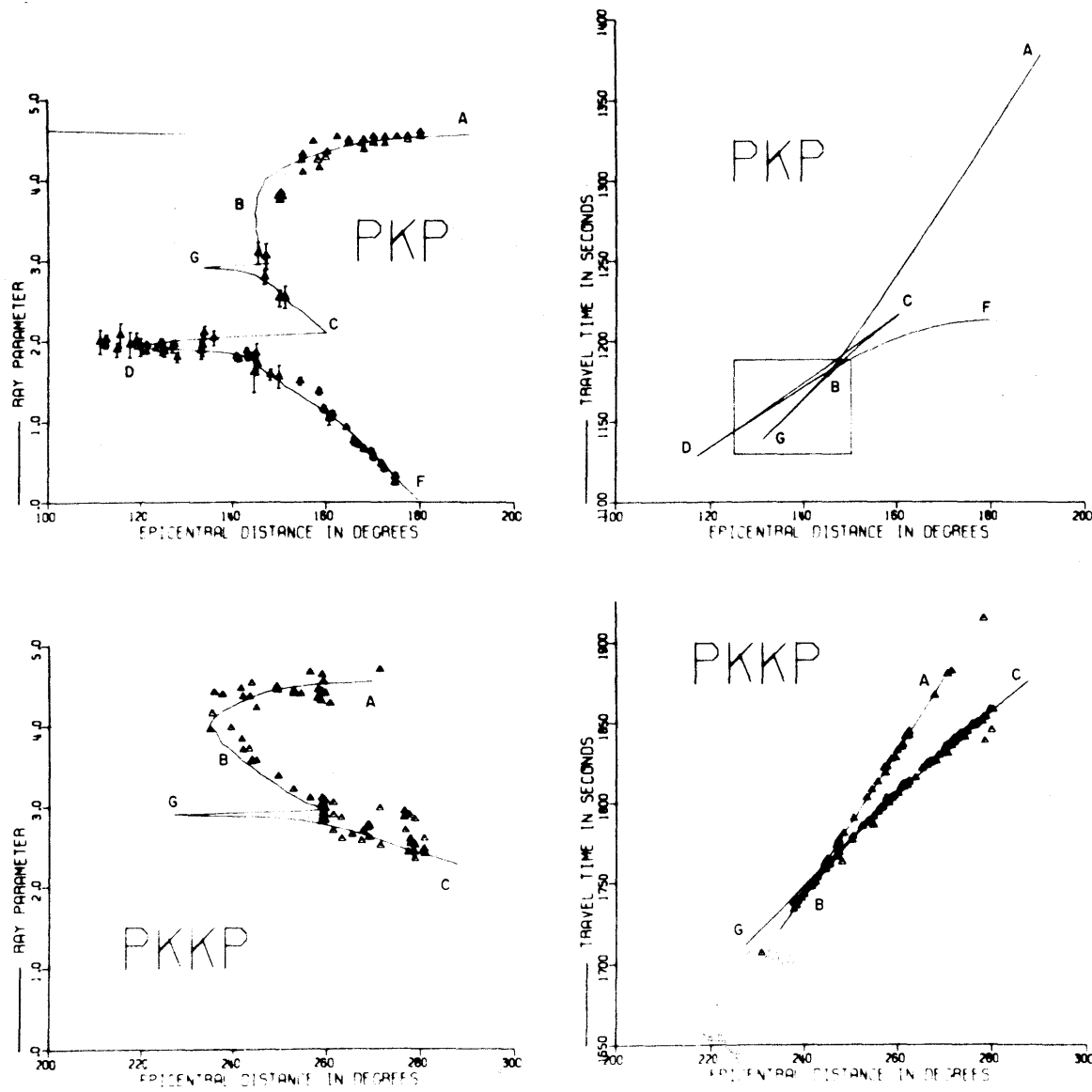


FIGURE 4.3

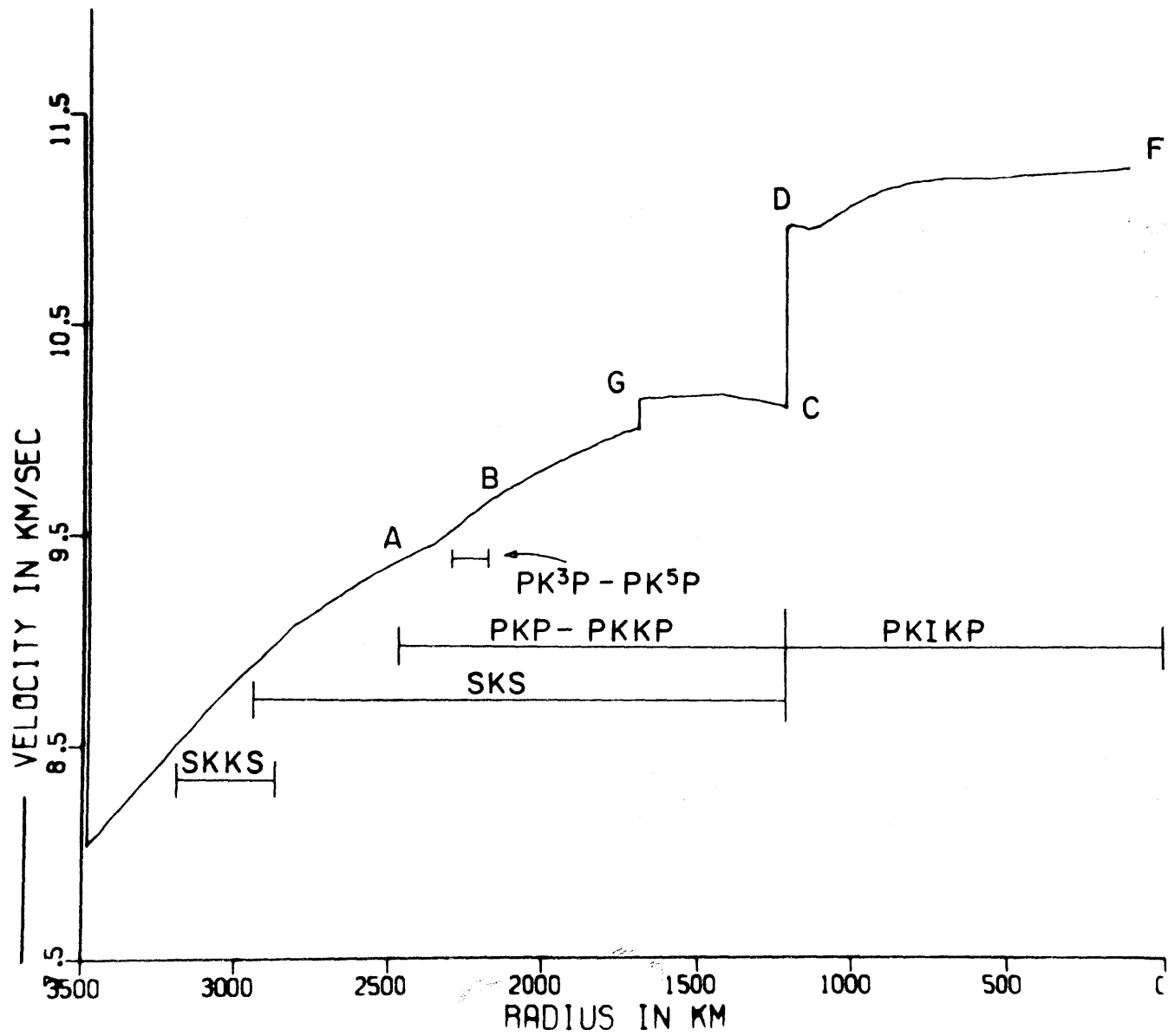


FIGURE 4.4

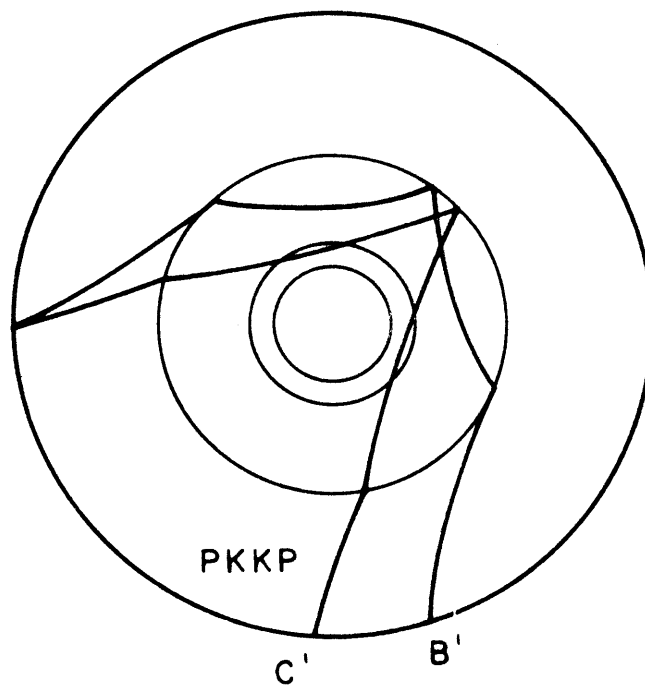
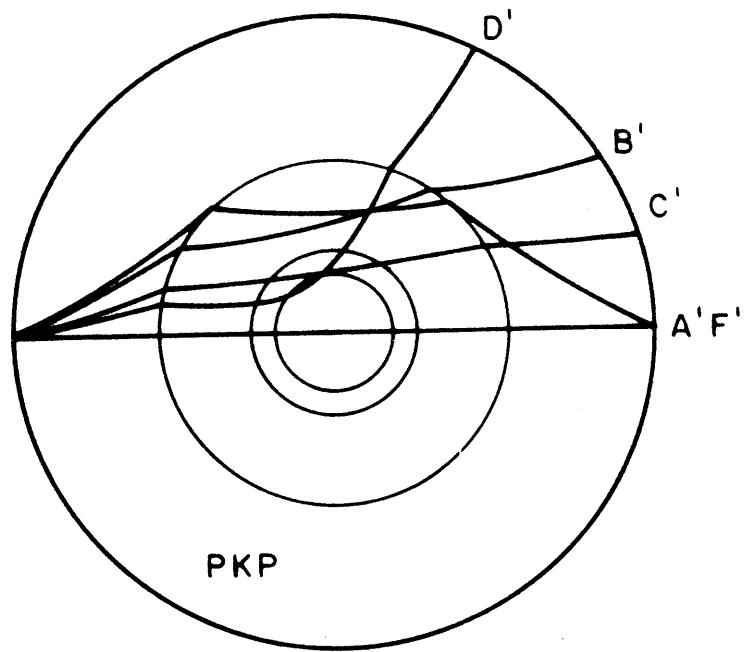


FIGURE 4.5

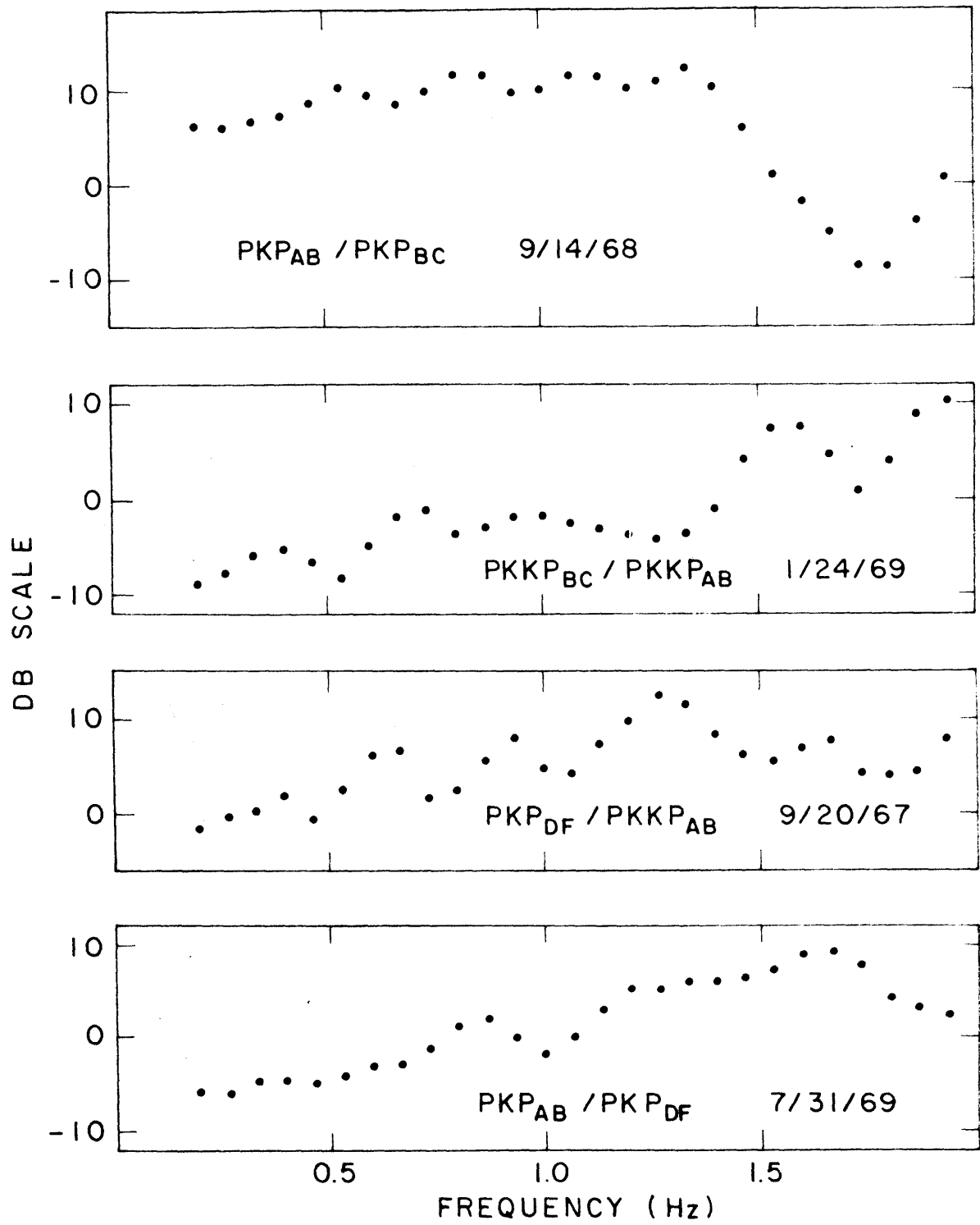


FIGURE 4.6

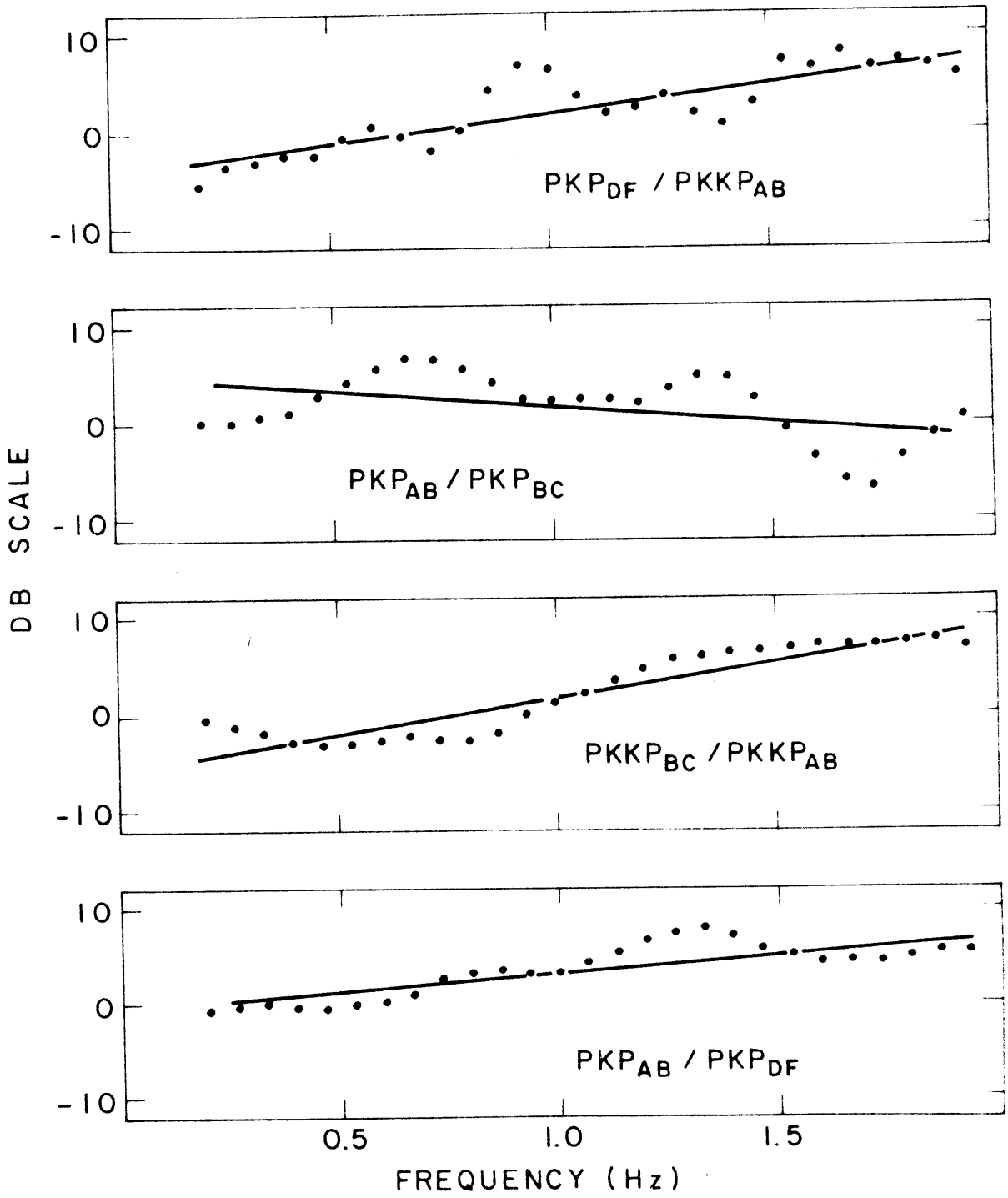


FIGURE 4.7

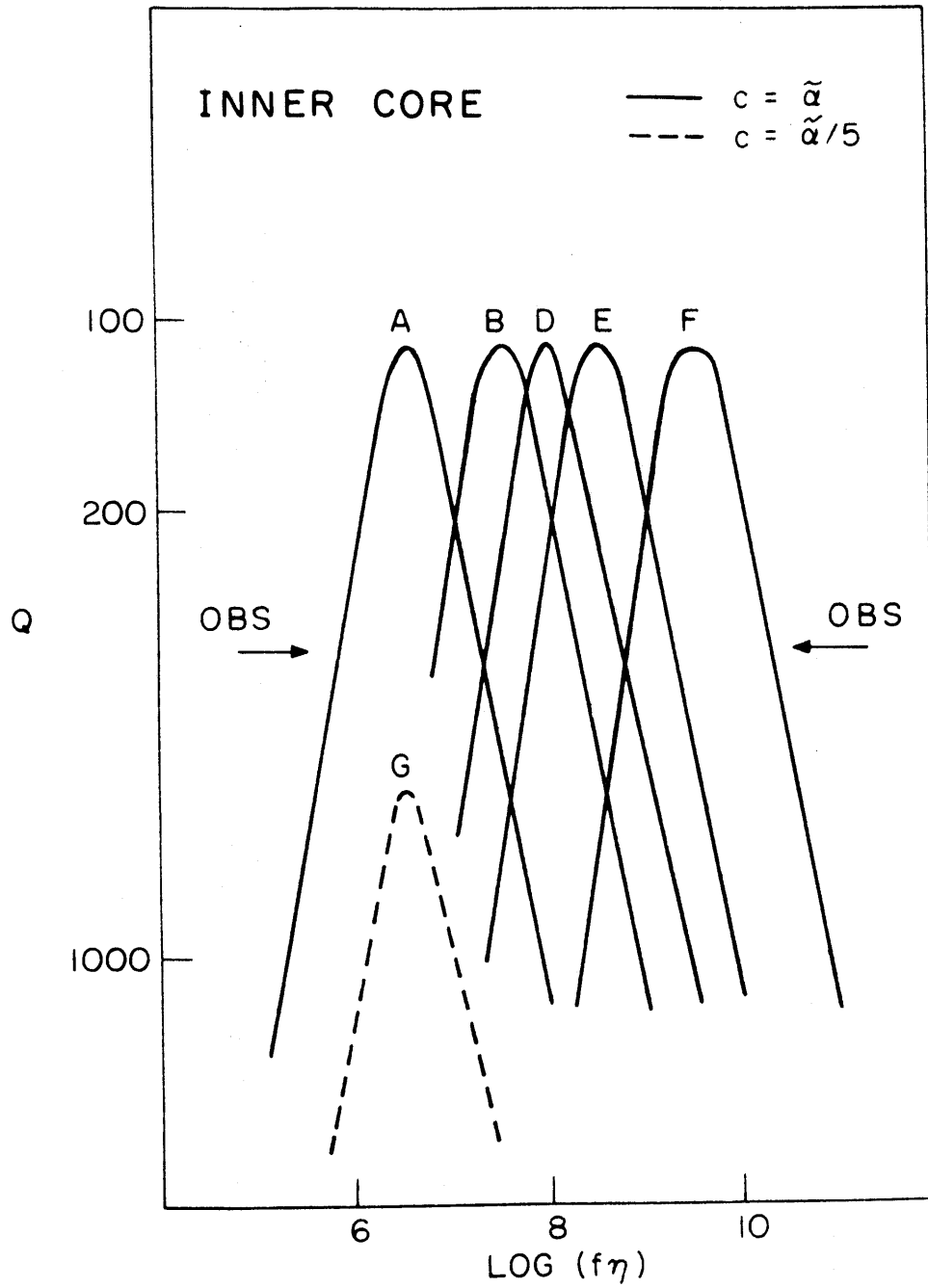


FIGURE 4.8

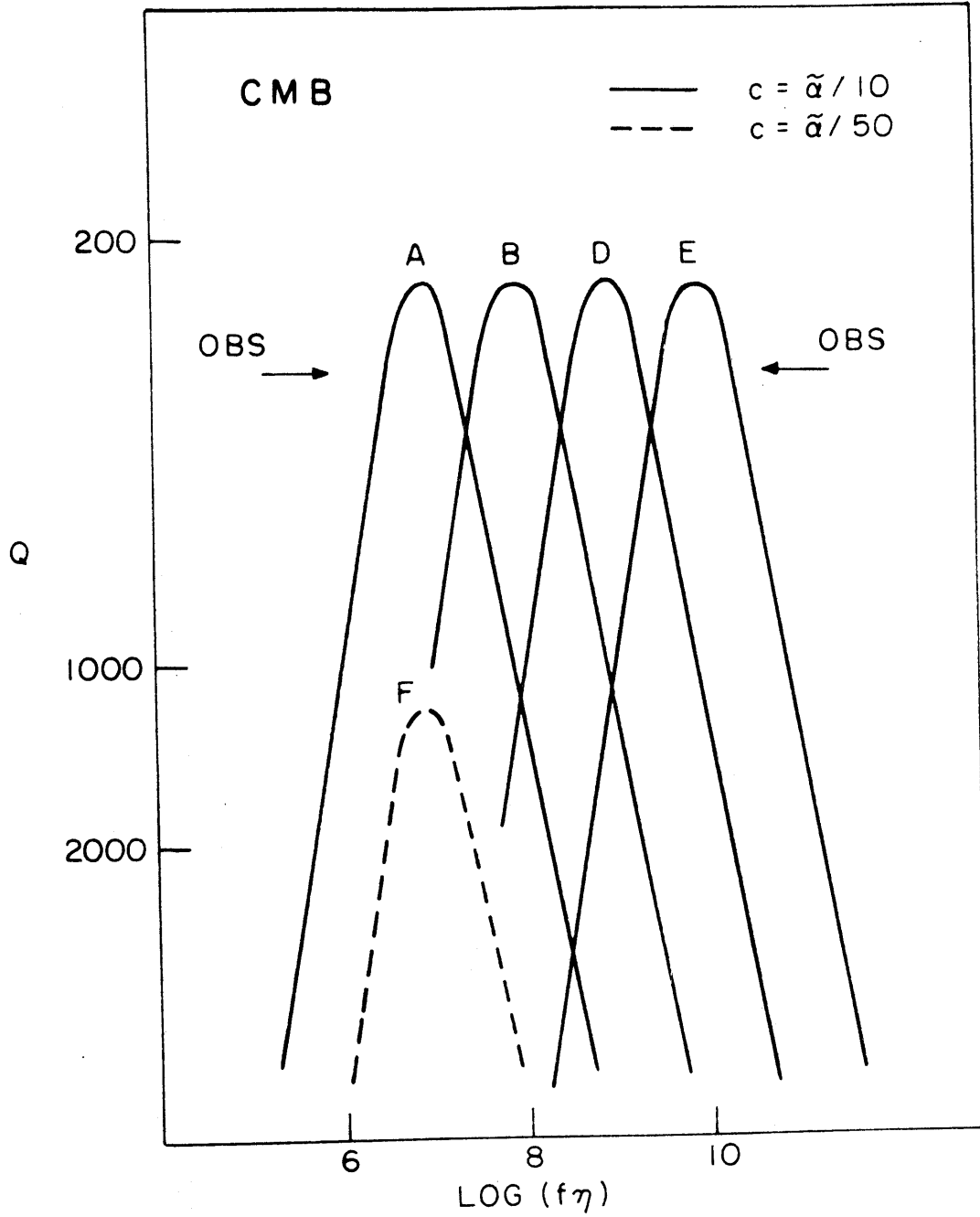


FIGURE 4.9

CHAPTER 5. CONCLUSIONS

In this study we examined several theoretical models for the propagation of seismic waves in two-phase media. We have tested these models against the velocity and attenuation of ultrasonic waves measured in suspensions of solid spheres in a viscous matrix. We have used our models to interpret the observed velocity and attenuation of seismic core phases in terms of partial melting in the inner core and at the base of the mantle and partial crystallization in the transition zone between the inner and outer core.

The results of the theoretical analysis are: (1) When the wavelengths are much longer than the size of the inclusions and when the matrix is solid, the effective elastic moduli derived dynamically are the same as those obtained by solving the corresponding static problem. In the non-interaction model, the effective elastic moduli are the same as the lower bounds of Hashin and Shtrikman (1963) and in our classical self-consistent models they are the same as those of Budiansky (1965) for spheres and Wu (1966) for spheroids. (2) When the matrix is a fluid, the effective dynamic and static bulk moduli are different, even when the wavelength is very long compared to the size of an inclusion.

This difference is due to the additional inertia effects stemming from the relative motion of the inclusion and the surrounding fluid.

(3) At intermediate wavelengths the effective properties of a two-phase medium depend on the wavelength and on the length within which interactions among neighboring inclusions are significant. The formulas we derived are of little predictive value on a quantitative basis since this effective interaction length is unknown. However, they indicate qualitatively that a two-phase medium is dispersive. (4) The measured velocities of ultrasonic waves in three separate suspensions of solid spheres in fluids with waves whose wavelength was of the order of fifty inclusion radii, were close to, but systematically below, the values calculated with our model containing the long wavelength approximation. The difference can be explained in terms of the above mentioned dispersive effects. The magnitude of the difference as well as its tendency to increase at larger concentrations indicate that interactions are significant, but only among very near neighboring inclusions (the effective interaction length is about 3 inclusion radii). Experimental data over a broad range of frequencies are needed to provide a more complete test of our theoretical analysis and lead to more general conclusions about the interaction processes. (5) The attenuation measurements with waves that penetrated the earth's core provide a means of exploring the properties of

the core. Attenuation is strong in the inner core and at the base of the mantle, whereas it is small in the outer core and intermediate in the transition zone between the outer and inner core. Joint interpretation of our attenuation data and available velocity models indicate that (a) in the inner core and at the base of the mantle a small amount (less than 5% in volume) of inclusions filled with liquid core material can explain the data; (b) the low velocity gradients in the transition zone are compatible with the presence of solid inclusions suspended in the viscous liquid core, the concentration of inclusions increasing as one approaches the inner core boundary. This interpretation implies that the inner core is slowly growing. The Q values found for the outer core and the transition zone indicate that the viscosity of the liquid core is of the order of 10^8 poises, if all attenuation is attributed to shear viscosity. If this assumption is extended to the inner core, our interpretation of the attenuation in terms of partial melting precludes the observability of phases propagating through the inner core as S waves.

REFERENCES

- Adams, R.D. and M.J. Randall, The fine structure of the earth's core, Bull. Seismol. Soc. Amer., 54, 5, 1299-1313, 1964.
- Aki, K., Scattering mechanism of teleseismic P waves under the Montana LASA, (abstract), Abstracts with Programs, Geol. Soc. Amer., Vol. 4, number 3, p. 121, 1972.
- Ament, W.S., Wave propagation in suspensions, U. S. Naval Res. Lab., Report 5307, 1959.
- Anderson, D.L., A. Ben Menachem and C.B. Archambeau, Attenuation of seismic energy in the upper mantle, J. Geoph. Res., 70, 1441-1448, 1965.
- Anderson, D.L., C. Sammis and T. Jordan, Composition and evolution of the mantle and core, Science, 171, 3976, 1103-1112, 1971.
- Archambeau, C.B., E.A. Flinn and D.G. Lambert, Fine structure of the upper mantle, J. Geoph. Res., 74, 25, 5825-5866, 1969.

- Bland, D.R., The theory of linear viscoelasticity,
Pergamon Press, 1960.
- Bolt, B.A., Structure, composition and state of the
core, EOS, Transactions, Am. Geoph. Union, 52, 5,
175-178, 1971.
- Bolt, B.A., The density distribution near the base of
the mantle and near the earth's center, (reprint),
International Conference on the core-mantle interface,
1972.
- Born, W.T., The attenuation constant of earth materials,
Geophysics, 6, 2, 132-148, 1941.
- Buchbinder, G.G.R., A velocity structure of the earth's
core, Bull. Seismol. Soc. Amer., 61, 2, 429-456,
1971.
- Budiansky, B., On the elastic moduli of some hetero-
geneous materials, J. Mech. Phys. Solids, 13, 233,
1965.
- Bullen, K.E., An introduction to the theory of seismology,
Cambridge University Press, 1965.

Chernov, L.A., Wave propagation in a random medium,
Dover Publications, Inc., New York, 1967.

Dziewonski, A.M. and F. Gilbert, Observations of normal modes from 84 recordings of the Alaskan earthquake of 28 March 1964, in press, Geophys. J. Roy. Astron. Soc., 1972.

Engdahl, E.R., E.A. Flinn and C.F. Romney, Seismic waves reflected from the earth's inner core, Nature, 228, 852-853, 1970.

Epstein, P.S., On the absorption of sound waves in suspensions and emulsions, Theodore Von Karmen Anniversary Volume, 162-188, 1941.

Eshelby, J.D., The determination of the elastic field of an ellipsoidal inclusion, and related problems, Proc. Roy. Soc., A241, 376-396, 1957.

Ewing, W.M., W.S. Jardetzky and F. Press, Elastic waves in layered media, McGraw-Hill Book Co., 1957.

Fleck, P.L., A seismic data analysis console, Technical Note 1968 - 14, Lincoln Lab., Mass. Inst. of Techn., 1968.

Hashin, Z., The elastic moduli of heterogeneous materials, J. Appl. Mech., 29E, 143-150, 1962.

Hashin, Z., Theory of mechanical behavior of heterogeneous media, Appl. Mech. Reviews, 17, 1, 1-9, 1964.

Hashin, Z., Theory of composite materials, Proc. 5th Symposium on Naval Structural Mechanics, May 8-10, 1967, Pergamon Press, 1970.

Hashin, Z. and S. Shtrikman, A variational approach to the theory of the elastic behavior of multiphase materials, J. Mech. Phys. Solids, 11, 127, 1963.

Howe, M.S., Wave propagation in random media, J. Fluid Mech., 45, 4, 769-783, 1971.

Johnson, L.R., Array measurements of P velocities in the lower mantle, Bull. Seismol. Soc. Amer., 59, 2, 973-1008, 1969.

Julian, B.R., D. Davies and R.M. Sheppard, PKJKP, Nature,
vol. 235, 317-318, 1972.

Karal, F.C. and J.B. Keller, Elastic, electromagnetic and
other waves in a random medium, J. Math. Physics,
5, 4, 537-547, 1964.

Knopoff, L., Q, Reviews of Geophysics, 2, 4, 625-660,
1964.

Knudsen, V.O., The propagation of sound in the atmos-
phere, attenuation and fluctuations, J. Acous.
Soc. Amer., 18, 1, 90-96, 1946.

Kuster, G., Sound velocity in fluid-solid suspension,
M.S. thesis, Mass. Inst. of Tech., Cambridge,
1970.

Lamb, H., Hydrodynamics, Dover Publications, New York,
1932.

McDonal, F.J., F.A. Angona, R.L. Mills, R.L. Sengbush,
R.G. Van Nostrand and J.E. White, Attenuation of
shear and compressional waves in Pierre shale
Geophysics, 23, 3, 421-439, 1958.

- Mackenzie, J.K., The elastic constants of a solid containing spherical holes, Proc. Phys. Soc. London, sec. B, vol. 62, 2-11, 1949.
- Mal, A.K. and L. Knopoff, Elastic wave velocities in two-component systems, J. Inst. Maths. Applics., 3, 376-387, 1967.
- Morse, P.M. and H. Feshbach, Methods of theoretical physics, McGraw-Hill Book Co., 1953.
- Nur, A. and G. Simmons, The effect of viscosity of a fluid phase on velocity in low porosity rocks, Earth Plan. Sci. Letters, 7, 99, 1969.
- Press, F., Seismic velocities, in Handbook of Physical Constants, S.P. Clark editor, Geol. Soc. Amer., Memoir 97, 195-218, 1966.
- Press, F., Earth models obtained by Monte Carlo inversion, J. Geoph. Res., 73, 16, 5223-5233, 1968.
- Press, F., Earth models consistent with geophysical data, Phys. Earth Planet. Interiors, 3, 3-22, 1970.

- Qamar, A., Seismic wave velocity in the earth's core: a study of PKP and PKKP, Ph.D. thesis, Univ. of Calif., Berkeley, 1971.
- Qamar, A. and A. Eisenberg, Attenuation in the outer core, (abstract), Abstracts with Programs, Geol. Soc. Amer., vol. 4, number 3, p. 221, 1972
- Reuss, A., Berechnung der Fliessgrenze von Meschkristallen auf Grund der Plastizitätsbedingung für Einkristalle, Angew. Math. u. Mech., 9, 49, 1929.
- Rudd, J.F., Physical constants of polystyrene, in Polymer Handbook, J. Brandrup and E.H. Immergut editors, 1965.
- Sato, R. and A.F. Espinosa, Dissipation in the earth's mantle and rigidity and viscosity in the earth's core determined from waves multiply reflected from the core-mantle boundary, Bull. Seismol. Soc. Amer., 57, 829-856, 1967.
- Schreiber, C., Sound velocity in deep sea sediments, J. Geoph. Res., 73, 1259-1268, 1968.

Shumway, G., Sound speed and absorption studies of marine sediments by a resonance method, Geophysics, 25, 451-467, 659-682, 1960.

Solomon, S.C., Seismic wave attenuation and the state of the upper mantle, Ph.D. thesis, Massachusetts Institute of Technology, Cambridge, 1971.

Solomon, S.C., Seismic-wave attenuation and partial melting in the upper mantle of North America, J. Geoph. Res., 77, 8, 1483-1502, 1972.

Spetzler, H. and D.L. Anderson, Effect of temperature and partial melting on velocity and attenuation in a simple binary system, J. Geoph. Res., 73, 6051-6060, 1968.

Stacey, F.D., Physics of the earth, John Wiley and Sons, Inc., 1969.

Teng, T.L., Body-wave and earthquake source studies, Ph.D. thesis, Calif. Inst. of Tech., Pasadena, 1966.

- Teng, T.L., Attenuation of body waves and the Q structure of the mantle, J. Geoph. Res., 73, 6, 2195-2208, 1968.
- Timur, A., Velocity of compressional waves in porous media at permafrost temperatures, Geophysics, 33, 584-595, 1968.
- Tittman, B.R., M. Abdel-Gawad and R.M. Housley, Rayleigh wave studies of lunar and synthetic rocks, (abstract), Third Lunar Science Conference, 755-757, 1972.
- Todd, T., H. Wang, W.S. Baldrige and G. Simmons, Elastic properties of Apollo 14 and 15 rocks, Proc. Third Lunar Science Conference (in press), 1972.
- Toksoz, M.N., Husebye and R. Wiggins, Structure and properties of the earth's core, to be published in Geophys. J. Roy. Astron. Soc., 1972.
- Verhoogen, J., Heat balance of the earth's core, Geophys. J. Roy. Astron. Soc., 4, 276-281, 1961.
- Walsh, J.B., New analysis of attenuation in partially melted rock, J. Geoph. Res., 74, 17, 4333-4337, 1969.

Weast, R.C., Handbook of Chemistry and Physics, The Chemical Rubber Co., 1971.

Wu, T.T., The effect of inclusion shape on the elastic moduli of a two-phase material, Int. J. Solids Structures, 2, 1-8, 1966.

Wyllie, M.R.J., A.R. Gregory and L.W. Gardner, Elastic wave velocities in heterogeneous and porous media, Geophysics, 21, 41-70, 1956.

Wyllie, M.R.J., A.R. Gregory and G.M.F. Gardner, An experimental investigation of factors affecting elastic wave velocities in porous media, Geophysics, 23, 459-493, 1958.

Yamakawa, N., Scattering and attenuation of elastic waves, Geophysical Magazine (Tokyo), 31, 63-103, 1962.

Appendix A

Scattering of a Plane P Wave by a Spherical Obstacle

Our method of deriving effective properties of a two-phase medium requires the estimation of the waves scattered by the representative sphere or a spherical inclusion (equation 2.9). Here we present the expressions of the scattered waves found by Yamakawa (1962),

Consider a plane P wave incident on a spherical elastic inclusion embedded in an infinite elastic matrix (figure 2.1a). The displacement \underline{u} at any point in the space is the solution of the vector Helmholtz equation if we assume an $e^{i\omega t}$ time dependence for all waves.

$$(\tilde{\lambda} + 2\mu) \text{grad div } \underline{u} - \mu \text{curl curl } \underline{u} + \omega^2 \rho \underline{u} = 0 \quad (\text{A1})$$

where $\tilde{\lambda}, \mu$ and ρ are the Lamé constants and density. Using the Helmholtz theorem

$$\underline{u} = \text{grad } \phi + \text{curl } \underline{A} \quad (\text{A2})$$

and assuming without loss of generality

$$\underline{A} = (r \psi_1, 0, 0) + \text{curl } (r \psi_2, 0, 0) \quad (\text{A3})$$

Equation (A1) reduces to three scalar Helmholtz equations

$$\nabla^2 \phi + p^2 \phi = 0 \quad (\text{A4})$$

$$\nabla^2 \psi_i + s^2 \psi_i = 0 \quad i = 1 \text{ or } 2$$

with $p^2 = \frac{\omega^2 \rho}{\lambda + 2\mu}$ and $s^2 = \omega^2 \rho / \mu$

Because the incident wave is a P wave, and because of the axial symmetry, we can set $\psi_1 = 0$ and we need not consider the ϕ dependence of the solutions in spherical coordinates. Then

$$\phi = \sum_{n=0}^{\infty} K_n f_n(pr) P_n(\cos \theta) e^{-i\omega t} \quad (\text{A5})$$

where K_n are constant coefficients, $P_n(\cos \theta)$ is the Legendre polynomial of order n , p is the wavenumber of a P wave (for ψ the argument of f_n would be sr where s is the wavenumber of an S wave), and f_n is a spherical Bessel or Hankel function; if the solution is to be finite at the origin $f_n(x)$ will be $j_n(x)$ and $h_n^{(1)}(x)$ represents waves travelling outwards.

Let the dilatation due to the plane incident P wave in the matrix be

$$\Delta_0 = A e^{i(pr \cos \theta - \omega t)} \quad (\text{A6})$$

where A is amplitude and p the wavenumber; from here on we omit the $e^{-i\omega t}$ time dependence and primed and unprimed variables refer to inclusion and matrix respectively. The presence of the sphere generates four additional waves; using the series expansion of (A6) and the combination of (A2), (A3) and (A5) we can formulate the problem in spherical coordinates as follows:

Incident P wave:

$$u_0 = -\frac{A}{p^2} \sum_{n=0}^{\infty} (2n+1) i^n \frac{d}{dr} j_n(pr) P_n(\cos \theta) \quad (A7)$$

$$v_0 = -\frac{A}{p^2} \sum_{n=1}^{\infty} (2n+1) i^n \frac{j_n(pr)}{r} \frac{d}{d\theta} P_n(\cos \theta)$$

Scattered P wave:

$$u_1 = -\frac{1}{p^2} \sum_{n=0}^{\infty} B_n \frac{d}{dr} h_n^{(1)}(pr) P_n(\cos \theta) \quad (A8)$$

$$v_1 = -\frac{1}{p^2} \sum_{n=1}^{\infty} B_n \frac{h_n^{(1)}(pr)}{r} \frac{d}{d\theta} P_n(\cos \theta)$$

Scattered S wave:

$$u_2 = -\frac{1}{s^2} \sum_{n=1}^{\infty} C_n n(n+1) \frac{h_n^{(1)}(sr)}{r} P_n(\cos \theta) \quad (A9)$$

$$v_2 = -\frac{1}{s^2} \sum_{n=1}^{\infty} \frac{C_n}{r} \frac{d}{dr} (r h_n^{(1)}(sr)) \frac{d}{d\theta} P_n(\cos \theta)$$

Transmitted P wave:

$$u_3 = -\frac{1}{p'^2} \sum_{n=0}^{\infty} D_n \frac{d}{dr} j_n(p'r) P_n(\cos \theta) \quad (A10)$$

$$v_3 = -\frac{1}{p'^2} \sum_{n=1}^{\infty} \frac{D_n}{r^n} j_n(p'r) \frac{d}{d\theta} P_n(\cos \theta)$$

Transmitted S wave:

$$u_4 = -\frac{1}{s'^2} \sum_{n=1}^{\infty} E_n n(n+1) \frac{j_n(s'r)}{r} P_n(\cos \theta) \quad (A11)$$

$$v_4 = -\frac{1}{s'^2} \sum_{n=1}^{\infty} \frac{E_n}{r} \frac{d}{dr} (r j_n(s'r)) \frac{d}{d\theta} P_n(\cos \theta)$$

where u and v stand respectively for radial and transverse displacement. The boundary conditions at $r=a$ (a is the radius of the sphere) are continuity of displacement and normal stresses.

$$u_0 + u_1 + u_2 = u_3 + u_4$$

$$v_0 + v_1 + v_2 = v_3 + v_4$$

(A12)

$$\tilde{\lambda}(\Delta_0 + \Delta_1) + 2\mu \frac{\partial}{\partial r} (u_0 + u_1 + u_2) = \tilde{\lambda}' \Delta_3 + 2\mu' \frac{\partial}{\partial r} (u_3 + u_4)$$

$$\mu T_e = \mu' T_r$$

where

$$\Delta_j = \frac{1}{r^2 \sin \theta} [(\partial/\partial r)(r^2 \sin \theta u_j) + (\partial/\partial \theta)(r \sin \theta v_j)]$$

$$j = 0, 1 \text{ or } 3$$

(A13)

$$T_e = \frac{\partial}{\partial r} (v_0+v_1+v_2) - \frac{1}{r}(v_0+v_1+v_2) + \frac{1}{r} \frac{\partial}{\partial \theta} (u_0+u_1+u_2)$$

$$T_r = \frac{\partial}{\partial r} (v_3+v_4) - \frac{1}{r}(v_3+v_4) + \frac{1}{r} \frac{\partial}{\partial \theta} (u_3+u_4)$$

Substituting (A7) to (A11) in (A12), we obtain the following vector equation for each $n \geq 1$:

$$-\underline{b}_n B_n + \underline{c}_n C_n + \underline{d}_n D_n - \underline{e}_n E_n = (2n+1) i^n \underline{a}_n A \quad (A14)$$

where

$$\begin{aligned} \underline{b}_n [\tilde{\lambda}, \mu, h_n^{(1)}(y)] &= \underline{a}_n [\tilde{\lambda}, \mu, j_n(y)] \\ \underline{d}_n [\tilde{\lambda}', \mu', j_n(y')] &= \underline{a}_n [\tilde{\lambda}, \mu, j_n(y)] \\ \underline{e}_n [\tilde{\lambda}', \mu', j_n(z')] &= \underline{c}_n [\tilde{\lambda}, \mu, h_n^{(1)}(z)] \end{aligned} \quad (A15)$$

$$y=pa \qquad y'=p'a$$

$$z=sa \qquad z'=s'a$$

$$\underline{a}_n [\tilde{\lambda}, \mu, j_n(y)] = \begin{cases} [2\mu(n+1)(n+2)/y^2 - (\tilde{\lambda}+2\mu)] j_n(y) - (4\mu/y) j_{n-1}(y) \\ \frac{2\mu}{y^2} [y j_{n-1}(y) - (n+2) j_n(y)] \\ \frac{1}{y} j_{n-1}(y) - \frac{(n+1)}{y^2} j_n(y) \\ \frac{j_n(y)}{y^2} \end{cases} \quad (A16)$$

$$c_{-n}[\tilde{\lambda}, \mu, h_n^{(1)}(z)] = \begin{cases} \frac{2\mu n(n+1)}{z^2} [(n+2)h_n^{(1)}(z) - zh_{n-1}^{(1)}(z)] \\ \frac{\mu}{z^2} [2zh_{n-1}^{(1)}(z) + (z^2 - 2(n+2)n)h_n^{(1)}(z)] \\ - \frac{n(n+1)}{z^2} h_n^{(1)}(z) \\ \frac{n}{z^2} h_n^{(1)}(z) - \frac{h_{n-1}^{(1)}(z)}{z} \end{cases} \quad (A17)$$

When $n = 0$, (A14) becomes a two-row vector equation

$$-\underline{b}_0 B_0 + \underline{d}_0 D_0 = \underline{a}_0 A \quad (A18)$$

$$\text{where } \underline{a}_0[\tilde{\lambda}, \mu, j_n(y)] = \begin{cases} \frac{4\mu}{y} j_1(y) - (\tilde{\lambda} + 2\mu) j_0(y) \\ - \frac{j_1(y)}{y} \end{cases} \quad (A19)$$

and where \underline{b}_0 and \underline{d}_0 can be obtained from \underline{a}_0 by using (A15).

We can solve system (A14) and (A18) by Cramer's rule for the coefficients B_n, C_n, D_n, E_n for all n . It is therefore formally possible to obtain exact solutions for the scattered waves in the form of infinite series; the solution depends on the properties of the matrix and inclusion, on the radius of the sphere and the frequency of the incident wave.

In general we shall use the far field expressions of the scattered waves; using the asymptotic formula for large argument ($x \gg 1$)

$$h_n^{(1)}(x) = (-i)^{n+1} \frac{e^{ix}}{x} \quad (\text{A20})$$

we obtain the following results:

For the scattered P waves

$$u = -\frac{1}{p^2} \frac{e^{ipr}}{r} \sum_{n=0}^{\infty} i^{3n} B_n P_n(\cos \theta) \quad (\text{A21})$$

For the scattered S wave

$$v = -\frac{1}{s^2} \frac{e^{isr}}{r} \sum_{n=1}^{\infty} i^{3n} C_n \frac{d}{d\theta} P_n(\cos \theta) \quad (\text{A22})$$

Of particular importance to us is the expression of the scattered waves when the wavelengths are much larger than the inclusion radius; if y, y', z, z' are all very small we can use the expansions of the spherical functions for small arguments (Yamakawa, 1962).

When $x \ll 1$

$$j_n(x) \approx \frac{2^n n!}{(2n+1)!} x^n \left[1 - \frac{x^2}{2(2n+3)} + \frac{x^4}{8(2n+3)(2n+5)} \right]$$

$$h_0^{(1)}(x) \approx -\frac{i}{x} + 1 + \frac{ix}{2} \quad (\text{A23})$$

$$h_n^{(1)}(x) \approx -i \frac{(2n)!}{2^n n! x^{n+1}} \left[1 + \frac{x^2}{2(2n-1)} \right]$$

$$n \geq 1$$

Substituting (A23) in (A15), (A16), (A17) and (A19), we solve the systems (A14) and (A20) for each n , retaining only the lowest order terms; the coefficients in the expansions of the scattered P waves are

$$B_0 = Aiy^3 \frac{K-K'}{3K'+4\mu}$$

$$B_1 = Ay^3 \frac{\rho-\rho'}{3\rho} \quad (\text{A24})$$

$$B_2 = \frac{20A}{3} i Y^3 \frac{\mu(\mu'-\mu)}{\mu(9K+8\mu) + 6\mu'(K+2\mu)}$$

where $K = \tilde{\lambda} + 2\mu/3$; and for $n \geq 3$,

$$(\text{A25}) \quad B_n = \frac{-i^{n+1} A \ 2n(n-1)(2n+1)(2n-1) [2^n n! / (2n)!]^2 \ \mu(\mu'-\mu) y^{2n-1}}{2(n-1)(3n+2)\mu\mu' + 2(n+1)(n-1)\tilde{\lambda}\mu' + (2n^2+1)\tilde{\lambda}\mu + 2(n^2+n+1)\mu^2}$$

For the scattered S waves they are given by

$$(\text{A26}) \quad C_n = (z/y)^{n+3} (B_n/n) \quad n \geq 1$$

All coefficients with $n \geq 3$ are negligible compared

to B_0 , B_1 , B_2 , C_1 and C_2 because the latter are of lower order in y . Thus we obtain the following important result: when all wavelengths are much longer than the radius of the spherical obstacle, the series expansions giving the scattered P and S waves in the far field can be approximated by keeping only the first few terms. Then the scattered P wave is

$$u = - \frac{iA}{p^2} (pa)^3 \frac{e^{i(pr-\omega t)}}{r} [Be_0 - Be_1 \cos \theta - \frac{Be_2}{4} (3 \cos 2\theta + 1)] \quad (A27)$$

and the scattered S wave is

$$v = - \frac{iA(sa)^3}{sp} \frac{e^{i(sr-\omega t)}}{r} [Be_1 \sin \theta + \frac{3s}{4p} Be_2 \sin 2\theta] \quad (A28)$$

$$\text{where } Be_0 = \frac{K-K'}{3K' + 4\mu} \quad (A29)$$

$$Be_1 = \frac{\rho-\rho'}{3\rho} \quad (A30)$$

$$Be_2 = \frac{20}{3} \frac{\mu(\mu'-\mu)}{6\mu'(K+2\mu) + \mu(9K+8\mu)} \quad (A31)$$

The above results were derived for a solid sphere in a solid matrix; they are applicable to the cases of a fluid sphere ($\mu'=0$) or a spherical cavity ($\tilde{\lambda}'=\mu'=\rho'=0$) in a solid matrix by making the appropriate modifications in the final results (A29), A(30) and (A31). However, when the matrix is a fluid ($\mu=0$), this procedure cannot be used.

Suppose for simplicity that the inclusion is also fluid; then (A9) and (A11) are to be omitted and the second and fourth boundary conditions in (A12) are not required. Making use of the long wavelength approximation (equations A23), we obtain the following systems of equations. For $n=0$

$$\frac{i\tilde{\lambda}}{Y} B_0 + \tilde{\lambda}' D_0 = \tilde{\lambda} A \quad (\text{A32})$$

$$\frac{i}{Y^3} B_0 + \frac{D_0}{3} = \frac{A}{3}$$

which gives, since $K=\tilde{\lambda}$ for a fluid,

$$B_0 = Aiy^3 \frac{K-K'}{3K'} \quad (\text{A33})$$

For $n = 2$

$$-3i\tilde{\lambda} \frac{B_2}{Y} - \tilde{\lambda}' Y'^2 \frac{D_2}{15} = \tilde{\lambda} Y^2 \frac{A}{3} \quad (\text{A34})$$

$$-\frac{9i}{Y^3} B_2 + \frac{2D_2}{15} = -\frac{2A}{3}$$

which gives

$$B_2 = \frac{2iAy^5}{9} \frac{(\rho-\rho')}{3\rho'+2\rho} \quad (\text{A35})$$

B_2 is of order y^5 and therefore negligible in our

approximation. This result as well as (A33) could have been obtained from (A24) by setting $\mu=0$. But for $n=1$ we have

$$\frac{i\tilde{\lambda}}{y^2} B_1 + \frac{\tilde{\lambda}'}{3} y' D_1 = iA\tilde{\lambda}y \quad (\text{A36})$$

$$-\frac{2i}{y} B_1 + \frac{D_1}{3y'} = \frac{iA}{y}$$

which gives

$$B_1 = Ay^3 \frac{\rho - \rho'}{\rho + 2\rho'} \quad (\text{A37})$$

This result is different from the one in (A24). This difference can be interpreted as follows. In the long wavelength approximation, the waves scattered by the sphere are the same as the waves one would observe if the sphere was replaced by a system of three sources. The simple radial source whose strength is B_0 represents the periodic variations in the volume of the inclusion. B_1 is the strength of a single force source which expresses the change in inertia due to the replacement of matrix material by inclusion material. When the matrix is solid, the change in inertia arises only from the density difference since there is no relative motion between matrix and inclusion

(all displacements are continuous across the boundary);
but when the matrix is a fluid, relative motion does
occur and the net effect of the fluid motion is to increase
the inertia of the sphere (Lamb, art. 92, 298 and 300).
(A37) was derived by taking a fluid inclusion for simplicity,
but one would obtain the same results if the inclusion is
solid, as long as the matrix is fluid.

APPENDIX B: SELF-CONSISTENT MODELS

In this appendix we derive the effective properties when a self-consistent scheme is used to take interactions into account.

We recall that with our method of derivation, the effective laws will contain the effect of interactions if we can compute the wave scattered by an individual inclusion without neglecting multiple scattering from the neighbouring inclusions. At the surface of an inclusion we can write the boundary condition as

$$\underline{\tilde{u}} + \underline{\tilde{u}}_S = \underline{\tilde{u}}_T \quad (\text{B1})$$

where $\underline{\tilde{u}}$, $\underline{\tilde{u}}_S$, $\underline{\tilde{u}}_T$ are six-row vectors whose elements are the three displacements and the three normal stresses. $\underline{\tilde{u}}$ refers to a wave travelling in the matrix towards the inclusion, it is the superposition of the original incident wave and all multiply scattered waves (including back-scattering); $\underline{\tilde{u}}_S$ is the scattered wave which we want to estimate. $\underline{\tilde{u}}_T$ is the wave inside the inclusion. Each one of $\underline{\tilde{u}}$, $\underline{\tilde{u}}_S$, $\underline{\tilde{u}}_T$ is completely determined by three potentials (See Equations A1 to A4 in Appendix A). In general, the boundary condition (B1)

is a system of six equations with nine unknowns. The solution is possible only if either $\underline{\tilde{u}}$ or $\underline{\tilde{u}}_T$ is known. When neglecting interactions we assumed $\underline{\tilde{u}}$ was known and that it was the original incident wave. But when multiple scattering is included, it seems very difficult to estimate $\underline{\tilde{u}}$, even in an average sense. Therefore, we attempt to estimate the wave inside the inclusion without neglecting interactions.

We assume that in an average sense the effect of multiple scattering on the wave inside an inclusion can be represented with a self-consistent scheme. The wave inside is found by solving the boundary conditions when a plane P wave is incident on the geometry shown on Figure 2.3. The radius b of the matrix shell is treated as a free parameter, but it is assumed that b^3 is much smaller than R^3 , R being the radius of the representative sphere with effective properties. Because of the axial symmetry we can again omit the φ dependence and since we want only the far field expression of the scattered wave, the wavelength being of course much larger than R , we need only the first three terms in the series expression of the wave inside the inclusion. The solution involves very long algebra for $n = 1$ and $n = 2$ (12 by 12 determinants), and we will only give the final result for the density and shear modulus laws, but we give in detail the calculation for $n = 0$, which yields the effective bulk modulus.

In general, the waves to be considered for solving the problem, illustrated in Figure 2.2, are

- (i) in the infinite matrix, the incident plane P wave and the scattered P and S waves
- (ii) in the shell of effective properties, ingoing and outgoing P and S waves
- (iii) in the shell of matrix material, ingoing and outgoing P and S waves
- (iv) in the inclusion, transmitted P and S waves.

All waves can be expanded in series (cf. Appendix A), and at each boundary ($r=R$, $r=b$, $r=a$) the boundary conditions are those written in Equation A12. Therefore, we obtain a system of 12 equations with 12 unknowns for an arbitrary n . As seen in Appendix A, the ingoing waves in the shells depend on the Hankel function of the second kind.

The term $n=0$ is missing in the expansions of the S waves and the transverse displacement of P waves. Thus the boundary conditions for $n=0$ reduce to a system of 6 equations with 6 unknowns.

Using the equality

$$h_n^{(2)}(x) + h_n^{(1)}(x) = 2j_n(x) \quad (\text{B2})$$

and the expansions for small argument (long wavelength approximation) given in Appendix A (Equation A23) and retaining only the lowest-order terms, we can write the system of 6 equations as

$$\begin{bmatrix}
 -\frac{i}{Y_R^3} & -\frac{2}{3} & \frac{i}{Y_R^{*3}} & 0 & 0 & 0 \\
 \frac{4i\mu}{Y_R^3} & -2K^* & -\frac{4i\mu^*}{Y_R^{*3}} & 0 & 0 & 0 \\
 0 & \frac{2}{3} & -\frac{i}{Y_b^{*3}} & -\frac{2}{3} & \frac{i}{Y_b^3} & 0 \\
 0 & 2K^* & \frac{4i\mu^*}{Y_b^{*3}} & -2K & -\frac{4i\mu}{Y_b^3} & 0 \\
 0 & 0 & 0 & \frac{2}{3} & -\frac{i}{Y_a^3} & -\frac{1}{3} \\
 0 & 0 & 0 & 2K & \frac{4i\mu}{Y_a^3} & -K'
 \end{bmatrix}
 \begin{bmatrix}
 P_0 \\
 Q_0 \\
 R_0 \\
 S_0 \\
 T_0 \\
 U_0
 \end{bmatrix}
 =
 \begin{bmatrix}
 -\frac{A}{3} \\
 -AK \\
 0 \\
 0 \\
 0 \\
 0
 \end{bmatrix}
 \quad (B3)$$

where

$$\begin{aligned}
 Y_R &= 2\pi R/\lambda \\
 Y_b &= 2\pi b/\lambda \\
 Y_a &= 2\pi a/\lambda \\
 Y_R^* &= 2\pi R/\lambda^* \\
 Y_b^* &= 2\pi b/\lambda^*
 \end{aligned}
 \quad (B4)$$

R , b , a are the radii of the representative sphere, the matrix shell and the inclusion respectively; λ and λ^* are the wavelengths of P waves in matrix and effective materials; μ and K refer to shear and bulk modulus; A is the amplitude of the incident wave; P_0 , Q_0 , R_0 , S_0 , T_0 , U_0 are the coefficients for

$n = 0$ in the series expansions of respectively the wave scattered in the infinite matrix, the ingoing and outgoing wave in the shell of effective material, the ingoing and outgoing wave in the matrix shell and the wave inside the inclusion. The latter is what we want to find. Using Cramer's rule and neglecting b^3/R^3 and a^3/R^3 with respect to 1, we have

$$U_0 = \frac{(3K^*+4\mu^*)(3K+4\mu)^2 A}{(3K+4\mu^*)(3K^*+4\mu)(3K'+4\mu) + 12(K-K')(\mu^*-\mu)(3K^*+4\mu)d^3} \quad (B5)$$

where $d^3 = a^3/b^3$.

Knowing the wave inside, we can find the wave scattered by this inclusion when it is isolated in the matrix with an unknown incident wave. The system to solve is

$$\begin{bmatrix} -\frac{i}{3} & -\frac{1}{3} \\ y_a & \end{bmatrix} \begin{bmatrix} B_0 \\ U_0 \end{bmatrix} = \begin{bmatrix} -\frac{I_0}{3} \\ -KI_0 \end{bmatrix} \quad (B6)$$

We find

$$B_0 = iy_a^3 U_0 \frac{K-K'}{3K+4\mu} \quad (B7)$$

where B_0 is the coefficient of the scattered P wave. Combining (B5) and (B7) we have

$$B_0 = iy_a^3 A \frac{(K-K') (3K^*+4\mu^*) (3K+4\mu)}{(3K^*+4\mu) [(3K+4\mu^*) (3K'+4\mu) + 12(K-K') (\mu^*-\mu) d^3]} \quad (B8)$$

Since U_0 contains the effect of interactions through the self-consistent scheme, so will B_0 . Equating the wave scattered by the representative sphere and the sum of all waves scattered by the inclusions we obtain the effective bulk modulus by using

$$B_0^* = \sum_{j=1}^N B_0^j \quad (B9)$$

where B_0^j is given by (B8). The wave scattered by the representative sphere is defined in terms of effective properties of the composite medium:

$$B_0^* = iy_R^3 A \frac{K-K^*}{3K^*+4\mu} \quad (B10)$$

Thus

$$K^* = K + \frac{c(K'-K) (3K^*+4\mu^*) (3K+4\mu)}{(3K+4\mu^*) (3K'+4\mu) + 12(K-K') (\mu^*-\mu) d^3} \quad (B11)$$

In general, the effective bulk modulus depends on the radius of the matrix shell. For $d = 1$, the result corresponds to the classical self-consistent scheme:

$$K^* = K + \frac{c(K'-K) (3K^*+4\mu^*)}{3K'+4\mu^*} \quad (B12)$$

When $d^3 = c$, which is the analog of Hashin's spherical composite element assumption, we obtain the same result as when interactions are neglected

$$K^* = K + \frac{c(K' - K)}{1 + \frac{3(K' - K)(1 - c)}{3K + 4\mu}} \quad (\text{B13})$$

Solving the boundary conditions for $n = 1$, we obtain the effective law on densities

$$\rho^* = \rho(1 - c) + \rho'c \quad (\text{B14})$$

It is independent of d which is not surprising since the term for $n = 1$ in the expansion of the wave inside is the same as that in the expansion of the incident wave under the long wavelength approximation (See Appendix C, Equations C34 to C36).

The algebra involved in obtaining the effective shear modulus is extremely complicated. The final result is

$$\mu^* - \mu = - \frac{7c(\tilde{\lambda}^* + 2\mu^*)(\tilde{\lambda} + 2\mu)\mu'}{24\mu(\mu' - \mu)f^2} X$$

where

$$X = \frac{A + Bd^5 + Cd^7}{D + Ed^3 + Fd^5 + Gd^7 + Hd^{10}} \quad (\text{B15})$$

with

$$d = a/b \quad f = 19\tilde{\lambda}'\mu' + 16\tilde{\lambda}'\mu + 14\mu'^2 + 56\mu\mu'$$

$$A = fg/14$$

$$B = 84(\tilde{\lambda}+\mu)(\tilde{\lambda}'+\mu')(\mu-\mu^*)(\mu-\mu')$$

$$C = -B + \frac{4(\mu-\mu^*)}{7} [f(2\tilde{\lambda}+7\mu) - 35\mu(\tilde{\lambda}+2\mu)(2\tilde{\lambda}'+7\mu')]$$

$$D = -\frac{gk\ell}{210 \times 36\mu^2\mu^*(\mu'-\mu)}$$

$$\begin{aligned} 252\mu\mu^*E &= -(\tilde{\lambda}+2\mu)(3\tilde{\lambda}'+8\mu^*)g + k[(3\tilde{\lambda}+8\mu)(5\tilde{\lambda}+7\mu)(8\mu^*-\mu) \\ &\quad - 21\mu(\lambda+\mu)(3\tilde{\lambda}+8\mu^*)]/16\mu \end{aligned}$$

$$F = \frac{2k}{15\mu^2} (\tilde{\lambda}+\mu)^2 (\mu-\mu^*)$$

$$945\mu^2\mu^*(\mu'-\mu)G = (\mu^*-\mu)k[(\tilde{\lambda}+\mu)63(\mu'-\mu) + (2\tilde{\lambda}+7\mu)\ell]$$

$$\begin{aligned} 945\mu^*\mu^2H &= 2(\mu^*-\mu)(2\tilde{\lambda}+7\mu)[\mu(9\tilde{\lambda}+14\mu)(3\tilde{\lambda}'+8\mu^*) - \\ &\quad - \mu^*(3\tilde{\lambda}+8\mu)(9\tilde{\lambda}'+14\mu^*)] \end{aligned}$$

$$f = 19\tilde{\lambda}'\mu' + 16\tilde{\lambda}'\mu + 14\mu'^2 + 56\mu\mu'$$

$$g = 19\tilde{\lambda}\mu + 16\tilde{\lambda}\mu^* + 14\mu^2 + 56\mu\mu^*$$

$$k = 6\tilde{\lambda}^*\mu + 16\mu\mu^* + 9\tilde{\lambda}^*\mu^* + 14\mu^*{}^2$$

$$\ell = 6\tilde{\lambda}\mu' + 16\mu\mu' + 9\tilde{\lambda}\mu + 14\mu^2$$

For an arbitrary value of d , μ^* and K^* have to be found numerically from (B11) and (B15).

APPENDIX C: SCATTERING BY SPHEROIDAL INCLUSIONS

In this appendix we derive the effective properties of a two-phase medium containing spheroidal inclusions. The method is discussed in Chapter 2 (Equation 2.9). It relies on the estimation of the waves scattered by the representative sphere on one hand and an individual inclusion on the other.

1. Isolated Inclusion of Arbitrary Shape.

Consider an elastic body of arbitrary shape imbedded in an infinite elastic medium. Let the incident wave have an $e^{i\omega t}$ time dependence, which we shall suppress for brevity. The displacement outside and inside the volume V occupied by the inclusion can be written as:

Outside the inclusion

$$\underline{u}(\underline{x}) = \underline{u}^0(\underline{x}) + \underline{\Delta u}(\underline{x}) \quad (C1)$$

Inside the inclusion

$$\underline{v}(\underline{x}) = \underline{u}^0(\underline{x}) + \underline{\Delta v}(\underline{x}) \quad (C2)$$

where $\underline{u}_0 =$ incident field. $\underline{\Delta u}$ and $\underline{\Delta v}$ are the scattered displacement fields. \underline{u} , \underline{u}^0 and $\underline{\Delta u}$ satisfy the same wave equation

$$c_{ijpq} \frac{\partial^2 u_p}{\partial x_q \partial x_j} + \rho \omega^2 u_i(\underline{x}) = 0 \quad (C3)$$

and v satisfies

$$c'_{ijpq} \frac{\partial^2 v_p}{\partial x_q \partial x_j} + \rho' \omega^2 v_i(\underline{x}) = 0 \quad (C4)$$

where primed and unprimed variables refer to inclusion and matrix material (both assumed homogeneous), ρ is density and

$$c_{ijpq} = \tilde{\lambda} \delta_{ij} \delta_{pq} + \mu (\delta_{ip} \delta_{jq} + \delta_{iq} \delta_{jp}) \quad (C5)$$

with $\tilde{\lambda}$ and μ being Lamé's constants and δ_{ij} the Kronecker delta. The boundary conditions at the surface S of the inclusion are

$$\underline{\Delta u}(\underline{\eta}) = \underline{\Delta v}(\underline{\eta})$$

$$c_{ijpq} \left(\frac{\partial \Delta v_p}{\partial \eta_q} - \frac{\partial \Delta u_p}{\partial \eta_q} \right) n_j = -\Delta c_{ijpq} \frac{\partial v_p}{\partial \eta_q} n_j \quad (C6)$$

where $\underline{\eta}$ is a point on S , \underline{n} is the outward unit normal at $\underline{\eta}$ and $\Delta c_{ijpq} = c'_{ijpq} - c_{ijpq}$. Then one can write the total field outside V as follows (Mal and Knopoff, 1967)

$$u_k(\underline{x}) = u_k^0(\underline{x}) + \int_V \left[\omega^2 \Delta \rho v_i(\underline{z}) G_{ki}(\underline{x}, \underline{z}) + \Delta c_{ijpq} \frac{\partial v_p}{\partial z_q} \frac{\partial G_{ki}}{\partial x_j} \right] dz \quad (C7)$$

where $\Delta\rho = \rho' - \rho$ and $G_{ki}(\underline{x}, \underline{z})$ is the i th component of the Green's function due to a point force acting in the k th direction at a point \underline{z} in the infinite matrix. If the field inside is known, the scattered field is computable.

2. Spherical Inclusion--Long Wavelength Limit

Assume that the obstacle is a sphere and that its radius is much smaller than the wavelength of the incident wave. The displacement inside the sphere can be estimated by Born's approximation

$$\underline{v}(\underline{z}) \approx \underline{u}^0(\underline{y}) \quad (\text{C8})$$

where \underline{y} is the center of the sphere. It is shown by Mal and Knopoff (1967) that the lowest-order approximation to the strain inside is given by

$$e_{kl} = (\tilde{P} - \tilde{Q}) \frac{e_{ii}^0}{3} \delta_{kl} + \tilde{Q} e_{kl}^0 \quad (\text{C9})$$

where

$$e_{kl} = \frac{1}{2} \lim_{\underline{z} \rightarrow \underline{y}} \left(\frac{\partial v_k}{\partial z_l} + \frac{\partial v_l}{\partial z_k} \right) \quad (\text{C10})$$

$$e_{kl}^0 = \frac{1}{2} \lim_{\underline{z} \rightarrow \underline{y}} \left(\frac{\partial u_k^0}{\partial z_l} + \frac{\partial u_l^0}{\partial z_k} \right) \quad (\text{C11})$$

$$\tilde{P} = \frac{3K + 4\mu}{3K' + 4\mu} \quad \tilde{Q} = \frac{5\mu(3K + 4\mu)}{6\mu'(K+2\mu) + \mu(9K+8\mu)} \quad (C12)$$

where K and μ are the bulk and shear moduli. This approximation is valid for any contrast of the matrix and inclusion moduli. The same result was obtained by Eshelby (1961) for the static strain inside a sphere when a uniform strain is applied at infinity. We shall make use of this relationship later.

Because of the symmetries of the c_{ijpq} tensor (Equation C5) we have

$$\Delta c_{ijpq} \frac{\partial v_p}{\partial z_q} = \Delta \tilde{\lambda} e_{pp} \delta_{ij} + 2\Delta \mu e_{ij} \quad (C13)$$

and by use of (C9)

$$\Delta c_{ijpq} \frac{\partial v_p}{\partial z_q} \approx (\tilde{P}\Delta K - \frac{2}{3}\tilde{Q}\Delta\mu) e_{pp}^0 \delta_{ij} + 2\tilde{Q}\Delta\mu e_{ij}^0 \quad (C14)$$

Introducing (C8) and (C14) into (C7) we can write the lowest-order approximation to the scattered field as

$$\Delta u_k(\underline{x}, \underline{y}) = V \left[\omega^2 \Delta \rho u_i^0(\underline{y}) G_{ki}(\underline{x}, \underline{y}) - \delta_{ij} \left(\tilde{P}\Delta K - \frac{2}{3}\tilde{Q}\Delta\mu \right) e_{pp}^0 \frac{\partial G_{ki}}{\partial y_i} - 2\tilde{Q}\Delta\mu e_{ij}^0 \frac{\partial G_{ki}}{\partial y_j} \right] \quad (C15)$$

3. Spheroidal Inclusion--Long Wavelength Approximation

Equation (C7) is valid for any shape of the inclusion. The displacement inside the spheroid can also be approximated by (C8) if we assume that the wavelength is much larger than the inclusion size. Eshelby (1957) has computed the strain inside an oblate spheroid when a uniform strain is applied at infinity. For an arbitrary orientation of the spheroid with respect to the fixed coordinate system taken for the matrix, the static field inside is given by

$$e_{ij} = U_{ijkl} e_{kl}^0 \quad (C16)$$

where

$$U_{ijkl} = l_{\alpha i} l_{\beta j} l_{\gamma k} l_{\delta l} T_{\alpha\beta\gamma\delta} \quad (C17)$$

The l_{mn} are direction cosines and $T_{\alpha\beta\gamma\delta}$ is a fourth-order tensor; the exact expression of each of its terms is not needed for the time being, but its symmetries are important. They are, for an oblate spheroid

$$\begin{aligned} T_{1111} &= T_{2222} & T_{1133} &= T_{2233} \\ T_{1122} &= T_{2211} & T_{3322} &= T_{3311} \\ T_{1212} &= T_{1221} = T_{2121} = T_{2112} & & \\ T_{1313} &= T_{1331} = T_{3113} = T_{3131} & & \\ T_{2323} &= T_{2332} = T_{3223} = T_{3232} & & \end{aligned} \quad (C18)$$

We also have the relation

$$T_{1111} - T_{1122} - 2T_{1212} = 0 \quad (C19)$$

The scalars T_{iijj} and T_{ijij} are important in the following analysis; their expressions are

$$T_{iijj} = \frac{3F_1}{F_2} \quad (C20)$$

$$T_{ijij} - \frac{1}{3}T_{iijj} = \frac{2}{F_3} + \frac{1}{F_4} + \frac{F_4 F_5 + F_6 F_6 - F_8 F_9}{F_2 F_4}$$

$$F_1 = 1 + A \left[\frac{3}{2}(g+\phi) - R \left(\frac{3}{2}g + \frac{5}{2}\phi - \frac{4}{3} \right) \right]$$

$$F_2 = 1 + A \left[1 + \frac{3}{2}(g+\phi) - \frac{R}{2}(3g+5\phi) \right] + B(3-4R) \\ + \frac{A}{2}(A+3B)(3-4R) \left[g + \phi - R(g-\phi+2\phi^2) \right]$$

$$F_3 = 1 + \frac{A}{2} \left[R(2-\phi) + \frac{(1+\tilde{\alpha}^2)}{\tilde{\alpha}^2} g(R-1) \right]$$

$$F_4 = 1 + \frac{A}{4} \left[3\phi + g - R(g-\phi) \right]$$

$$F_5 = A \left[R\left(g + \phi - \frac{4}{3}\right) - g \right] + B\phi(3-4R)$$

$$F_6 = 1 + A \left[1 + g - R(g+\phi) \right] + B(1-\phi)(3-4R)$$

$$F_7 = 2 + \frac{A}{4} \left[9\phi + 3g - R(5\phi+3g) \right] + B\phi(3-4R)$$

$$F_8 = A \left[1 - 2R + \frac{g}{2}(R-1) + \frac{\phi}{2}(5R-3) \right] + B(1-\phi)(3-4R)$$

$$F_9 = A \left[g(R-1) - R\phi \right] + B\phi(3-4R)$$

$$A = \frac{\mu'}{\mu} - 1$$

$$B = \frac{1}{3} \left(\frac{K'}{K} - \frac{\mu'}{\mu} \right)$$

$$R = \frac{3\mu}{3K + 4\mu}$$

$$\phi = \frac{\tilde{\alpha}}{(1 - \tilde{\alpha}^2)^{3/2}} [\cos^{-1} \tilde{\alpha} - \tilde{\alpha}(1 - \tilde{\alpha}^2)^{1/2}]$$

$$g = \frac{\tilde{\alpha}^2}{1 - \tilde{\alpha}^2} (3\phi - 2)$$

Now Mal and Knopoff showed that the lowest-order approximation to the strain inside a sphere in the dynamic case is the same as Eshelby's exact result in the static case. By analogy, we assume that this is also true when the inclusion is an oblate spheroid. Using (C8), (C13) and (C16) in (C7) we obtain

$$\Delta u_k(\underline{x}, \underline{y}) = \omega^2 u_i^0(\underline{y}) \int_V G_{ki}(\underline{x}, \underline{z}) d\underline{z} + \quad (C21)$$

$$\left[\Delta \tilde{\lambda} U_{pprs} e_{rs}^0 \delta_{ij} + 2\Delta \mu U_{ijrs} e_{rs}^0 \right] \frac{\partial}{\partial x_j} \int_V G_{ki}(\underline{x}, \underline{z}) d\underline{z}$$

The integrals in (C21) can be easily evaluated when $r = |\underline{x} - \underline{y}|$ is large:

$$\int_V G_{ki}(\underline{x}, \underline{z}) d\underline{z} \approx V G_{ki}(\underline{x}, \underline{y}) \quad (C22)$$

Then at a large distance from the inclusion, the lowest-order approximation to the field scattered by an oblate spheroid of arbitrary orientation can be written as

$$\Delta u_{\underline{k}}(\underline{x}, \underline{y}) = V \left[\omega^2 \Delta \rho u_i^0(\underline{y}) G_{ki}(\underline{x}, \underline{y}) - \left(\Delta \tilde{\lambda} \delta_{ij} U_{pprs} + \right. \right. \\ \left. \left. + 2 \Delta \mu U_{ijrs} \right) e_{rs}^0 \frac{\partial}{\partial y_j} G_{ki}(\underline{x}, \underline{y}) \right] \quad (C23)$$

4. Effective Properties: Non-Interaction Model

Consider a quasi-homogeneous and quasi-isotropic two-phase medium where the inclusions are oblate spheroids. For an isotropic model, we can take a sphere as the representative volume element. Then the scattered wave expressed in terms of the effective properties is given by (C15)

$$\Delta u_{\underline{k}}^*(\underline{x}, \underline{y}) = V \left\{ \omega^2 (\rho^* - \rho) u_i^0(\underline{y}) G_{ki}(\underline{x}, \underline{y}) - \right. \\ \left. - \frac{\partial G_{ki}}{\partial y_j} \left[\delta_{ij} e_{pp}^0 (\tilde{P}^* (K^* - K) - \frac{2}{3} \tilde{Q}^* (\mu^* - \mu)) + 2 \tilde{Q}^* (\mu^* - \mu) e_{ij}^0 \right] \right\} \quad (C24)$$

where

$$\tilde{P}^* = \frac{3K + 4\mu}{3K^* + 4\mu} \quad \tilde{Q}^* = \frac{5\mu(3K + 4\mu)}{6\mu^*(K + 2\mu) + \mu(9K + 8\mu)}$$

We assume that all interactions can be neglected so that the field incident on each spheroid is also \underline{u}^0 . Because the medium is quasi-isotropic, the orientation of the spheroids must be uniform over all directions. Then the sum of the fields scattered by all inclusions in the representative sphere is

$$\Delta u_k^T(\underline{x}, \underline{y}) = \left\{ \omega^2 (\rho' - \rho) u_i^0(\underline{y}) G_{ki}(\underline{x}, \underline{y}) \right. \\ \left. - \left[\delta_{ij} A_{pprs} (\tilde{\lambda}' - \tilde{\lambda}) + 2(\mu' - \mu) A_{ijrs} \right] e_{rs}^0 \frac{\partial G_{ki}}{\partial y_j} \right\} \sum_{n=1}^N V_n \quad (C25)$$

where V_n is the volume of the nth inclusion, N is the total number of inclusions and

$$A_{ijkl} = \frac{1}{4\pi} \int_0^\pi \sin \theta \, d\theta \int_0^{2\pi} U_{ijkl} \, d\varphi \quad (C26)$$

In obtaining (C25) it is also assumed that each inclusion is approximately located at the center of the representative sphere since the observation point is at a large distance. The effective laws are obtained by equating (C25) and (C24) and setting

$$\frac{1}{V} \sum_{n=1}^N V_n = c$$

the volume concentration of inclusions.

The first term yields the density law

$$\rho^* - \rho = (\rho' - \rho)c \quad (C27)$$

and the last term yields the effective elastic constants.

Let the incident field be purely dilational.

$$e_{ij}^0 = e \delta_{ij} \quad (C28)$$

The effective law is then

(C29)

$$3e\tilde{P}^*(K^*-K)G_{ki,i} = c \left(2(u'-\mu)A_{ijnn} + \delta_{ij}(\tilde{\lambda}'-\tilde{\lambda})A_{ppnn} \right) eG_{ki,j}$$

From the symmetries of the tensor $T_{\alpha\beta\gamma\delta}$ and the integration in (C26) we find that

$$A_{ppnn} = \frac{1}{3} T_{iijj} \quad (C30)$$

$$A_{ijnn} = 0 \quad \text{if } i \neq j$$

Finally, by combining (C29) and (C30) we obtain

$$\frac{K^* - K}{3K^* + 4\mu} = c \frac{K' - K}{3K + 4\mu} \frac{T_{iijj}}{3} \quad (C31)$$

The effective shear modulus law is obtained in a very similar way by taking the incident field as

$$e_{ij}^0 = \begin{cases} 0 & i = j \\ e & i \neq j \end{cases} \quad (C32)$$

and making use of (C19). Then

$$\frac{\mu^* - \mu}{6\mu^*(K+2\mu) + \mu(9K+8\mu)} = \frac{c(\mu' - \mu)}{25\mu(3K+4\mu)} \left(T_{ijij} - \frac{1}{3} T_{iijj} \right) \quad (C33)$$

5. Effective Properties Including Interactions

Whether interactions are neglected or not, the field scattered by the representative sphere is given by (C24). We also know that the field scattered by each inclusion is given by (C7), where the matrix is the surrounding material. If we can estimate the effect of the interactions on the field inside an inclusion, then we can determine its effect on the effective laws. We assume that the interactions can be taken into account by a self-consistent scheme in an average sense. We estimate the field inside an inclusion which is surrounded by effective material up to a distance R (the radius of the representative sphere) where matrix material starts and extends to infinity.

The displacement inside the inclusion is approximated by

$$\underline{v}(\underline{y}) \approx \underline{u}^*(\underline{y}) \quad (C34)$$

where \underline{u}^* is the displacement which would exist at the center of the representative sphere if the inclusion was absent.

But \underline{u}^* is itself given by

$$\underline{u}^*(\underline{y}) \approx \underline{u}^0(\underline{y}) \quad (C35)$$

so that

$$\underline{v}(\underline{y}) \approx \underline{u}^0(\underline{y}) \quad (C36)$$

where \underline{u}^0 is the incident field.

The strain inside the inclusion is given as in (C16) by

$$e_{ij} = U_{ijkl}^* e_{kl}^* \quad (C37)$$

where e_{kl}^* is the strain which would exist at \underline{y} if the inclusion was absent. U^* is the analog of U in (C16). U^* depends on inclusion and effective properties, whereas U depends on inclusion and matrix properties. Now e_{kl}^* is the strain inside the representative sphere and it is given by

$$e_{kl}^* = \frac{1}{3}(\tilde{P}^* - \tilde{Q}^*) e_{pp}^0 \delta_{kl} + \tilde{Q}^* e_{kl}^0 \quad (C38)$$

The above relationship was used in (C24). Combining (C37) and (C38) we obtain

$$e_{ij} = \frac{1}{3}(\tilde{P}^* - \tilde{Q}^*) U_{ijn}^* e_{pp}^0 + \tilde{Q}^* U_{ijkl}^* e_{kl}^0 \quad (C39)$$

The derivation follows exactly the same steps as in the preceding section. We use (C13), integrate over all orientations, make use of the symmetries of the T tensor, and we obtain the following results

$$\rho^* - \rho = (\rho' - \rho)c \quad (C40)$$

$$K^* - K = c(K' - K) \frac{1}{3} T_{iijj}^* \quad (C41)$$

$$\mu^* - \mu = \frac{c(\mu' - \mu)}{5} (T_{ijij}^* - \frac{1}{3} T_{iijj}^*) \quad (C42)$$

Equations (C41) and (C42) were also obtained by Wu (1966) for the corresponding static case.

APPENDIX D: EFFECTIVE PROPERTIES FOR INTERMEDIATE WAVELENGTHS

In this appendix we treat the case where the wavelength of the incident P wave is much longer than the radius of the inclusions, but only slightly longer than the radius of the representative sphere. When a plane P wave is incident on a spherical inclusion, the dilation of the scattered P waves can be written as an infinite series. As shown in Appendix A, the far field expression is

$$\Delta = \frac{e^{i(pr-\omega t)}}{pr} \sum_{n=0}^{\infty} (-i)^{n+1} B_n' P_n(\cos \theta) \quad (D1)$$

The coefficients B_n are found from the boundary conditions for each n . Let us assume for simplicity that the matrix is a non-viscous fluid. Then for any wavelength the coefficients are (See Appendix A, Equations A14 to A19)

$$B_0 = -A \left[\frac{xKj_0(x)j_1(x') + x'j_1(x) \left(+\frac{4\mu'}{x'} j_1(x') - (K' + \frac{4\mu'}{3}) j_0(x') \right)}{xKh_0^{(1)}(x)j_1(x') + x'h_1^{(1)}(x) \left(\frac{4\mu'}{x'} j_1(x') - (K' + \frac{4\mu'}{3}) j_0(x') \right)} \right] \quad (D2)$$

$$B_n = -(2n+1) i^{n_A} \frac{x^2 K j_n(x) \Delta_1 + [x j_{n-1}(x) - (n+1) j_n(x)] \Delta_2}{x^2 K h_n(x) \Delta_1 + [x h_{n-1}^{(1)}(x) - (n+1) h_n^{(1)}(x)] \Delta_2} \quad n \geq 1$$

(D3)

where

$$\Delta_1 = d_{n3} e_{n2} - d_{n2} e_{n3}$$

$$\Delta_2 = d_{n2} e_{n1} - d_{n1} e_{n2}$$

$$d_{n1} = \left[\frac{2\mu' (n+1) (n+2)}{x'^2} - \left(\kappa' + \frac{4\mu'}{3} \right) \right] j_n(x') - \frac{4\mu'}{x'} j_{n-1}(x')$$

$$d_{n2} = \frac{2\mu'}{x'^2} \left[x' j_{n-1}(x') - (n+2) j_n(x') \right]$$

$$d_{n3} = \frac{j_{n-1}(x')}{x'} - \frac{(n+1)}{x'^2} j_n(x')$$

$$e_{n1} = + \frac{2\mu' n(n+1)}{z'^2} \left[(n+2) j_n(z') - z' j_{n-1}(z') \right]$$

$$e_{n2} = \frac{\mu'}{z'^2} \left[2z' j_{n-1}(z') + (z'^2 - 2(n+2)n) j_n(z') \right]$$

$$e_{n3} = - \frac{n(n+1)}{z'^2} j_n(z')$$

$$x = 2\pi a / \lambda'_\alpha$$

$$x' = 2\pi a / \lambda'_\alpha$$

$$z' = 2\pi a / \lambda'_\beta$$

λ_α is the wavelength of a P wave in the matrix; λ'_α and λ'_β are the wavelengths of P and S waves in the inclusion.

We restrict our analysis to values of x , x' , z' smaller than 1 because of the quasi-homogeneity assumption inherent to our study of the effective properties. We can use the expansions of the spherical Bessel and Hankel functions for small arguments even if x is close to one, provided that the truncation of the series takes place after a sufficient number of terms. For small n , the expansions are

$$j_0(x) \approx 1 - \frac{x^2}{6} + \frac{x^4}{120} - \frac{x^6}{120 \times 42}$$

$$j_1(x) \approx \frac{x}{3} - \frac{x^3}{30} + \frac{x^5}{840} + \frac{x^7}{120 \times 378}$$

$$j_2(x) \approx \frac{x^2}{15} - \frac{x^4}{210} + \frac{121x^6}{120 \times 1008}$$

$$h_0^{(1)}(x) \approx -\frac{i}{x} + 1 + \frac{ix}{2} - \frac{x^2}{6} - \frac{ix^3}{24} + \frac{x^4}{120} + \frac{ix^5}{720}$$

$$h_1^{(1)}(x) \approx -\frac{i}{x^2} - \frac{i}{2} + \frac{x}{3} + \frac{ix^2}{8} - \frac{x^3}{30} - \frac{ix^4}{144} + \frac{x^5}{840}$$

$$h_2^{(1)}(x) \approx -\frac{3i}{x^3} - \frac{i}{2x} - \frac{ix}{8} + \frac{x^2}{15} + \frac{ix^3}{48} - \frac{x^4}{210}$$

We will simplify the problem to the case of a fluid representative sphere embedded in a fluid matrix. This covers our experimental data, since the effective medium for a suspension

of solid inclusions in a fluid matrix is essentially a fluid (i.e., $\mu^* = 0$). Using (D2) and (D3) and letting $\mu^* = 0$, we have

$$B_0 = -A \frac{K j_0(Y_R) j_1(Y_R^*) Y_R - K^* j_0(Y_R^*) j_1(Y_R) Y_R^*}{K j_1(Y_R^*) h_0^{(1)}(Y_R) Y_R - K^* j_0(Y_R^*) h_1^{(1)}(Y_R) Y_R^*} \quad (D5)$$

Using the expansions given in (D4) we obtain

$$B_0 \approx -\frac{A Y_R^3}{3i} \frac{K-K^*}{K^*} \left[1 + (\tilde{Y} - \tilde{Z}) (1 - \tilde{Z} + \tilde{Z}^2 - \tilde{Z}^3 \dots) \right] \quad (D6)$$

where

$$\begin{aligned} \tilde{Y} - \tilde{Z} = & - Y_R^2 \frac{3}{5} - \frac{K}{3K^*} + \frac{K(Y_R^{*2} - Y_R^2)}{15(K-K^*)} - \frac{Y_R^3(K-K^*)}{3iK^*} \\ & + \frac{15Y_R^4 + 12Y_R^2 Y_R^{*2} - Y_R^{*4}}{120} - \frac{K Y_R^2}{30K^*} (5Y_R^2 + Y_R^{*2}) \\ & + \frac{Y_R^{*4}(3K-7K^*) + Y_R^4(7K-3K^*)}{840(K-K^*)} \end{aligned} \quad (D7)$$

$$\tilde{z} = \frac{Y_R^2}{2} - \frac{Y_R^{*2}}{6} - \frac{KY_R^2}{3K^*} + \frac{Y_R^3(K-K^*)}{3iK^*} + \frac{Y_R^{*4} - 10Y_R^2Y_R^{*2} - 15Y_R^4}{120} + \frac{KY_R^2}{30K^*} (Y_R^{*2} + 5Y_R^2)$$

Writing B_0 as

$$B_0 = Y_R^3 [B_{00} + B_{02}Y_R^2 + B_{03}Y_R^3 + \dots] \quad (D8)$$

we find

$$B_{00} = -\frac{A(K-K^*)}{3iK^*}$$

$$B_{02} = -\frac{A(K-K^*)}{3iK^*} \left[\frac{K([Y_R^{*2}/Y_R^2] - 1)}{15(K-K^*)} - \frac{(9K^* - 5K)}{15K^*} \right] \quad (D9)$$

$$B_{03} = -\frac{A(K-K^*)^2}{9K^{*2}}$$

B_{00} is usually smaller than 1, since K and K^* are generally close. Since Y_R is smaller than 1, the term $B_{03}Y_R^3$ can be neglected with respect to B_{00} . For the water-polystyrene suspension at 50% concentration, $B_{03}Y_R^3/B_{00}$ is about 10^{-3} . With a similar procedure, we find

$$B_1 = Y_R^3 [B_{10} + B_{12}Y_R^2 + B_{13}Y_R^3 + \dots] \quad (D10)$$

with

$$\begin{aligned}
 B_{10} &= 3i \frac{\rho - \rho^*}{\rho + 2\rho^*} A \\
 B_{12} &= \frac{3i \left[60\rho\rho^* \left(1 - \frac{y_R^{*2}}{2Y_R} \right) - 6(\rho^2 - \rho^{*2}) \right]}{10(\rho + 2\rho^*)^2} A \\
 B_{13} &= - \frac{A(\rho - \rho^*)^2}{(\rho + 2\rho^*)^2}
 \end{aligned} \tag{D11}$$

Neglecting $B_{13}y_R^3$ with respect to B_{10} introduces an error of the order of 10^{-4} for our suspension. We thus truncate the series after $B_{12}y_R^2$. To the same order we obtain

$$B_2 \approx B_{22}y_R^5 \tag{D12}$$

where

$$B_{22} = \frac{2A}{9i} \frac{\rho^* - \rho}{2\rho + 3\rho^*}$$

The effective laws are derived by equating the coefficients B_n estimated for the representative sphere and for the individual inclusions. B_{n0} is the coefficient in the long wavelength limit. By including B_{n2} we perturb the solution. For $n = 2$, B_{20} vanishes and thus the effective law for $n = 2$ is very sensitive to the higher order term. We also know that the coefficient B_2 yields the law for the effective shear modulus, which vanishes for any wavelength

when the matrix is a fluid. Thus, because our method is essentially a perturbation of the long wavelength effective laws, we only consider the equations for the leading coefficients B_0 and B_1 . Assuming that the wavelength is sufficiently larger than the inclusion size for neglecting the higher-order terms, we can write the effective laws as

$$c \frac{\rho - \rho'}{\rho + 2\rho'} = \frac{\rho - \rho^*}{\rho + 2\rho^*} \left[1 + y_R^2 \frac{60\rho\rho^*(\rho K^* - \rho^* K) - 6\rho K^*(\rho^2 - \rho^{*2})}{10(\rho + 2\rho^*)(\rho - \rho^*)\rho K^*} \right] \quad (D13)$$

$$c \frac{K - K'}{K'} = \frac{K - K^*}{K^*} \left[1 + y_R^2 \frac{\rho^* K^2 + \rho(5K^2 + 9K^{*2}) - 15\rho K K^*}{15\rho K^*(K - K^*)} \right]$$

Denoting by K_L and ρ_L the value of K^* and ρ^* in the long wavelength limit, this approximation gives

$$K^* \approx K_L \left[1 - y_R^2 + \frac{y_R^2}{3} \frac{K}{K_L} \left(1 + \frac{\rho_L}{5\rho} \right) + \frac{3}{10} \frac{y_R^2}{y_R} \frac{K_L}{K} \right] \quad (D14)$$

$$\rho^* \approx \rho_L \left[1 - \frac{2y_R^2}{(\rho - 2\rho_L)^2} \left((\rho^2 - 4\rho_L^2) + \frac{(\rho - 2\rho_L)(\rho + 2\rho_L)^2}{50\rho_L} \right) - \frac{(\rho + 2\rho_L)(\rho - 2\rho_L)^2}{20\rho} + \frac{K}{10K_L\rho} (\rho + 2\rho_L) \{ 5(\rho - 2\rho_L)^2 + (\rho + 2\rho_L)\rho \} \right]$$

BIOGRAPHICAL NOTE

The author was born in Mulhouse, France on July 9, 1946. He attended the Lycée d'Etat de Mulhouse and in 1964 went to the Université de Strasbourg where he received his licence ès sciences in 1967. He enjoyed a summer of paleomagnetic field work and gastronomic experiences in the South of France with the Société Nationale des Petroles d'Aquitaine and earned the degree of ingénieur géophysien at the Institut de Physique du Globe de Strasbourg in 1968. He happily left the Old Continent to enter MIT where a research assistantship and a fellowship from Chevron Oil Company allowed him to stay without facing bankruptcy. He received the degree of Master of Science in 1970. He held a summer position with the Seismic Discrimination Group at Lincoln Laboratory the same year and finally completed this work before the call of the French Army.

Publications

Kuster, G.T., Influence du forage sur l'aimantation des roches -- Etudes paléomagnétiques dans la bande dioritique du massif du Champ-du-Feu, Mémoire,

Faculté des Sciences, Université de Strasbourg,
1968.

Kuster, G.T., Effect of drilling on rock magnetization
(abstract), EOS, 50, 4, 134, 1969.

Kuster, G.T., Sound velocity in fluid-solid suspensions,
M.S. thesis, Massachusetts Institute of Technology,
Cambridge, 1970.

Lacoss, R.T. and Kuster, G.T., Processing a partially
coherent large seismic array for discrimination,
Technical Note 1970-30, MIT Lincoln Laboratory,
1970.

Kuster, G.T. and M.N. Toksöz, Sound velocity in fluid-
solid suspension, (abstract), 40th Annual Meeting,
Society of Exploration Geophysicists, 1970.

Kuster, G.T. and M.N. Toksöz, Elastic wave propagation
in suspensions, (abstract), Meeting of the Eastern
Section of the Seismological Society of America,
1971.